AD-A114 457 FOREIGN TECHNOLOGY DIV WRIGHT-PATTERSON AFB OH F/G 20/9
PRINCIPLES OF RADIO ENGINEERING (SELECTED PAGES),(U)
APR 82 Y A FILATOVA, I I CHUGUNOV
UNCLASSIFIED FTD-ID(RS)T-0647-81 NL

1 of 2

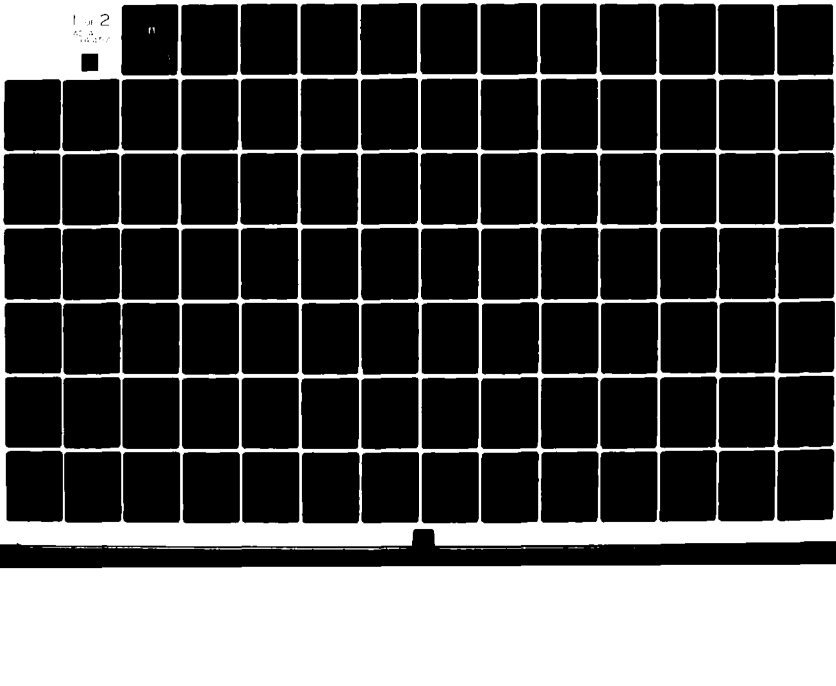

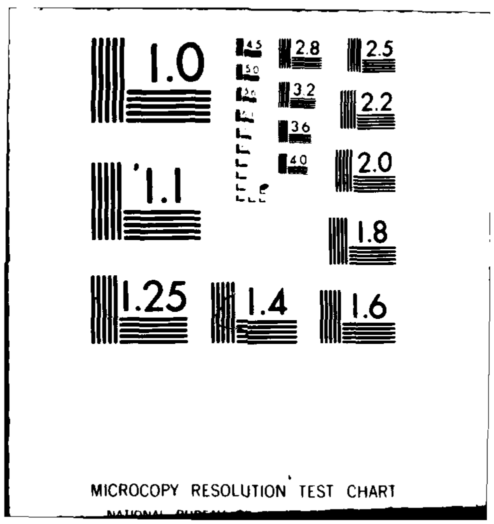
1.0
1.1
1.25
1.4
1.6
1.8
2.0
2.2
2.5
2.8
3.2
3.6
4.0
MICROCOPY RESOLUTION TEST CHART

(2)

FTD-ID(RS)T-0647-81

FOREIGN TECHNOLOGY DIVISION

AIR FORCE SYSTEMS COMMAND

PRINCIPLES OF RADIO ENGINEERING

(Selected Pages)

FOREIGN TECHNOLOGY DIVISION

82 05 17 005

EDITED TRANSLATION

FTD-ID(RS)T-0647-81 22 April 1982

MICROFICHE NR: FTD-82-C-000507

PRINCIPLES OF RADIO ENGINEERING (Selected Pages)

English pages: 141

Source: Osnovy Radiotekhniki, Trudy 100, Moscow, 1972, pp. 2-127

Country of origin: USSR
Translated by: LEO KANNER ASSOCIATES
F33657-81-D-0264
Requester: NISC

TABLE OF CONTENTS

U. S. BOARD ON GEOGRAPHIC NAMES TRANSLITERATION SYSTEM

Block	Italic	Transliteration	Block	Italic	Transliteration
А а	*А а*	A, a	Р р	*Р р*	R, r
Б б	*Б б*	B, b	С с	*С с*	S, s
В в	*В в*	V, v	Т т	*Т т*	T, t
Г г	*Г г*	G, g	У у	*У у*	U, u
Д д	*Д д*	D, d	Ф ф	*Ф ф*	F, f
Е е	*Е е*	Ye, ye; E, e*	Х х	*Х х*	Kh, kh
Ж ж	*Ж ж*	Zh, zh	Ц ц	*Ц ц*	Ts, ts
З з	*З з*	Z, z	Ч ч	*Ч ч*	Ch, ch
И и	*И и*	I, i	Ш ш	*Ш ш*	Sh, sh
Й й	*Й й*	Y, y	Щ щ	*Щ щ*	Shch, shch
К к	*К к*	K, k	Ъ ъ	*Ъ ъ*	"
Л л	*Л л*	L, l	Ы ы	*Ы ы*	Y, y
М м	*М м*	M, m	Ь ь	*Ь ь*	'
Н н	*Н н*	N, n	Э э	*Э э*	E, e
О о	*О о*	O, o	Ю ю	*Ю ю*	Yu, yu
П п	*П п*	P, p	Я я	*Я я*	Ya, ya

*ye initially, after vowels, and after ъ, ь; e elsewhere.
When written as ё in Russian, transliterate as yё or ё.

RUSSIAN AND ENGLISH TRIGONOMETRIC FUNCTIONS

Russian	English	Russian	English	Russian	English
sin	sin	sh	sinh	arc sh	$\sinh^{-1}$
cos	cos	ch	cosh	arc ch	$\cosh^{-1}$
tg	tan	th	tanh	arc th	$\tanh^{-1}$
ctg	cot	cth	coth	arc cth	$\coth^{-1}$
sec	sec	sch	sech	arc sch	sech^{-1}
cosec	csc	csch	csch	arc csch	csch^{-1}

Russian	English
rot	curl
lg	log

GRAPHICS DISCLAIMER

All figures, graphics, tables, equations, etc. merged into this translation were extracted from the best quality copy available.

FOREWORD

This collection contains articles written by staff members of the department of radio engineering fundamentals and antenna feed installations of the Radio Engineering Division, Moscow Power Institute, in 1971.

As to subject matter orientation, the collection is divided into four parts. Part 1 includes studies on problems of the electrodynamics of inhomogeneous media. Presented in Part 2 are articles in which problems of the excitation and diffraction of electromagnetic waves are examined. Part 3 contains investigations on the recording of electromagnetic radiation in the microwave band. Part 4 considers problems of the theory and application of dielectric waveguides.

Because of the subject matter orientation of the collection, the references cited are general. In this collection, a three-digit arrangement is used in citing articles. Thus, in referring to article 7, the number 107 is given, and in citing article 23, the number 123.

Much of the work involved in collecting the articles and editing the collection was done by candidate of technical sciences V. V. Shtykov. Considerable work in the technical preparation of the collection was performed by degree-seeking student I. T. Krylova.

PART 1

ELECTRODYNAMICS OF INHOMOGENEOUS MEDIA

SOLVING PULSED PROBLEMS OF ELECTRODYNAMICS IN INHOMOGENEOUS MEDIA BY THE METHOD OF FINITE-DIFFERENCE NETS

Ye. A. Filatova

Modeling of Initial Equations in the Case of Magnetic Type Waves

An examination is made of modeling with finite-difference electrical nets of two-dimensional Maxwell operator equations in spherical coordinates originating in cases when the conductivity $\sigma(\omega)$ and the dielectric constant $\varepsilon_a(\omega)$ of a plasma medium vary with respect to radius and the angular coordinate θ. Schemes of net models are presented in an investigation of waves of the magnetic or electrical type.

When problems of the propagation of pulsed signals in dispersive media are investigated, the initial Maxwell equations for instantaneous values are best represented in the form of operator equations. In the case under study, this is a system of scalar operator equations. Here the system of scalar operator equations can be written in the following form:

$$\begin{aligned}
&\frac{1}{r\sin\theta}\frac{\partial}{\partial\theta}[E_\varphi(p)\sin\theta] = -p\mu_a H_r(p),\\
&\frac{1}{r}\frac{\partial}{\partial r}[rE_\varphi(p)] = p\mu_a H_\theta(p),\\
&\frac{1}{r}\frac{\partial}{\partial r}[rH_\theta(p)] - \frac{1}{r}\frac{\partial H_r(p)}{\partial\theta} = p\tilde{\varepsilon}_a(p)E_\varphi(p),
\end{aligned} \tag{1}$$

where $E_\varphi(p), H_r(p), H_\theta(p)$ are the component images of the vectors of electromagnetic field intensity after Laplace

$\tilde{\varepsilon}_a(p) = \varepsilon_a(p) + \frac{\sigma(p)}{p}$ is the complex dielectric constant of a medium in operator form

The resulting operator equations are valid, assuming zero initial conditions.

The method of modeling operator equations consists of writing the initial equations in the form of equations in finite differences for a constant quantization step between the nodes of a two-dimensional net mn and mn+1 or mn-1 and mn, respectively, for the step Δθ between the nodes and m+1n or m-1n and mn. By introducing the constant modeling coefficients k_1, k_2, and the following notation:

$$
\begin{aligned}
&\frac{K_1[rE_\varphi(p)\sin\theta]'_{mn}}{\Delta r} = U_{mn}(p),\\
&\frac{K_1[rE_\varphi(p)\sin\theta]_{(mn\pm 1)}}{\Delta r} = U_{(mn\pm 1)}(p),\\
&\frac{K_1[rE_\varphi(p)\sin\theta]_{(m\pm 1n)}}{\Delta r} = U_{(m\pm 1n)}(p),\\
&\frac{K_2[rH_\theta(p)]_{(mn\pm 0.5)}}{\Delta r} = \mathcal{J}_{(mn\pm 0.5)}(p),\\
&\frac{K_2 H_{r\,m\pm 0.5n}(p)}{\Delta\theta} = \mathcal{J}_{m\pm 0.5n}(p),
\end{aligned}
\tag{2}
$$

we can write Eq. (1) in finite differences in the form of the following system:

$$
\begin{aligned}
&U_{m+1n}(p) - U_{mn}(p) = -p\mu_a\frac{K_1}{K_2}\sin\theta_{m+0.5}\frac{r_n^2\Delta\theta^2}{\Delta r}\mathcal{J}_{m+0.5n}(p),\\
&U_{mn}(p) - U_{m-1n}(p) = -p\mu_a\frac{K_1}{K_2}\sin\theta_{m-0.5}\frac{r_n^2\Delta\theta^2}{\Delta r}\mathcal{J}_{m-0.5n}(p),\\
&U_{mn+1}(p) - U_{mn}(p) = p\mu_a\Delta r\frac{K_1}{K_2}\sin\theta_m\mathcal{J}_{mn+0.5}(p),\\
&U_{mn}(\bar{p}) - U_{mn-1}(p) = p\mu_a\Delta r\frac{K_1}{K_2}\sin\theta_m\mathcal{J}_{mn-0.5}(p),\\
&\mathcal{J}_{mn+0.5}(p) - \mathcal{J}_{mn-0.5}(p) - \mathcal{J}_{m+0.5n}(p) + \mathcal{J}_{m-0.5n}(p) =\\
&\quad = \frac{K_2}{K_1}p\tilde{\varepsilon}_{a\,mn}(p)\frac{\Delta r}{\sin\theta_m}U_{mn}(p).
\end{aligned}
\tag{3}
$$

The system of equations (1) can be reduced to operator equations (8) of the voltage U(p) balance and of the current $\mathcal{J}$(p) balance in the node of the two-dimensional net. The two-port networks of the model can be calculated with the following formulas:

$$Z_{m\pm\frac{1}{2},n}(p) = p\mu_a \frac{K_1}{K_2} \frac{r_n^2 \Delta\theta^2}{\Delta r} \sin\theta_{m\pm\frac{1}{2}}, \tag{4}$$

$$Z_{m,n\pm\frac{1}{2}}(p) = p\mu_a \frac{K_1}{K_2} \Delta r \sin\theta_m, \tag{5}$$

$$Y_{mn}(p) = p\tilde{\varepsilon}_{a\,mn}(p) \frac{K_2}{K_1} \frac{\Delta r}{\sin\theta_m}. \tag{6}$$

The model can be obtained if from the resulting equations (4), (5), (6) the target is synthesized for the known law $\tilde{\varepsilon}_a$(p). For the case of a plasma medium, the dielectric constant ε_a(p) and the conductivity σ(p) in operator form can be written as follows:

$$\varepsilon_a(p) \doteq \left(1 - 3{,}19\cdot 10^9 \frac{n_e}{\nu^2 - p^2}\right)\varepsilon_0, \tag{7}$$

$$\sigma(p) = 2{,}82 \cdot 10^{-2} \frac{n_e \nu}{\nu^2 - p^2}, \tag{8}$$

where n_e is the electron concentration in the plasma

ν is the effective rate of electron collisions in the plasma, 1/s

By the synthesis of the two-port networks, the model diagram as shown in Fig. 1 was obtained.

The model elements can be calculated with the formulas:

$$L_{m\pm\frac{1}{2},n} \doteq \mu_a \frac{K_1}{K_2} \frac{r_n^2 \Delta\theta^2}{\Delta r} \sin\theta_{m\pm\frac{1}{2}}, \tag{9}$$

$$L_{m,n\pm\frac{1}{2}} = \mu_a \frac{K_1}{K_2} \Delta r \sin\theta_m, \tag{10}$$

$$C_{mn} = \varepsilon_0 \frac{K_2}{K_1} \frac{\Delta r}{\sin\theta_m}, \tag{11}$$

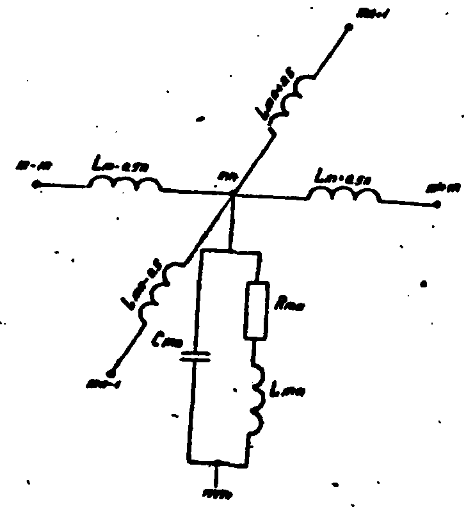

Fig. 1.

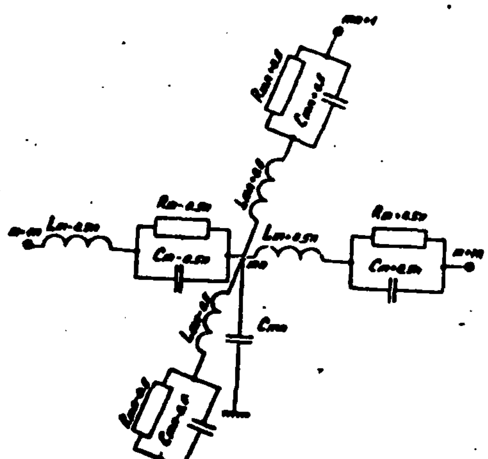

Fig. 2.

$$L_{mn} = \frac{K_1 \sin\theta_m}{K_2\, 3{,}19\cdot 10^8\, n_{emn}\, \varepsilon_0 \Delta r}, \tag{12}$$

$$R_{mn} = \frac{K_1 \nu_{mn} \sin\theta_m}{K_2\, 3{,}19\cdot 10^8\, n_{emn}\, \varepsilon_0 \Delta r}. \tag{13}$$

Modeling Initial Equations in the Case of Electric Type Waves

Operator Maxwell equations for this case can be written in the following form:

$$\begin{aligned} &\frac{1}{r\sin\theta}\frac{\partial}{\partial\theta}\left[H_\varphi(p)\sin\theta\right] = p\bar{\varepsilon}_a(p)E_r(p), \\ &\frac{1}{r}\frac{\partial}{\partial r}\left[rH_\varphi(p)\right] = -p\bar{\varepsilon}_a(p)E_\theta(p), \\ &\frac{1}{r}\frac{\partial}{\partial r}\left[rE_\theta(p)\right] - \frac{1}{r}\frac{\partial E_r(p)}{\partial\theta} = -p\mu_a H_\varphi(p). \end{aligned} \tag{14}$$

Modeling of system (14) is analogous to modeling of Eqs. (1). The model diagram is given in Fig. 2. The model elements for the case of a plasma medium can be calculated with the following formulas:

$$C_{mn} = \mu_a \frac{K_2}{K_3}\frac{\Delta r}{\sin\theta_m}, \tag{15}$$

$$L_{m\pm q,n} = \varepsilon_0 \frac{K_3}{K_4}\frac{r_n^2\Delta\theta^2}{\Delta r}\sin\theta_{m\pm q}, \tag{16}$$

$$C_{m\pm q,n} = \frac{K_4 \Delta r}{K_3 \varepsilon_0\, 3{,}19\cdot 10^8\, n_{em\pm q,n}\, r_n^2 \Delta\theta^2 \sin\theta_{m\pm q}}, \tag{17}$$

$$R_{m\pm q,n} = \frac{\varepsilon_0 \frac{K_3}{K_4}\, 3{,}19\cdot 10^8\, n_{em\pm q,n}\, r^2\Delta\theta^2 \sin\theta_{m\pm q}}{\Delta r\, \nu_{m\pm q,n}}, \tag{18}$$

$$L_{mn\pm q} = \varepsilon_0 \frac{K_3}{K_4}\Delta r \sin\theta_m, \tag{19}$$

$$C_{mn\pm q} = \frac{K_4}{K_3 \varepsilon_0\, 3{,}19\cdot 10^8\, n_{emn\pm q}\, \Delta r \sin\theta_m}, \tag{20}$$

$$R_{mn\pm q} = \frac{K_3 \varepsilon_0\, 3{,}19\cdot 10^8\, n_{emn\pm q}\, \Delta r \sin\theta_m}{K_4\, \nu_{mn\pm q}}. \tag{21}$$

In this diagram the components of the electromagnetic field can be determined from the following relationships:

$$k_3 \frac{[rH_\varphi(p)\sin\theta]_{mn}}{\Delta r} = U_{mn}(p), \tag{22}$$

$$k_4 \frac{[rE_\theta(p)]_{mn\pm 0.5}}{\Delta r} = J_{mn\pm 0.5}(p), \tag{23}$$

$$k_4 \frac{E_{rm\pm 0.5n}(p)}{\Delta\theta} = J_{m\pm 0.5n}(p), \tag{24}$$

where k_3, k_4 are constant coefficients of modeling.

The solution of the practical problems can be reduced to setting up the diagram of the models according to Fig. 1, when the required boundary conditions are satisfied [1].

The calculations and the experiments showed that it is entirely possible to exactly synthesize the modeling diagrams in the frequency band exceeding the band used in actual radio systems. The advantages of the modeling method consist of the fact that in this case use is made only of quantization along the coordinates along which the parameters of the medium vary. In contrast to numerical methods, this method does not require quantization with respect to frequency and to time. The model is best constructed for a frequency distinct from the working frequency of the pulse system. All elements of the diagram and the pulse signals tested are recalculated to the model frequency according to the principle of electrodynamic similitude. The excitation condition is attained by connecting a radio pulse generator to the corresponding node. When the shape or duration of the radio pulse is varied, the model elements remain unchanged. A pulse signal is observed in the electrical circuit, at different points in it corresponding to certain spatial points of the electrodynamic problem.

SOLUTION OF ONE-DIMENSIONAL PROBLEMS OF LONG-RANGE ELECTRODYNAMIC PROBLEMS BY METHOD OF MODELING ON MODELS WITH SHORT ELECTRICAL LENGTH

I. I. Chugunov and L. P. Abasheyeva

When a plane electromagnetic wave is incident at an angle ϕ on a plane inhomogeneous layer, the complex dielectric constant being $\tilde{\varepsilon}_a = \varepsilon_a - j\frac{\sigma}{\omega}$ and varying along the coordinate z, depending on the polarization, the process can be described with either the equation

$$\frac{d^2U}{dz^2} + f(z)U = 0 \qquad (1)$$

or the equation

$$\frac{d^2U}{dz^2} + \tilde{\varepsilon}_a \frac{d}{dz}\left(\frac{1}{\tilde{\varepsilon}_a}\right)\frac{dU}{dz} + f(z)U = 0, \qquad (2)$$

where

$$f(z) = \omega^2 \mu_a \varepsilon_0 [\tilde{\varepsilon}(z) - \sin^2\varphi].$$

Using the discrete partitioning of the layer into m equal parts Δz, within whose limits the variation in the parameters of the medium is insignificant, and by applying the principle of electrodynamic similitude, let us model Eqs. (1) and (2) [2].

By modeling the equations, we get the circuit diagrams shown in Fig. 1a and 1b.

For Eq. (1), Fig. 1a, given the values f(z)>0, and Fig. 1b, given the values f(z)<0. In these diagrams, according to [1]

$$z_m = \frac{1}{j\omega C_m} = \frac{K_1}{K_2 j\omega \mu_a \Delta z}.$$

Hence we have

$$C_m = \frac{K_2}{K_1}\mu_a \Delta z,$$

$$\begin{aligned} z_{m\pm qs} &= j\omega \frac{K_1}{K_2}\Delta z\,\varepsilon_0 \tilde{\varepsilon}_{\varphi m\pm qs} = \\ &= j\omega \frac{K_1}{K_2}\Delta z\,\varepsilon_0 \left[(\varepsilon_{m\pm qs} - \sin^2\varphi) - j\frac{\sigma_{m\pm qs}}{\omega\varepsilon_0}\right] \end{aligned} \tag{3}$$

or

$$L_{m\pm qs} = \frac{K_1}{K_2}\Delta z\,\varepsilon_0 (\varepsilon_{m\pm qs} - \sin^2\varphi), \tag{4}$$

$$R_{m\pm qs} = \frac{K_1}{K_2}\Delta z\,\sigma_{m\pm qs}. \tag{5}$$

For the case when $(\varepsilon_{m\pm qs} - \sin^2\varphi) < 0$, the inductance $L_{m\pm 0.5}$ can be replaced with the inductance $C_{m\pm 0.5}$ determined with the formula

$$C_{m\pm qs} = \frac{K_2}{K_1\omega^2\Delta z\,\varepsilon_0(\varepsilon_{m\pm qs} - \sin^2\varphi)} \tag{6}$$

In these circuits the voltage at the nodes determine the magnitude of the magnetic field intensity at the corresponding points of the inhomogeneous layer. The value of the current $J_{m\pm qs}$ determines the electric field intensity. By modeling Eq. (2), we get circuits of the form shown in Fig. 1b, for f(z)>0, and Fig. 1d, for the values f(z)<0.

As can be shown in Fig. 1c and 1d, in place of the constant capacitance C_m in the parallel branch of the circuit the parallel connection of capacitance C_m and resistance R_m, determined with the following formulas, now appear:

$$R_m = \frac{K_1}{K_2}\,\frac{\left[\varepsilon_m^2 + \left(\frac{\sigma_m}{\omega\varepsilon_0}\right)^2\right]\varepsilon_0}{\mu_0\,\Delta z\,\sigma_m \sin^2\psi}\,, \tag{7}$$

$$C_m = \frac{K_2}{K_1}\mu_0\,\Delta z\left[1 - \frac{\varepsilon_m \sin^2\psi}{\varepsilon_m^2 + \left(\frac{\sigma_m}{\omega\varepsilon_0}\right)^2}\right], \tag{8}$$

$$R_{m\pm0.5} = \frac{K_1}{K_2}\,\Delta z\,\sigma_{m\pm0.5}\,, \tag{9}$$

$$L_{m\pm0.5} = \frac{K_1}{K_2}\,\Delta z\,\varepsilon_0\varepsilon_{m\pm0.5} \tag{10}$$

For the negative values $\varepsilon_{m\pm0.5}$, the inductance $L_{m\pm0.5}$ is replaced with the capacitance

$$C_{m\pm0.5} = \frac{K_2}{\omega^2 K_1\,\Delta z\,\varepsilon_0\left|\varepsilon_{m\pm0.5}\right|} \tag{11}$$

If

$$\frac{\varepsilon_m \sin^2\psi}{\varepsilon_m^2 + \left(\frac{\sigma_m}{\omega\varepsilon_0}\right)^2} > 1,$$

then the capacitance C_m must be replaced with the inductance

$$L_m = \frac{K_1}{K_2\,\omega^2\mu_0\,\Delta z}\cdot\frac{1}{\left|1 - \frac{\varepsilon_m \sin^2\psi}{\varepsilon_m + \left(\frac{\sigma_m}{\omega\varepsilon_0}\right)^2}\right|} \tag{12}$$

In this diagram, the voltage at the nodes U_m determine the value of the component of the magnetic field intensity, and the currents $I_{m\pm0.5}$, the value of the electric field intensity.

In Eqs. (3) through (12), k_1 and k_2 are constant coefficients selected in accordance with the principle of electrodynamic similitude.

The design of the universal model (one-dimensional) makes it possible to rapidly select different diagrams shown in Fig. 1, and to match the model input with the generator output. Additionally, there is the option of changing the model $z_{вх}$ according to the necessary boundary conditions.

When electromagnetic waves pass through an inhomogeneous plasma layer, the attenuation constant α is the main parameter. But when the electrical length of an inhomogeneous plasma layer exceeds the electrical length of the model or when the inhomogeneous plasma layer has large attenuations, $U_{прош.}$ cannot always be measured. In these cases, the problem must be solved by stages. To do this, the inhomogeneous plasma layer is divided into parts.

A block diagram for determining attenuation by parts is shown in Fig. 2a. The letters A and D designate the start and end of the model, respectively; the letters B and ~~D~~ C, the points dividing the inhomogeneous layer into three parts: I, II, III. When the problem was formulated, it was assumed that the plane wave is incident from free space at an inhomogeneous layer and exits into unbounded free space.

As can be seen in Fig. 2b, the solution is carried out to completion, that is, first part III of the layer is considered. The $z_{вх.1}$ of the section of the model CD is determined by connecting the generator to the model at point C across resistance R, serving for determining the complex amplitude of the current, and α_{III}, the attenuation constant for layer III.

By replacing the section of the model CD with the resistance $z_{вх.1}$ obtained, we determine α_{II} and $z_{вх.2}$ and so on. If the number of partitionings is m, total attenuation is obtained by summing the attenuation constants α_m.

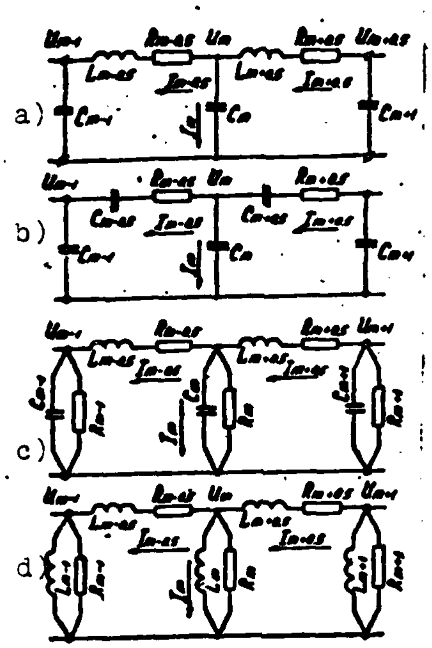

Fig. 1.

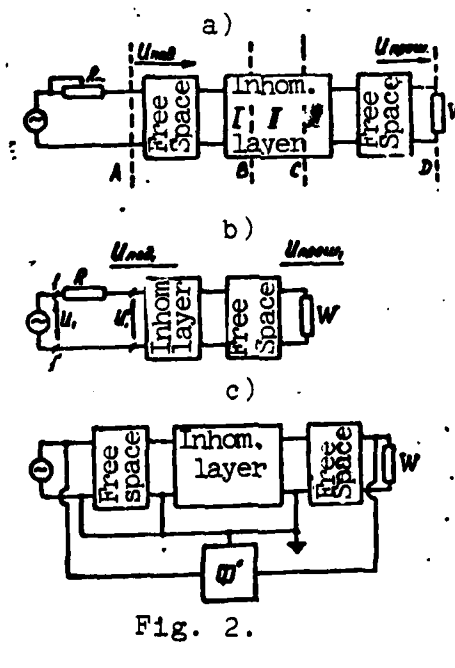
a)
Free Space
Inhom.
layer
Free Space
W
A
B
C
D
b)
Inhom layer
Free Space
W
c)
Free space
Inhom.
layer
Free Space
W

Fig. 2.

When the signal passes through the inhomogeneous layer, the phase of the arriving signal with respect to the input is measured in the usual way: by connecting a phasemeter to the model input and output. Shown in Fig. 2c is a phasemeter connection diagram. But if the signal does not pass through the layer, the above-described method of dividing the model into parts is used. Then the total phase ϕ_{AD} will be

$$\varphi_{AD} = \varphi_{CD} + \varphi_{BC} + \varphi_{AB}$$

The phasemeter connection diagram for connecting the phasemeter to each individual model part is the same as in Fig. 2c. Measuring the phase by parts yielded good agreement with the result of measuring the phase for the entire model. The error of measurement was ± 10. Actual working with the universal model showed that, by successively replacing the model parts with their $z_{вх}$, because of rapid commutation of the model elements the problem can be solved without significant degradation of solution accuracy.

REFLECTION OF A PLANE TM WAVE FROM A HOMOGENEOUS PLASMA HALF-SPACE

I. G. Yakushkin and V. A. Permyakov

1. As is known, when a TM wave is reflected from an inhomogeneous plane stratified plasma with the law of variation of the dielectric constant $\varepsilon(z)=\varepsilon'(0)\cdot z$, $\varepsilon'(0)\neq 0$, in the neighborhood of zero ε, resonance absorption of the field occurs. In this case, the modulus of the reflection coefficient is different from unity even when there are infinitesimal heat losses in the layer. Although the phenomenon of resonance absorption has been investigated in a large number of publications [3-6], they lack detailed numerical results and approximate expressions suitable for determining the reflection coefficient when there are arbitrary gradients of the dielectric constant. Below we analyze the function of the reflection coefficient of a TM wave reflected from a plasma half-space, with the linear law $\varepsilon(z)=-az\,,\ z>-\frac{1}{a}$ when there are arbitrary gradients of ε.

The reflection coefficient for the magnetic field is defined by the expression

$$R=\frac{\cos\theta-Z}{\cos\theta+Z}\,, \tag{1}$$

where Z is the normalized (divided by free-space impedance) impedance of the layer, equal to

$$Z = -i\,\frac{U'(z)}{\kappa\varepsilon(z)U(z)} \tag{2}$$

and U(z) satisfies the equation

$$U'' - \frac{\varepsilon'(z)}{\varepsilon(z)}U' + \kappa^2(\varepsilon(z) - \sin^2\theta)U = 0 \tag{3}$$

The angle of incidence of the wave θ is measured from the normal to the interface.

2. When there are arbitrary gradients of ε, the solution of Eq. (3) is sought for by the power series method at the point ε=0 and has the form [4, 9]

$$U(t) = \left(f(\lambda) - \frac{1}{2}\ln t\right)U_1(t) + U_2(t), \tag{4}$$

where

$$t = -\left(\frac{\kappa}{a}\right)^{2/3}\varepsilon(z), \qquad \lambda = \left(\frac{\kappa}{a}\right)^{2/3}\sin^2\theta$$

$$U_1(t) = \sum_{n=0}^{\infty} A_n t^{n+1}, \; A_0 = 1,\; A_1 = 0,\; A_n = \frac{1}{n(n+1)}(\lambda A_{n-2} + A_{n-3}),\; n \geq 2$$

$$U_2(t) = \sum_{n=0}^{\infty} B_n t^n, \; B_0 = -\frac{1}{2},\; B_1 = B_2 = 0,$$

$$B_n = \frac{1}{n(n-1)}\left[\lambda\left(\frac{n-1}{2}A_{n-2} + B_{n-2}\right) + B_{n-3}\right],\; n \geq 3.$$

The unknown function f(λ) appearing in Eq. (4) is determined on the condition that the solution of U(t) decreases as $t \to +\infty$ ($\varepsilon \to -\infty$). Different formulas are presented in [9] for determining the functions f(λ) suitable for both analytic and machine calculations. According to [9], when $|\lambda| \lesssim 1$, the function f(λ) is equal, with at least an accuracy of 5 percent, to its value when θ=0:

$$f(\lambda) \approx f(0) \approx 0{,}848.$$

Using this value of the function f(λ) and retaining the terms of the power series (4) to the order $(k/a)^2$ inclusively, we get the following asymptotic formula for skin impedance that is suitable for large gradients of ε:

$$Z = i\,\frac{1{,}372\left(\frac{\kappa}{a}\right)^{1/3} + \frac{\kappa}{a} - \left[0{,}5 - \frac{2}{3}\ln\frac{a}{\kappa} + i\pi\right]\frac{\kappa}{a}\sin^2\theta}{1 - 0{,}686\left(\frac{\kappa}{a}\right)^{2/3} - \frac{1}{3}\left(\frac{\kappa}{a}\right)^2 - 0{,}5\sin^4\theta\left(\frac{\kappa}{a}\right)^2\left[\frac{2}{3}\ln\frac{a}{\kappa} - i\pi\right]} \tag{5}$$

Beginning with Eq. (5), we can show that when a>>1, the modulus of the reflection coefficient takes on the minimum value of $|R|_{min} \sim 1$ to $2.3(k/a)^{2/3}$ when $\theta \sim \arccos \operatorname{Im} Z$. With increase in a R_{min} tends to unity and is observed at grazing angles of incidence.

3. When a<<k and for not very shallow incidence, the phase integral method [7] can be applied for an approximate solution of Eq. (3). The phase integral method solution of Eq. (3) can be constructed in both the region of large positive z, that is, where $\varepsilon<0$, as well as in the region of negative z. After the substitutions $U=\sqrt{\varepsilon}F;\ \xi=\left(\frac{k}{a}\right)^{4/3}\varepsilon(z)$, Eq. (3) takes on the form

$$F''+\left(\xi-\lambda-\frac{3}{4\xi^2}\right)F=0, \tag{6}$$

where

$$\lambda=\left(\frac{k}{a}\right)^{4/3}\sin^2\theta$$

For large ξ, in Eq. (6) the term $(3/4)\xi^{-2}$ can be neglected. So the phase integral method solution of Eq. (6) for large negative ξ, selected on the conditions of decreasing in the domain where $\varepsilon<0$, takes on the form

$$F=\frac{C}{\sqrt[4]{\lambda-\xi}}\exp\int_{\lambda}^{\xi}\sqrt{\lambda-\xi}\,d\xi \tag{7}$$

For large positive ξ, based on the radiation conditions, we can write

$$F=\frac{A}{\sqrt[4]{\xi-\lambda}}\left\{\exp\left(-i\int_{\lambda}^{\xi}\sqrt{\xi-\lambda}\,d\xi\right)+R\exp\left(i\int_{\lambda}^{\xi}\sqrt{\xi-\lambda}\,d\xi\right)\right\} \tag{8}$$

The coefficient A, in the case if we can neglect reflection from the interface of media, can be determined simply on the condition of interlinking with the incident wave. The reflection coefficient of the wave R from an inhomogeneous half-space is the principal quantity to be determined. For large values of λ, generally the energy does not penetrate to the point $\xi=0$. In this case, Eq. (6) can be reduced to the Airy differential equation and it turns out that R=1. The situation is more involved when $\lambda \sim 1$, since in this case the reflection is determined by the

function $\xi-\lambda-\frac{3}{4}\xi^{-2}$. This function has already three inflection points, two of which are located at complex values of ξ.

To take this reflection into account, by using the phase integral method it is important to be able to consider the phase integral method approximation to be applicable even in the neighborhood of a pole. For this purpose, the function $p(\xi)$ used in constructing the phase integral method solution [7], Eqs. (6) must be selected so that the error of the phase integral method solution remains finite when $\xi=0$. The selection [6] of

$$p(\xi)=\xi-\lambda-\xi^{-2} \tag{9}$$

leads to this result.

In the following treatment, the notation below will be used:

$$\begin{gathered}(\alpha,\xi)=p^{-\frac{1}{4}}\exp\left(-i\int_{\alpha}^{\xi}\sqrt{p(\xi)}\,d\xi\right),\quad(\xi,\alpha)=p^{-\frac{1}{4}}\exp\left(-i\int_{\xi}^{\alpha}\sqrt{p(\xi)}\,d\xi\right),\\ [\xi,\alpha]=\exp\left(-i\int_{\xi}^{\alpha}\sqrt{p(\xi)}\,d\xi\right).\end{gathered} \tag{10}$$

To apply the phase integral method in determining the coupling coefficient associating the asymptotic representations of the solution for positive and negative ξ, we must know the structure of the Stokes lines, that is, the lines where

$Im\int_{\xi_i}^{\xi}\sqrt{p(\xi)}\,d\xi=0$ (ξ is the root of the equation $p(\xi)=0$).

The pattern of the Stokes lines for the function $p(\xi)$ assigned by Eq. (9) is shown in Fig. 1. The dashed line shows the conjugate Stokes lines at which $Re\int_{\xi_i}^{\xi}\sqrt{p(\xi)}\,d\xi=0$.

For large negative ξ, the solution must be sought in the form of (7), that is, in region IV the solution is of the form $F=C(\xi,\xi_2)$.

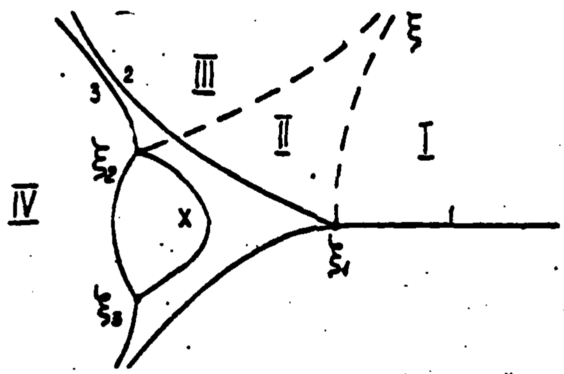

Fig. 1

In region III this solution is growing and therefore in the transition to region II, in accordance with the conventional rules for transition through conjugate Stokes lines [7,8], we get

$$F = C\{(\xi, \xi_2)[\xi_1, \xi_2] + i(\xi_1, \xi)[\xi_2, \xi_1]\}.$$

At Stokes line I we have

$$F = C\{(\xi, \xi_1)[\xi_1, \xi_2] + i(\xi_1, \xi_2)[\xi_1, \xi_2] + i(\xi_1, \xi)[\xi_2, \xi_1]\}.$$

By selecting C so that the solution is brought to the form (8), that is, $C = [\xi_2, \xi_1]\Psi$, where

$$\Psi = \exp\left\{-i\int_{\xi_1}^{\infty}\sqrt{\xi - \lambda - \xi^{-2}}\,d\xi + i\int_{\lambda}^{\infty}\sqrt{\xi - \lambda}\,d\xi\right\},$$

we get

$$R = i\Psi^2\{1 + [\xi_2, \xi_1]^2\} \qquad (11)$$

To derive the formula for the reflection coefficient, we used the complex inflection point lying in the upper half-space. Use of the lower inflection point does not lead to, and must not lead to the same result, since Eq. (4), at point $\xi=0$, has a branch point of infinite order, therefore by bypassing this point in the lower half-space, we arrive at another sheet of a manifold plane on which the solution is defined.

The cofactor appearing in Eq. (11) ahead of the brackets for the modulo is equal to unity and describes the phase shift of the reflected wave. The cofactor in the brackets describes the resonance absorption of the TM wave.

In the limiting cases, the solution obtained coincides with known results.

As can be seen from (11), $R \to 1$ as $\lambda \to \infty$. When $\lambda=0$, the same value $R=1$ is obtained from the exact solution and from Eq. (11).

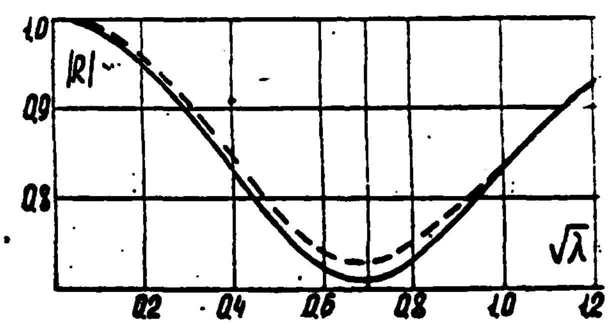

Fig. 2

4. Figs. 2 and 3 present the results of computing the reflection coefficient by the power series method (4) on a computer (solid line), and their comparison with the approximation of a strongly inhomogeneous plasma (5) (crosses) with the approximation of a weakly inhomogeneous plasma (dashed line) (11). From a comparison, there must be close agreement of the approximation of the weakly inhomogeneous plasma with the rigorous calculation when $a \leq 0.1k$ in the entire range of angles of incidence for plane waves. From the graphs it follows that $|R|$ has a minimum equal to ~ 0.7 when $\lambda \sim 0.5$, and beginning with $\lambda \sim 2.25$, $|R|$ is in practice equal to unity. For large gradients of ε ($1 \gtrsim \dot{a}/k \gtrsim 0.1$), the phase integral method is suitable in the range of angles close to zero ($\theta \lesssim 40$ to 60°). The inaccuracy of approximation (11) at grazing angles of incidence in this region of gradients of ε is explained by the fact that in its derivation the layer is assumed unbounded, while the numerical results were obtained when the wave was incident on a half-space.

The approximation of a strongly inhomogeneous plasma (5) proves to be suitable when $a \gtrsim k$. It bears noting that when $a \sim (1$ to $0.5)k$ in the region of grazing angles of incidence, this approximation agrees closely with the rigorous calculation.

Thus, in the aggregate the approximate solutions for the weakly inhomogeneous and strongly inhomogeneous plasma make it possible to describe the behavior of the reflection coefficient of the TM wave for arbitrary gradients of ε.

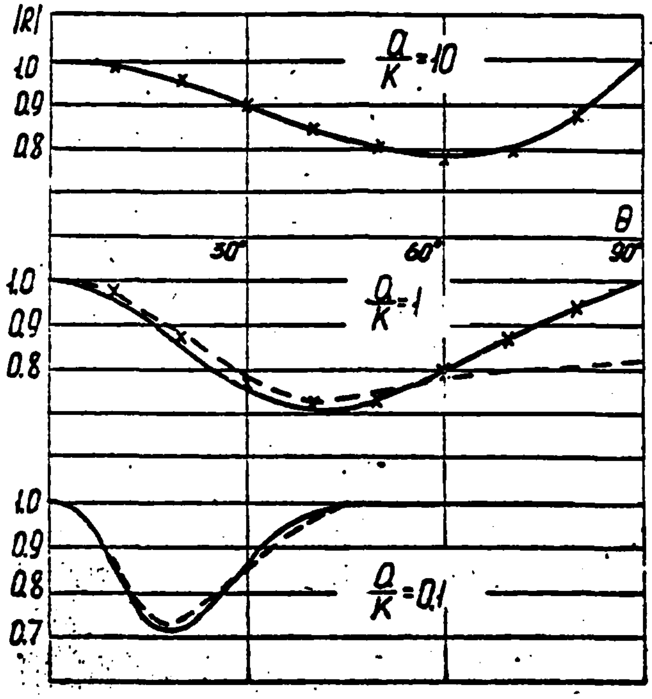
|R|
1.0
0.9
0.8
$\frac{a}{K}=10$
θ
30°
60°
90°
1.0
0.9
0.8
$\frac{a}{K}=1$
1.0
0.9
0.8
0.7
$\frac{a}{K}=0.1$

Fig. 3

EFFECT OF LINEAR TRANSITION LAYER ON THE ATTENUATION OF WAVES IN A PLANE STRATIFIED WAVEGUIDE

V. K. Polishchuk

1. Derivation of Dispersion Equations

Let us examine a plane-stratified waveguide, with relative dielectric constant ε_r, which is a continuous even function of the coordinate x (Fig. 1) and which, when x>0, can be expressed by the formulas

$$\varepsilon_r(x) = \begin{cases} \varepsilon_+, & 0<x<l, \\ a(x_0-x), & l<x<l+d, \\ -\varepsilon_-, & x>l+d, \end{cases}$$

$$a = \frac{\varepsilon_+ + \varepsilon_-}{d}; \quad x_0 = l + \frac{\varepsilon_+ d}{\varepsilon_+ + \varepsilon_-}.$$

If a slit in a screen symmetrically positioned and symmetrically excited with respect to the waveguide axis is excited with a source, only even TM waves will exist in the waveguide [10].

There is a single component of the magnetic field H_y in the TM wave propagating along the z axis. Considering that the dependence of H_y on coordinates is of the form

$$H_y = H(x)e^{-ihz}$$

(we assume that the field does not depend on the coordinate y)

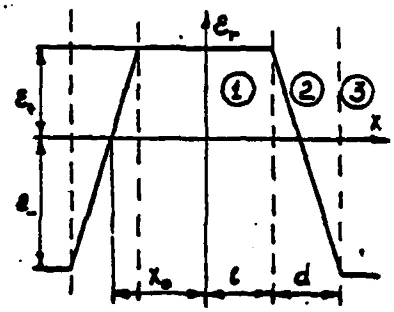

Fig. 1

$$H'' + \frac{\varepsilon_r'}{\varepsilon_r} H' + (k_0^2\varepsilon_r - h^2)H = 0, \tag{1}$$

where k_0 is the free-space wave number.

The component of the electric field E_z that is tangent to the layer boundaries can be determined in terms of H(x) with the formulas

$$E_z = E(x)e^{-ihz}, \quad E(x) = (i\omega\varepsilon_0\varepsilon_r)^{-1}H'(x).$$

where ε_0 is the absolute dielectric constant of a vacuum. Let us find the expressions for the functions H(x) and E(x) in different regions of the waveguide; in view of symmetry, we will consider the field only when x>0.

Region I. $0<x<\ell$

Eq. (1) takes on the form: $H''+q^2H=0$. Solving it, for the even wave types we get

$$H(x) = \cos qx, \quad E(x) = -q(i\omega\varepsilon_0\varepsilon_+)^{-1}\sin qx,$$
$$q^2 + h^2 = k_0^2\varepsilon_+. \tag{2}$$

The expression for H(x) is determined, strictly speaking, with an accuracy to an arbitrary constant cofactor. But since the amplitude of the waves in the waveguide is not of interest to us, we assume that in region 1 it is equal to unity, for H(x).

Region 3. $x>\ell+d$

Eq. (1) takes on the following form: $H''-p^2H=0$. With allowance for the weakening of the field as $x\to\infty$, we find

$$H(x)=H_0e^{-px},\quad E(x)=p(i\omega\varepsilon_0\varepsilon_-)^{-1}H_0e^{-px},\quad p^2-h^2=\kappa_0^2\varepsilon_-. \tag{3}$$

Region 2 [sic]. $\ell<x<\ell+d$

In region 2 we have the equation

$$H''+\frac{1}{x_0-x}H'+(\kappa_0^2a(x_0-x)-h^2)H=0 \tag{4}$$

We will solve it using series in powers of the difference x_0-x and, considering the width of region 2 to be small ($d/\ell<<1$), in the result we will limit ourselves to a finite number of terms.

It is known [11] that the general solution of Eq. (4) is of the form

$$H(x)=c_1u(x)+c_2v(x),$$

where u and v are two linearly independent solutions of Eq. (4), represented in the form of the expansions

$$u=\sum_{n=0}a_n(x_0-x)^{n\cdot 2},\quad v=su\ln\kappa_0(x_0-x)+\sum_{n=0}b_n(x_0-x)^n,$$

whose coefficients, determined from the recursion formulas, are equal to, respectively:

$$a_0=1,\quad a_1=0,\quad a_2=\frac{h^2}{8},\ \ldots,$$

$$s=\frac{h^2}{2},\quad b_0=1,\quad b_1=b_2=0,\quad b_3=-\frac{\kappa_0^2a}{3},\quad b_4=-\frac{3h^2}{64},\ \ldots .$$

Using these expressions, by limiting ourselves to terms not higher than the first order of smallness in x_0-x and d, we get

$$H(x)=A,\quad E(x)=-(i\omega\varepsilon_0 a)^{-1}(Ah^2 \ln \varkappa_0(x_0-x)+B) \tag{5}$$

By here equating the corresponding Eqs. (2), (3), and (5) at the boundaries of regions 1 through 3, we get the following system of dispersion equations:

$$\begin{gathered} q \operatorname{tg} ql=-\frac{\varepsilon_+}{\varepsilon_-}p+\frac{\varepsilon_+ d}{\varepsilon_+ +\varepsilon_-}h^2\left(\ln\frac{\varepsilon_+}{\varepsilon_-}+i\pi\right), \\ p^2+q^2=\varkappa_0^2(\varepsilon_+ +\varepsilon_-) \end{gathered} \tag{6}$$

2. Analysis of Dispersion Equations

By neglecting waves of all types except for the principal wave, we analyze system (6) for the symmetrical transition layer $\varepsilon_+=\varepsilon_-=\varepsilon$.

If we convert to the quantities $\sigma=pl$, $\tau=ql$, $\rho=hl$, $\varkappa=\varkappa_0 l$, and $\delta=\frac{\pi d}{2l}$, and if we use Eqs. (2) and (3), we can get the following system of equations:

$$\left.\begin{aligned} \sigma+\tau \operatorname{tg}\tau &= i(\sigma^2-\tau^2)\delta, \\ \sigma^2+\tau^2 &= 2\varkappa\varepsilon, \end{aligned}\right\} \tag{7}$$

or the single dispersion equation for the longitudinal wave number

$$\sqrt{\varkappa^2-\rho^2}+\sqrt{\varkappa^2-\rho^2}\operatorname{tg}\sqrt{\varkappa^2-\rho^2}=i\rho^2\delta. \tag{8}$$

To find the solutions of the system (7) or Eq. (8), we assume that they are known to use when $\delta=0$ and $\operatorname{Im}\varepsilon=0$. We denote the quantities σ, τ, and ρ corresponding to this case with σ_0, τ_0, and ρ_0, that is, under our assumption the following relationships obtain:

$$\left.\begin{aligned} \sigma_0+\tau_0\operatorname{tg}\tau_0 &= 0 \\ \sigma_0^2+\tau_0^2 &= 2\varkappa^2 \end{aligned}\right\} \tag{9}$$

$$\sqrt{\varkappa^2-\rho_0^2}+\sqrt{\varkappa^2-\rho_0^2}\operatorname{tg}\sqrt{\varkappa^2-\rho_0^2}=0 \tag{10}$$

Suppose now $\varepsilon=1-i\varepsilon_1$, $\varepsilon_1>0$, and $\delta\neq 0$. Let us represent the longitudinal wave number ρ_0 in the form $\rho=\rho_0+\rho_1$ and substitute it in Eq. (8). By expanding the left and right parts of (8) in series in terms of the small parameters δ, ε_1, and ρ_1 and referring to

Eq. (9), we get

$$\rho = \rho_0 (1 - i(\alpha\delta + \beta\varepsilon_1)),$$

with an accuracy to the infinitesimals of the second order, where

$$\alpha = \frac{(\varkappa^2-\rho_0^2)\sqrt{\varkappa^2+\rho_0^2}}{2\varkappa^2(\sqrt{\varkappa^2+\rho_0^2}-1)}, \quad \beta = \frac{\varkappa^2\sqrt{\varkappa^2+\rho_0^2}-\rho_0^2}{2\rho_0^2(\sqrt{\varkappa^2-\rho^2}-1)}. \qquad (11)$$

We see that to the first approximation of the method of perturbations, the corrections to the constant of propagation due to the transition layer and to the imaginary part of the dielectric constant are additive and therefore can be examined independently of each other. In addition, in the case of a symmetric transition layer these corrections are purely imaginary for propagating wave types, that is, their phase velocities remain unchanged.

Presented in the study [12] are the solutions of the "unperturbed" equation (10) for different $\varkappa$. When investigating the behavior of the correction coefficients α and β, it is convenient for us to use Eq. (10) as well as system (9). And as the independent variable we select not the frequency $\varkappa$, but the transverse wave number τ_0.

Let us find the critical values of $\varkappa$ determining the resonance in the cross-section of the waveguide at which $\rho_0=0$.

By substituting $\rho_0=0$ in Eq. (10), we get the equation

$$\varkappa(1+tg\,\varkappa)=0,$$

from which we find

$$\varkappa_m = \begin{cases} 0, & m=0 \\ \pi(m-\frac{1}{4}), & m>0. \end{cases}$$

By differentiating Eq. (10) at the point $\varkappa=\varkappa_1$, we can show that when $\varkappa<\varkappa_1=\frac{3\pi}{4}$ the longitudinal wave number ρ_0 is imaginary, and when $\varkappa>\varkappa_1$ it is real, that is, the critical value of for the fundamental wave is $\varkappa_1=\frac{3\pi}{4}$, and at $\varkappa_0=0$. If the frequency $\varkappa$ takes on the values within the limits $\frac{3\pi}{4}<\varkappa<\frac{7\pi}{4}$, all waves of the higher types will be attenuating.

When $\frac{3\pi}{4} < \varkappa < \frac{7\pi}{4}$, the longitudinal wave number τ_0 takes on values in the interval $1.1\,\frac{\pi}{2} \leq \tau_0 \leq \frac{3\pi}{4}$.

The solutions of Eqs. (9) and (10) in the interval $\frac{\pi}{2} < \tau_0 < \frac{3\pi}{4}$ (for the fundamental wave) are shown in Fig. 2 in the form of the functions $\sigma_0(\tau_0)$, $\varkappa_0(\tau_0)$ and $\rho_0(\tau_0)$. Also presented there are the plots for the coefficients $\alpha(\tau_0)$ and $\beta(\tau_0)$ determining the behavior of the imaginary part of the constant of propagation ρ, that is, the decrement of attenuation. From Fig. 2 we see that for the fundamental wave the curve $\beta(\tau_0)$ trends everywhere higher than the curve $\alpha(\tau_0)$, such that when there are identical values of δ and ε_1, the resonance absorption will always be less than the heat losses. In addition, when $\tau_0 \to \pi/2$, $\varkappa \to \infty$ (at higher frequencies) the function $\beta(\tau_0)$ tends to a finite value, and $\alpha(\tau_0)$, to zero. So by increasing the frequency (or, which amounts to the same thing, the electrical dimension of the waveguide), the resonance absorption can be made small enough.

In the other limiting case, when the frequency is near-critical in value, we can find

$$\alpha = \frac{3\pi}{2(3\pi-4)}, \quad \beta = \frac{12\pi}{(3\pi-4)(3\pi-4\tau_0)} \quad \left(\tau_0 \to \frac{3\pi}{4}\right).$$

In this case we observe the strong dependence of β on frequency and, in addition, $\beta \to \infty$ $(\tau \to \tau_{cr})$. So at near-critical frequencies, Eq. (11) may prove to be invalid for β obtained by the method of perturbations.

Calculations show that in estimational calculations of the attenuation of radio waves in an inhomogeneous waveguide the losses due to the transition region can be neglected.

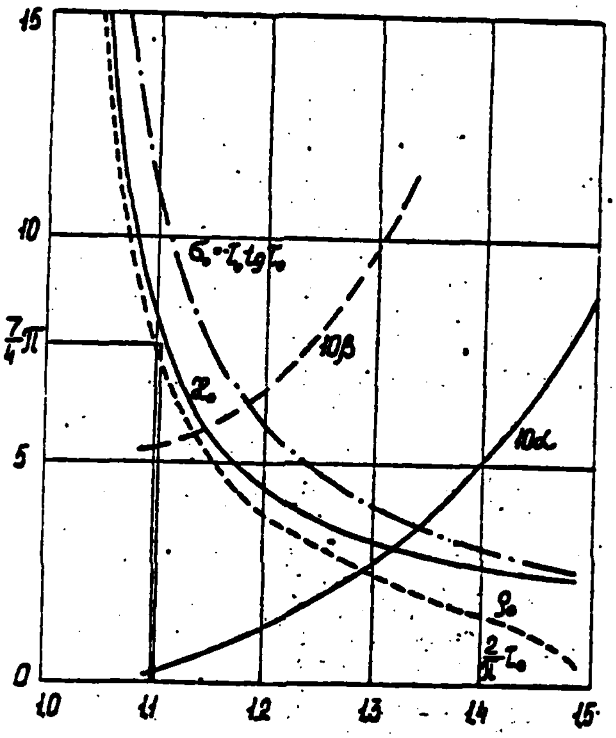

15
10
$\frac{7}{4}\pi$
5
0
1.0
1.1
1.2
1.3
1.4
1.5
$\sigma_0 = \tau_0 \, tg \, \tau_0$
10β
τ_0
10α
ρ_0
$\frac{2}{\pi}\tau_0$

Fig. 2

CHARACTERISTICS OF RADIATION OF APERTURE ANTENNAS IN A PLANE-STRATIFIED MEDIUM

A. P. Anyutin, V. A. Permyakov, and V. K. Polishchuk

Presented in this study are working formulas and the results of calculation of radiation patterns of a (circular) waveguide located in an infinite metal plane under a dielectric layer and a plasma layer. In deriving the formulas for the radiation patterns it is assumed that: 1) the field distribution in the open end of the rectangular (circular) waveguide coincides with the field distribution of the wave H_{01} (H_{11}) propagating in the waveguide; 2) the reflection coefficient p of the wave H_{01} (H_{11}) from the open end of the waveguide is given; and 3) the complex dielectric constant of the plasma varies only along the normal to the surface and is defined by the formula [3]:

$$\varepsilon(z) = 1 - \frac{3.18 \cdot 10^9 N_e(z)}{\omega^2 + \nu_e^2} - i \frac{\nu_e}{\omega} \frac{3.18 \cdot 10^9 N_e(z)}{\omega^2 + \nu_e^2},$$

where ω is the working frequency, ν_e is the effective number of electron collisions in the plasma, and $N_e(z)$ is the electron concentration in the plasma. These assumptions allow us to reduce the initial problem to a problem of the radiation of a current sheet in a two-sheet medium (Fig. 1). A method of solving this problem consists in the following [13]: by applying the Fourier transform to the wave equation with respect to the coordinates x, y, and by satisfying the boundary conditions, a system of

linear algebraic equations results for the spectral representations of the fields. The dependence of all spectral representations on the coordinate z is determined with ordinary differential equations with variable coordinates (in the case of an inhomogeneous plasma).

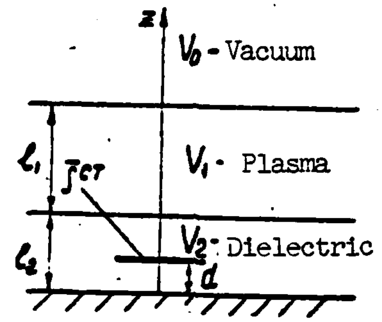

Fig. 1

By applying the inverse Fourier transform to the solution of the system of linear algebraic equations, we get the integral representation of the fields. To define the fields in the far zone, the double integrals representing them are calculated with the method of the integral [14]. The final expressions for the components of the electric field in the far zone are as follows:

a) rectangular waveguide

$$E_\varphi = A\,\frac{\left[(1+p)\gamma_2\cos\Delta + i(1-p)\frac{\alpha}{K_0}\sin\Delta\right]}{\gamma_2\cos\Delta_2\,U(\zeta_2) - \frac{\sin\Delta_2}{K_0}U'(\zeta_2)} \times \frac{\sin(K_0 a\sin\theta\cos\varphi)}{K_0 a\sin\theta\cos\varphi} \times \frac{\cos(K_0 b\sin\theta\sin\varphi)}{1-\left(\frac{2K_0 b\sin\theta\sin\varphi}{\pi}\right)^2} \times \cos\theta \cdot \sin\varphi,$$

$$E_\theta = A\,\frac{\left[(1+p)(\varepsilon_2/\gamma_2)\cos\Delta + i(1-p)(\alpha/K_0)\sin\Delta\right]}{\cos\Delta_2\,V(\zeta_2) + \frac{\varepsilon_2\sin\Delta_2}{K_0\gamma_2\varepsilon_1(\zeta_2)}V'(\zeta_2)} \times \frac{\sin(K_0 a\sin\theta\cos\varphi)}{K_0 a\sin\theta\cos\varphi} \times \frac{\cos(K_0 b\sin\theta\sin\varphi)}{1-\left(\frac{2K_0 b\sin\theta\sin\varphi}{\pi}\right)^2} \times \cos\theta \cdot \cos\varphi, \quad (2)$$

$$A = (e^{-ik_0R} 4ab\kappa_0 l) \cdot (R\pi^2)^{-1}$$

b) circular waveguide

$$E_\varphi = B\,\frac{\left[(1+p)\gamma_2\cos\Delta + i(1-p)\frac{\alpha}{\kappa_0}\sin\Delta\right]}{\gamma_2\cos\Delta_2\,U(\ell_2) - (\sin\Delta_2/\kappa_0)\,U'(\ell_2)} \cdot \frac{J_1'(\kappa_0 a\sin\theta)\cos\theta\sin\varphi}{1-\left(\frac{\kappa_0 a\sin\theta}{\varkappa_a}\right)^2},$$

$$E_\theta = B\,\frac{\left[(1+p)\frac{\varepsilon_2}{\gamma_2}\cos\Delta + i(1-p)\frac{\alpha}{\kappa_0}\sin\Delta\right]}{\cos\Delta_2\,V(\ell_2) + \frac{\varepsilon_2\sin\Delta_2}{\kappa_0\gamma_2\varepsilon_1(\ell_2)}\,V'(\ell_2)} \cdot \frac{2J_1(\kappa_0 a\sin\theta)}{\kappa_0 a\sin\theta}\cos\theta\cos\varphi$$

$$B = i\kappa_0 a^2 E_0 J_0(\varkappa a)\, e^{-i\kappa_0 R} \cdot (2R)^{-1}.$$

In Eqs. (1)-(4), U(z) is the solution of the equation

$$\frac{d^2U}{dz^2} + \kappa_0^2[\varepsilon_1(z) - \sin^2(\theta)]\,U = 0 \qquad (5)$$

with the initial conditions $U(\ell_1) = 1$, $U'(\ell_1) = -i\kappa_0\cos\theta$ at the point $z=\ell_2$; V(z) is the solution of the equation

$$\frac{d^2V}{dz^2} - \frac{1}{\varepsilon_1(z)}\frac{d\varepsilon_1}{dz}\frac{dV}{dz} + \kappa_0^2[\varepsilon_1(z) - \sin^2\theta]\,V = 0 \qquad (6)$$

with the initial conditions $V(\ell_1) = 1$, $V'(\ell_1) = -i\kappa_0\varepsilon_1(\ell_1)\cos\theta$ at the point $z=\ell_2$;

a is the dimension of the narrow wall of the waveguide (waveguide radius)

b is the dimension of the wide wall of the waveguide

$\varepsilon_1(z)$ is the relative dielectric constant of the plasma

ε_1 is the relative dielectric constant of the dielectric;

$$\gamma_2 = \sqrt{\varepsilon_2 - \sin^2\theta};\ \Delta = \kappa_0\gamma_2 d;\ \Delta_1 = \kappa_0\gamma_2\ell_1;$$
$$\varkappa a = 1{,}84;\ W_0 = \sqrt{\frac{\mu_0}{\varepsilon_0}};$$

k_0 is the wave number of free space;

$$\alpha = \sqrt{1-\left(\frac{\lambda}{2b}\right)^2} \quad \left(\alpha = \sqrt{\varepsilon_2\kappa_0^2 - \varkappa^2}\right)$$

J, J_1 are Bessel functions

ℓ_1, ℓ_2, d are as shown in Fig. 1.

The solutions of Eqs. (5) and (6) are sought for numerically by the Runge-Kutta method [15]; where $\varepsilon_1(z)$ is approximated with the function $\varepsilon_1(z) = A_1 z^{r_1} + B_1$. Specifying $\varepsilon_1(z)$ in another analytic form poses no fundamental difficulties in calculations.

The expressions found for the fields in the far zone can be used in calculating the antenna efficiency η:

$$\eta = P_\Sigma / P_0 ,$$

where P_Σ is the antenna power,

$$P_\Sigma = R_2 \int_0^{2\pi} d\varphi \int_0^{\pi/2} \frac{1}{W_0} \left(|E_\theta|^2 + |E_\varphi|^2 \right) \sin\theta \, d\theta ,$$

P_0 is the power fed to the waveguide;

a) a rectangular waveguide

$$P_0 = \frac{2ab E_0^2 \sqrt{\varepsilon_1 K_0^2 - \left(\frac{\pi}{a}\right)^2} \left(1 - |\rho|^2\right)}{W_0 K_0} ,$$

b) a circular waveguide

$$P_0 = \left(1 - |\rho|^2\right) \frac{\pi \alpha a^2}{2 K_0 W_0} |E_0|^2 \left[(\varkappa a)^2 - 1 \right] J_1^2(\varkappa a).$$

These formulas for calculating the characteristics of antenna radiation and antenna efficiency in the plane-stratified medium were programmed for computations on a computer.

For $\lambda_0=6.28$; $\ell_2=0$; $\ell_1=1$; $\Delta\theta=4°$; $a=0.03\lambda_0$; $b=0.5\lambda_0$; $d=0$; shown in Fig. 2 are the radiation patterns of an antenna in the plane of an electric vector without allowing for plasma (dot-dashed line) and for two laws of variation in the dielectric constant of the plasma, the linear (solid line) and the quadratic (dashed line). The calculated distributions $\varepsilon(z)$ are also presented in Fig. 2. From the figure it follows that the plasma layer leads to an abrupt drop in the relative radiation level in the region of grazing angles of observation. We can also note the weak dependence of the radiation pattern on the law $\varepsilon(z)$ of the plasma, characteristic of thin, compared with

the wavelength, inhomogeneous plasma layers with approximately equal cumulative values of the electron concentration.

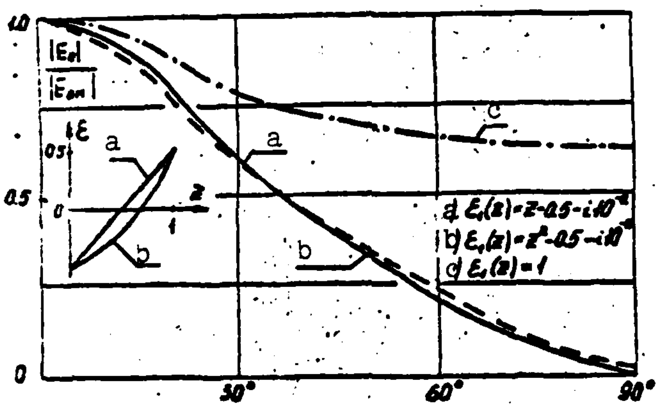

Fig. 2

APPROXIMATE METHOD OF DIAGNOSTICS OF INHOMOGENEOUS PLASMA

M. B. Aksenov, V. G. Kartashev, A. P. Mayorov, and V. L. Skachkov

Theoretical Analysis of Problem

In investigating plasma parameters there often appears the necessity of determining the law of spatial distribution of the main plasma parameters: concentration N_e and collision rate ν_{ef}. Known methods of microwave diagnostics of inhomogeneous plasma (for example, [16]), permitting the determination of the spatial distribution of concentration, are based on the geometric optical approximation and therefore are not always applicable. Rigorous methods of diagnostics (for example, [17]) are very complex and have not yet been fully worked out. But in some cases, when there is apriori information on the kind of distribution of plasma concentration, the problem of diagnostics can be considerably simplified. Examined in this study is a method of diagnostics of a plane-stratified plasma based on the assumption that the plasma concentration varies in space according to an exponential law, but the collision frequency is constant. The method is based on measuring the coefficient of reflection from the plasma when it is irradiated with a plane electromagnetic wave.

Let us examine the normal incidence of a plane electromagnetic wave from a homogeneous dielectric with dielectric constant

ε_1 on a plane-stratified plasma with a concentration that varies in the direction of the z-axis according to an exponential law

$$N_e(z) = N_0 e^{-\alpha z} \quad (z > 0). \tag{1}$$

The plane z=0 is the interface of plasma and the dielectric. Without constraints on generality, we will assume that the irradiating field has the components E_x and H_y.

As shown in [3], the equation for the electric field intensity in this case can be represented in the following form

$$\frac{d^2E}{dz^2} + \frac{\omega^2}{c^2}\varepsilon_z'(\omega, z)E = 0, \tag{2}$$

where

$$\varepsilon_z'(\omega, z) = 1 - \frac{4\pi e^2 N_e(z)(\omega + i\nu_{\text{эф}})}{m\omega(\omega^2 + \nu^2_{\text{эф}})} \tag{3}$$

The general solution of Eq. (2) with reference to (1) and (3) can be written in the form

$$E = C_1 J_{i\mu}(u) + C_2 J_{-i\mu}(u), \tag{4}$$

where

$$u = b e^{-\frac{1}{2}\gamma\zeta}; \quad b = i\frac{2}{\gamma}\kappa^{1/2};$$
$$\kappa = \frac{\omega_{p0}^2(\omega + i\nu_{\text{эф}})}{\omega(\omega^2 + \nu^2_{\text{эф}})}; \quad \mu = \frac{2}{\gamma};$$

$\zeta = \frac{\omega}{c}z$ is the dimensionless coordinate

$\gamma = \frac{\alpha c}{\omega}$ is the dimensionless constant of attenuation

ω_{p0} is the plasma frequency when z=0.

From inspection of the solution (4) for small values of the arguments u ($\zeta \to -\infty$) it follows that $J_{-i\mu}(u) \sim e^{i\zeta}$ and therefore, $c_2=0$. Finally, solution (4) can be written in the form

$$E = C_1 J_{i\mu}\left(i \frac{2\kappa^{1/2}}{\gamma} e^{-\frac{1}{2}\gamma\zeta}\right)$$

From the boundary conditions when z=0 let us find an expression for the complex reflection coefficient Γ

$$\dot{\Gamma} = \frac{\sqrt{\varepsilon_1} - \kappa^{1/2} J'_{i\mu}(u)/J_{i\mu}(u)}{\sqrt{\varepsilon_1} + \kappa^{1/2} J'_{i\mu}(u)/J_{i\mu}(u)}$$

Using the recurrence relationship for the Bessel functions, we get a final expression for the reflection coefficient

$$\dot{\Gamma} = \frac{\sqrt{\varepsilon_1} - 1 + \kappa^{1/2} J_{1+i\mu}(u)/J_{i\mu}(u)}{\sqrt{\varepsilon_1} + 1 - \kappa^{1/2} J_{1+i\mu}(u)/J_{i\mu}(u)} \qquad (5)$$

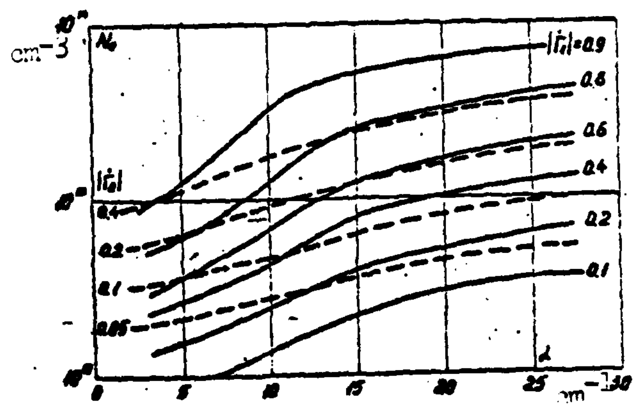

Fig. 1

By representing the Bessel functions in the form of series, after some transformations we get

$$\frac{J_{1+i\mu}(u)}{J_{i\mu}(u)} = \frac{u/2}{1+i\mu}\left[\frac{1 - \frac{u/2}{2+i\mu} + \frac{(u/2)^2}{(2+i\mu)(3+i\mu)2!} - \cdots}{1 - \frac{u/2}{1+i\mu} + \frac{(u/2)^2}{(1+i\mu)(2+i\mu)2!} \cdots}\right] \qquad (6)$$

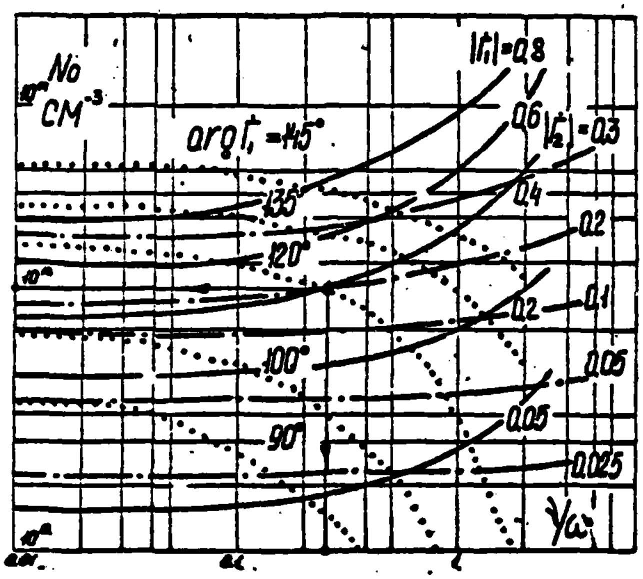

Fig. 2

By applying Eqs. (5) and (6), we can calculate the values of the modulus and the phase of the coefficient of reflection by the plasma for any value of the coefficient N_0 and any value of the parameter α. Some results of the calculations for $\varepsilon=1$ are presented in Figs. 1 and 2, where for convenience in further application, the lines of the modulus level and the phase of the reflection coefficient are presented for the frequencies of the probe field f_1=10 GHz and f_2=30 GHz.

Method of Determining the Plasma Parameters Based on Experimental Data

Let us examine the problem of the practical determination of the plasma parameters N_0, α, and ν_{eff} from measurements of the reflection coefficient.

If the collision rate is small, so that the effect of collisions on the reflection coefficient can be neglected, to determine the plasma parameters N_0 and α, it is sufficient to measure the modulus of the reflection coefficient $|\dot{\Gamma}_1|$ and $|\dot{\Gamma}_2|$ at two rates f_1 and f_2. Then from the plot shown in Fig. 1, we can find the points of intersection of the corresponding curves $|\dot{\Gamma}_1|$ and $|\dot{\Gamma}_2|$ and determine the values of N_0 and α.

When there are collisions in the plasma, the procedure of interpreting the experimental data is considerably more involved. In this case, to determine the three plasma parameters N_0, α, and $\nu_{эф}$, we must measure three parameters of the reflected waves. This can be either the modulus of the reflection coefficient at three rates $|\dot{\Gamma}_1|$, $|\dot{\Gamma}_2|$, and $|\dot{\Gamma}_3|$, or the modulus $|\dot{\Gamma}_1|$ and the phase θ_1 of the reflection coefficient at the same rate and the modulus of the reflection coefficient $|\dot{\Gamma}_2|$ at the second rate. Analysis shows that preference must be given to the second method, since the task of measuring the coefficient of reflection from one part of the plasma at three rates proves to be complex.

For the practical determination of the plasma parameters in this case, we must calculate and plot the graphs of the lines of the level $|\dot{\Gamma}_1|$, θ_1, $|\dot{\Gamma}_2|$ (Fig. 2) for different values of α, thus constructing an album of curves, each page of which corresponds to a certain α. Further, from the measured values of $|\dot{\Gamma}_1|$, θ_1, and $|\dot{\Gamma}_2|$ we seek the page in the album where all three curves of the levels $|\dot{\Gamma}_1|$, θ_1, $|\dot{\Gamma}_2|$ intersect at the same point. The coordinates of this point define the values of N_0 and $\nu_{эф}$, and the page number, the value of α.

This method of diagnostics of an inhomogeneous plasma proves to be quite simple, but it is suitable only when the plasma concentration exhibits an exponential distribution. If the distribution of the concentration differs from the exponential, rigorous methods of plasma diagnostics must be employed.

PROBLEM OF MEASURING THE PARAMETERS OF LOSSY INHOMOGENEOUS DIELECTRICS

V. G. Kartashev and A. P. Mayorov

Measurement of Parameters of Dielectrics in Normal Probing

Let us examine the normal incidence of a plane electromagnetic wave on the surface of an inhomogeneous plane-stratified dielectric with relative dielectric constant $\tilde{\varepsilon}(z)$. We assume the relative permeability of the dielectric μ to be constant. We take the direction of the coordinate axes and the polarization of the irradiating wave such that the boundary of the dielectric coincides with the z=0 plane, and the field has only the components E_x and H_y.

From Maxwell's equations, for the complex amplitudes of the field it is easy to derive the expressions

$$\left.\begin{aligned} \frac{\partial H_y}{\partial z} &= -i\omega\varepsilon_a' E_x \\ \frac{\partial E_x}{\partial z} &= -i\omega\mu_a H_y \end{aligned}\right\} \qquad (1)$$

where

$$\varepsilon_a' = \varepsilon_0\varepsilon - i\frac{\sigma}{\omega}; \quad \mu_a = \mu_0\mu$$

By performing the substitution of variables

$$\tau = \int_0^z \sqrt{\mu_a(\xi)}\, \mathrm{Re}\sqrt{\varepsilon_a'(\xi)}\, d\xi, \qquad (2)$$

we derive an equation for the component E_x

$$\frac{d^2E_x}{d\tau^2} = \frac{Z'}{Z}\frac{dE_x}{d\tau} - \omega^2 p(\tau)E_x, \tag{3}$$

where

$$Z = \frac{\sqrt{\mu_0}}{Re\sqrt{\varepsilon_a}}; \qquad p(\tau) = \frac{\varepsilon'}{(Re\sqrt{\varepsilon'})^2} \tag{4}$$

Employing the substitution $U = \sqrt{\frac{Z(0)}{Z(\tau)}}E_x$, we get the final equation

$$U'' + [\omega^2 p(\tau) - q(\tau)]U = 0, \tag{5}$$

where

$$q(\tau) = \left(\frac{Z'}{2Z}\right)^2 - \left(\frac{Z'}{2Z}\right)'. \tag{6}$$

If the dielectric under study is not lossy (σ=0), then $\rho(\tau)$=1, and Eq. (5) takes on the form for which the inverse Sturm-Liouville problem was solved in [18]. In this case, the problem of measuring the dielectric constant $\varepsilon(z)$ of a nonlossy dielectric can be reduced to the following:

The complex reflection coefficient $\dot{\Gamma}(\omega)$ is measured as a function of the field frequency; then the characteristic function of Eq. (5) is determined:

$$M(\omega) = \frac{\sqrt{\mu(0)\varepsilon(0)}}{i\omega}\,\frac{1+\dot{\Gamma}(\omega)}{1-\dot{\Gamma}(\omega)}$$

Then, according to [19], the spectral function $\rho(\lambda)$ is found:

$$\rho(\lambda) = \lim_{\delta\to 0}\lim_{\varkappa\to 0}\frac{1}{\pi}\int_{\delta}^{\lambda+\delta} \operatorname{Im} M(\omega+i\varkappa)\,d\omega$$

and using the method given in [18] the unknown coefficient $\phi(\tau)$ of Eq. (5) is determined. Then, by solving Eq. (6), using Eqs. (4) and (2) we can find the desired function $\varepsilon(z)$. Specific procedures for solving this problem as applied to inhomogeneous transmission lines are considered in detail in [20].

If the conductivity of the dielectric cannot be neglected, this method of solving the inverse problem is not applicable. In Eq. (5) the spectral parameter ω^2 is not separated from the

function of τ; the solution of the inverse problem for equations of this kind is not yet known.

Thus normal probing of an inhomogeneous dielectric with a plane electromagnetic wave, using now available mathematical methods, makes it possible to determine the dielectric parameters only when the dielectric is nonlossy.

Measuring the Parameters of Dielectrics in Slant Probing

The slant incidence of a plane electromagnetic wave on a plane-stratified medium is described with the equation [21]

$$F'' + \kappa_0^2[\varepsilon'(z) - \varepsilon_1 \sin^2\theta_1]F = 0 \tag{7}$$

where $\varepsilon'(z)$ is the complex dielectric constant of the test medium ($z>0$)

ε_1 is the dielectric constant of the medium for [text is missing]

θ_1 is the angle of incidence of the wave

Eq. (7) can be converted to the form

$$F'' + [\lambda - q(z)]F = 0, \tag{8}$$

where

$$\lambda = \frac{\omega^2}{c^2}(1 - \varepsilon_1 \sin^2\theta_1); \tag{9}$$

$$q(z) = \frac{\omega^2}{c^2}[\varepsilon'(z) - 1] \tag{10}$$

If the frequency ω is fixed, the spectral parameter λ and the function of the coordinate $q(z)$ are not related in Eq. (8) as with the real and the complex function $q(z)$. The method of solving the inverse problem for Eq. (8) with the complex-valued coefficient $q(z)$ was worked out in [22]. To carry out this method we must determine the complex reflection coefficient $\dot{\Gamma}$ as a function of the angle of incidence θ_1 and find the function $m(\lambda)$

$$m(\lambda) = \frac{1}{i\kappa_0\sqrt{\varepsilon_1}\cos\theta_1} \cdot \frac{1+\Gamma}{1-\Gamma},$$

which acts as the characteristic function of Eq. (8).

One feature of this method is the fact that when the angle of incidence θ_1 varies, the spectral parameter λ in accordance with Eq. (9) can vary over the limits from 0 to ω^2/c^2. Thus, the function $m(\lambda)$ proves to be specified not for the entire semiaxis $0<\lambda<\infty$, but only for the interval $(0,\omega^2/c^2)$. But by suitably selecting the field frequency ω and using the asymptotic relationships for $m(\lambda)$, the error caused by the incomplete specification of the function $m(\lambda)$ can be reduced to zero.

A second feature of the slant probing method is caused by the displacement of the beam of electromagnetic waves during reflection, leading to a reduction in the measured reflection coefficient and to loss of information about the deep-lying layers of the dielectric. To reduce the influence of this effect, it is best to irradiate the test object with a broad beam whose transverse dimensions are much larger than the assumed beam displacement.

PART TWO

EXCITATION AND DIFFRACTION OF ELECTROMAGNETIC WAVES

SOME SOLUTIONS OF MAXWELL'S EQUATIONS

G. T. Markov

Presented at the radio engineering section of the scientific-engineering conference of the Moscow Power Institute in April 1970

1. Suppose that in a spherical region with radius a, with parameters of the medium $\sigma=0$, ε_0, μ_0 (vacuum), there is given the distribution of the volume density of electric currents $\bar{j}^{e}$ varying with time according to the law $e^{i\omega_0 t}$. Imagine an electromagnetic field in the form of the superpositioning of oscillations of electrical and magnetic types: $E = E^e + E^m$, $\bar{H} = \bar{H}^e + \bar{H}^m$. The oscillations of the electrical type are excited with the currents $\bar{j}^{ee}$, and the oscillations of the magnetic type, with the currents $\bar{j}^{em}$, where $\bar{j}^e = \bar{j}^{ee} + \bar{j}^{em}$.

Let us write out the expressions for the complex amplitudes of the component vectors of current and field satisfying the inhomogeneous Maxwell's equations:

$$\begin{aligned} \operatorname{rot} \bar{H} &= i\omega_0 \varepsilon_0 \bar{E} + \bar{j}^{e}, & \operatorname{rot} \bar{E} &= -i\omega_0 \mu_0 \bar{H}, \\ \operatorname{div} \bar{E} &= \frac{\rho}{\varepsilon_0}, & \operatorname{div} \bar{H} &= 0. \end{aligned} \tag{1}$$

Using the general expressions given in [13, 23], we get the following relationships for one of the spatial harmonics.

Oscillations of the Electrical Type (H_r=0)

$$
\begin{aligned}
j_r^{ст} &= \frac{a_{nm}}{2}\frac{\partial^2 f^0(r)}{\partial r^2}\, r\,\psi_n(\kappa_n r)P_n^m(\cos\theta)\,e^{-im\varphi},\\
j_\theta^{ст} &= a_{nm}\frac{\partial f^0(r)}{\partial r}\,\psi_n(\kappa_n r)\frac{\partial P_n^m(\cos\theta)}{\partial\theta}\,e^{-im\varphi},\\
j_\varphi^{ст} &= a_{nm}\frac{\partial f^0(r)}{\partial r}\,\psi_n(\kappa_n r)\frac{(-im)}{\sin\theta}P_n^m(\cos\theta)\,e^{-im\varphi}.
\end{aligned}
\tag{2}
$$

$$
\begin{aligned}
&E_r+\frac{1}{i\omega_n\varepsilon_0}j_r^{ст}=\frac{n(n+1)}{r}U_{nm}^0,\\
&E_\theta^0+\frac{1}{i\omega_n\varepsilon_0}j_\theta^{ст}=\frac{1}{r}\frac{\partial^2(rU_{nm}^0)}{\partial\theta\,\partial r},\\
&E_\varphi^0+\frac{1}{i\omega_n\varepsilon_0}j_\varphi^{ст}=\frac{1}{r\sin\theta}\frac{\partial^2(rU_{nm}^0)}{\partial\varphi\,\partial r},\\
&H_\theta^0=\frac{i\omega_n\varepsilon_0}{\sin\theta}\frac{\partial U_{nm}^0}{\partial\varphi},\quad H_\varphi^0=-i\omega_n\varepsilon_0\frac{\partial U_{nm}^0}{\partial\theta},
\end{aligned}
\tag{3}
$$

where

$$
U_{nm}^0=-\frac{1}{i\omega_n\varepsilon_0}\frac{a_{nm}}{2}\left[f^0(a)-f^0(r)\right]\psi_n(\kappa_n r)P_n^m(\cos\theta)\,e^{-im\varphi}.
\tag{4}
$$

The frequency of the oscillations is determined from the condition

$$
\psi_n(\kappa_n a)=0,
\tag{5}
$$

where $\kappa_n=\omega_n\sqrt{\varepsilon_0\mu_0}$, n=1,2,3,....

In Eqs. (2) and (4), $f^0(r)$ is a real function, finite, and with its first and second derivatives on the interval from r=0 to r=a; outside this interval it is assumed equal to zero;

$P_n^m(\cos\theta)$ are adjoint Legendre functions,

$\psi_n(\kappa_n r)=\sqrt{\frac{\pi}{2\kappa_n r}}\,J_{n+\frac{1}{2}}(\kappa_n r)$ are radial spherical functions

r, e, ϕ are spherical coordinates

The coefficients a_{nm} in Eqs. (2) and (4) are not defined here.

The validity of the solutions presented is verified by the direct substitution of Eqs. (2), (3), and (4) in the Maxwell's equation (1). The vectors of the fields $\bar{E}^{э}$ and $\bar{H}^{э}$ on the surface of the sphere r=a are equal to zero and according to the theorem of equivalency [13] the electromagnetic field of currents (2) in the external region of the system (r>a) is identically equal to zero.

Thus, the system of currents (2) is nonradiating. The power of the electromagnetic oscillation generators is reactive and can be determined by the method of induced electromotive forces with the following formula [13]:

$$P^{э} = -\frac{1}{2}\int \bar{j}^{\,эм}\bar{E}\,dv \qquad (6)$$

By substituting Eqs. (2) and (3) in Eq. (6) and bearing in mind that

$$\int_{\varphi=0}^{2\pi} e^{-i(m-m')\varphi}\,d\varphi = \begin{cases} 0 & \text{when } m' \pm m \\ 2\pi & \text{when } m'=m \end{cases}$$

$$\int_{\theta=0}^{\pi} n(n+1)\,P_n^m(\cos\theta)\,P_{n'}^m(\cos\theta)\sin\theta\,d\theta =$$

$$\int_{\theta=0}^{\pi}\left[\frac{\partial P_n^m(\cos\theta)}{\partial\theta}\frac{\partial P_{n'}^m(\cos\theta)}{\partial\theta} + \frac{m^2}{\sin^2\theta}P_n^m(\cos\theta)P_{n'}^m(\cos\theta)\right]\sin\theta\,d\theta =$$

$$= \begin{cases} 0 & \text{при } n' \neq n \\ \frac{2n(n+1)}{2n+1}\frac{(n+m)!}{(n-m)!} & \text{when } n'=n, \end{cases}$$

we get the following expression for the generator power:

$$P^{э} = \frac{a_{nm}^2}{4}\frac{\pi}{i\omega_n\varepsilon_0}\frac{2n(n+1)(n+m)!}{(2n+1)(n-m)!}\int_{z=0}^{a}\left[\left(\frac{\partial^2 f^{э}(z)}{\partial z^2}\right)^2\frac{z^2}{n(n+1)} + 3\left(\frac{\partial f^{э}(z)}{\partial z}\right)^2\right]z^2\psi_n^2(\kappa_n z)\,dz, \qquad (7)$$

We note that the distribution of the volume density of electrical charges derived from the continuity equation $\operatorname{div}\bar{j}^{\,эм} + i\omega_n\rho = 0$ corresponds to the distribution of the volume density of electric currents (2):

$$\rho = \frac{1}{i\omega_n}\frac{a_{nm}}{2}\Big[2n(n+1)\frac{1}{z}\frac{\partial f^{э}(z)}{\partial z}\psi_n(\kappa_n z) - \qquad (8)$$

$$-\frac{1}{z^2}\frac{\partial}{\partial z}\left(\frac{\partial^2 f^{э}(z)}{\partial z^2}z^2\psi_n(\kappa_n z)\right)\Big]P_n^m(\cos\theta)\,e^{-im\varphi}$$

Oscillations of the Magnetic Type ($E_r=0$)

$$
\begin{aligned}
&j_r^{m}=0,\\
&j_\theta^{m}=-b_{nm}\left[\frac{\partial^2 f^m(r)}{\partial r^2}\psi_n(\kappa_n r)+2\frac{\partial f^m(r)}{\partial r}\frac{1}{r}\frac{\partial}{\partial r}(r\psi_n(\kappa_n r))\right]\frac{(-im)}{\sin\theta}P_n^m(\cos\theta)\,e^{-im\varphi},\\
&j_\varphi^{m}=b_{nm}\left[\frac{\partial^2 f^m(r)}{\partial r^2}\psi_n(\kappa_n r)+2\frac{\partial f^m(r)}{\partial r}\frac{1}{r}\frac{\partial}{\partial r}(r\psi_n(\kappa_n r))\right]\frac{\partial P_n(\cos\theta)}{\partial\theta}\,e^{-im\varphi}
\end{aligned}
\tag{9}
$$

$$
\begin{aligned}
&H_r=\frac{n(n+1)}{r}U_{nm}^{m},\quad H_\theta^{m}=\frac{1}{r}\frac{\partial^2(rU_{nm}^{m})}{\partial\theta\,\partial r},\quad H_\varphi^{m}=\frac{1}{r\sin\theta}\frac{\partial^2(rU_{nm}^{m})}{\partial\varphi\,\partial r},\\
&E_\theta^{m}=-\frac{i\omega_n\mu_0}{\sin\theta}\frac{\partial U_{nm}^{m}}{\partial\varphi},\quad E_\varphi^{m}=i\omega_n\mu_0\frac{\partial U_{nm}^{m}}{\partial\theta},
\end{aligned}
\tag{10}
$$

where

$$U_{nm}^{m}=-b_{nm}\left[f^m(a)-f^m(r)\right]\psi_n(\kappa_n r)P_n^m(\cos\theta)\,e^{-im\varphi} \tag{11}$$

The frequency of oscillations of the magnetic type is determined from the same condition (5). The function $f^m(r)$ is finite and continuous together with its derivatives on the interval from r=0 to r=a and is equal to zero outside this interval.

The validity of solutions (9), (10), and (11) is verified by their direct substitution in Maxwell's equation (1). The electromagnetic field of oscillations of the magnetic type on the surface of a sphere r=a and outside this sphere is equal to zero, that is, the system of currents (9) is also nonradiating.

Substitution of (9) and (10) in (6) leads to the following expression for the power of generators of oscillations of the magnetic type

$$P^m=b_{nm}^2\pi i\omega_n\mu_0\frac{2n(n+1)}{2n+1}\frac{(n+m)!}{(n-m)!}\int_{r=0}^{a}\left(\frac{\partial f^m(r)}{\partial r}\right)^2 r^2\psi_n^2(\kappa_n r)\,dr \tag{12}$$

We note that $\operatorname{div}\bar{j}^m=0$, and therefore the volume density of electric charges for oscillations of the magnetic type is always equal to zero.

2. Superimposing the electric and magnetic oscillations makes it possible to reduce the system to the resonance state, that is, a state in which the total energy of the electromagnetic field of the system with time remains constant and changes from electrical to magnetic energy, and vice versa. This will occur under the condition that the total reactive power of the generators of electromagnetic oscillations is equal to zero:

$$P = P' + P'' = 0 \tag{13}$$

From substituting (7) and (12) in (13), we get the expression

$$a_{mn}^2 \int_{r=0}^{a} \left[\left(\frac{\partial^2 f'(r)}{\partial r^2} \right)^2 \frac{r^2}{n(n+1)} + 3 \left(\frac{\partial f'(r)}{\partial r} \right)^2 \right] r^2 \psi_n^2(k_n r)\, dr = 4 b_{mn}^2 k_n^2 \int_{r=0}^{a} \left(\frac{\partial f''(r)}{\partial r} \right)^2 r^2 \psi_n^2(k_n r)\, dr \tag{14}$$

If we turn to Poynting's theorem for this system (as applied to instantaneous values)

$$-\int_v \bar{j}\,' \bar{E}\, dv = \frac{\partial}{\partial t} \int_v \left(\frac{\varepsilon_0 E^2}{2} + \frac{\mu_0 H^2}{2} \right) dv, \tag{15}$$

then we see that the left-hand side of (15), under condition (14), proves to be equal to zero. Thus, the total instantaneous power of generators of electromagnetic oscillations of the system is also equal to zero and the total energy of the electromagnetic field of the system remains constant with time.

3. The functions $f'(r)$ and $f''(r)$ are arbitrary in the sense indicated above. We can, in particular, assume $f'(r) = f''(r) = r$. Then condition (14) can be reduced to the following:

$b_{mn} = \frac{\sqrt{3}}{2} \frac{a_{mn}}{k_n}$.

If the following boundary conditions are imposed on these functions:

$$\left. \frac{\partial^2 f'(r)}{\partial r^2} \right|_{r=a} = 0, \quad \left. \frac{\partial f''(r)}{\partial r} \right|_{r=a} = 0, \tag{16}$$

the electrical charges and currents at the boundary of the system (r=a) prove to be equal to zero. So they will be continuous everywhere, including the boundary of the system.

ITERATIVE METHODS OF SYNTHESIZING REFLECTION ARRAYS

A. F. Chaplin, V. A. Mashkov, and V. F. Makkaveyeva

This paper examines certain iterative methods of synthesizing methods of synthesizing arrays of radiators loaded with reactances. Because there is no widely accepted name for this class of arrays, we will call them "reflection" arrays, as is done in a number of publications . The formulation of the problem of synthesizing these arrays was given in the study [25]. In examining reflection arrays, the system of Kirchhoff equations is conveniently written out in the form

$$\{[Z] + [E]\langle X\rangle\}\langle i\rangle = \langle \varepsilon\rangle , \qquad (1)$$

where [Z] is the matrix of the assigned intrinsic and muutal impedances of the radiators

[E] is the unit matrix

<X> is the vector-column of the load reactances

<i> is the vector-column of currents in the radiators

<ε> is the vector-column of the voltages induced by the active radiator.

The solution of this problem of synthesis can be reduced to finding the reactances <X> based on the given radiation pattern of an array; here the currents <i> must belong to the

set $\mathcal{J}$ providing the reactance of the impedances <X>. The approximation to the given radiation pattern can be root-mean-square of uniform. The problem of the root-mean-square approximation for a linear array consists of minimizing the function

$$\Gamma(i_1, \ldots i_n) = \int_{-\frac{\pi}{2}}^{\frac{\pi}{2}} \left| F(\theta) - \varphi(\theta) \sum_{n=1}^{N} i_n e^{jkdn\sin\theta} \right|^2 d\theta, \tag{2}$$

and the uniform approximation problem, to minimizing the function

$$\Gamma(i_1, i_2, \ldots i_n) = \max_{\theta} \left| F(\theta) - C\varphi(\theta) \sum_{n=1}^{N} i_n e^{jkdn\sin\theta} \right| \tag{3}$$

The final formulation of the problem of synthesizing a reflection array with arbitrary fixed geometry can be represented as follows: minimize $\Gamma\ (i_1, i_2, \ldots, i_n)$ with respect to <i> under the condition that $\langle i \rangle \in \mathcal{J}$, that is, find the $\langle \tilde{i} \rangle$ such that

$$\left. \Gamma(\tilde{i}_1, \tilde{i}_2, \ldots \tilde{i}_n) = \min_{\substack{\langle i \rangle \\ \langle \tilde{i} \rangle \in \mathcal{J}}} \Gamma(i_1, i_2, \ldots i_n). \right\} \tag{4}$$

In mathematics there is not yet an algorithm capable of solving problem (4) in the most general form, that is, when $\Gamma(i_1, \ldots, i_n)$ is an arbitrary function, and $\mathcal{J}$ is a set with arbitrary configuration. In the case of reflection arrays, the currents from the $\mathcal{J}$ must satisfy the following system of constraints [25]:

$$Re\left\{\left(\varepsilon_n - \sum_{\ell=1}^{N} Z_{n\ell} i_\ell\right) i_n^*\right\} = 0, \quad \kappa = 1, 2, \ldots N \tag{5}$$

This article presents the results obtained using different algorithms developed by the authors as applied to the problem of reflection arrays.

Let us assume we know certain initial values of the load impendances of the dipoles $\langle x \rangle^{(o)}$. Selection of the initial value of the loads can be done with different methods:

a) First Method of Selecting Initial Loads

Let us solve problem (4) without allowing for the constraints on the currents. For this purpose it is best to set up an overdetermined system of equations that can be solved for function (2) by the method of least squares, and for function (3), by the Stieffel exchange method [24]. After finding the currents $\langle i \rangle$, which generally do not belong to the set $\mathcal{J}$, let us calculate the load impedances based on a linewise solution of system (1) and, by eliminating the real part in this solution, we regard them as the initial loads.

b) Second Method of Selecting Initial Loads

Conditionally we assume that the mutual influence between the dipoles in the array is weak, that is, the matrix [Z] is a diagonal matrix. In this case, the currents from (1) are defined as

$$i_n^{m} = \frac{\varepsilon_n}{Z_{nn} + jX_n} \tag{6}$$

The right-hand side of Eq. (6) is a circle on a complex plane [25]. If we denote the current, which is the solution of problem (4) without the presence of constraints (5), by $\langle i' \rangle$, as the initial value of the load impedances we select the value that minimizes the expression

$$\left| i_n' - \frac{\varepsilon_n}{Z_{nn} + jX_n} \right| = \min_{\substack{X_n \\ n = 1, 2, \ldots N}} \left| i_n' - \frac{\varepsilon_n}{Z_{nn} + jX_n} \right|. \tag{7}$$

The solution of Eq. (7) has a simple geometrical significance and analytically can be reduced to solving a quadratic equation.

The simplest algorithm for solving the problem of synthesizing an array in the root-mean-square approximation is given in [26]. The problem can be reduced to minimizing the function Δ:

$$|i'_k - \tilde{i}_k|^2 = \Delta, \quad k = 1, 2, \ldots N \tag{8}$$

given the system of constraints on current (5). The algorithm above presupposes that the matrix [Z] has an emphasized diagonal and the current-column $\langle i \rangle^{(o)}$ is known, which we adopt as the zero approximation. The assumption that there is weak mutual influence between the dipoles enables us to minimize (8) for the k-th dipole, when there is the k-th constraint on system (5). The Lagrange method as applied to this problem leads to a system of two equations, one being quadratic, and the other, linear. The solution obtained in this case does not exactly satisfy conditions (8) and (5). For a revised solution, new computational cycles are carried out. This algorithm makes it possible to compute the arrays of a small number of dipoles quite widely dispersed in space ($d/\lambda > 0.1$). Its advantage is the simplicity of computations. The desire to allow for the influence of only two adjoining dipoles leads to much more complexity of computations. Elaborating this concept, we now must minimize (8) for the k-th dipole given the (k-1)-th, k-th, and (k+1)-th constraints on the current from system (5). The Lagrange method leads to a system of nine equations, three of which are quadratic. An incomplete allowance for the mutual influence leads to a situation in which the solution obtained will be inexact; and just as in the first case, repeated computations will be necessary. When the mutual influence between all dipoles is taken into account, a system of 3N equations must be solved, of which N are quadratic. In contrast to the first two cases examined, with an increase in the number of elements, the matrix order also grows larger. Allowing for mutual influence (partially or completely) leads to the need to solve a system of nonlinear equations. Existing mathematical methods enable this problem to be solved [27].

We present our further exposition on the example of the uniform synthesis of a reflection array. For the case of the root-mean-square synthesis, the algorithm functions quite analogously; there will be a difference only in the normalizing of the radiation pattern. The problem of uniform synthesis is formulated in the form of problem (4), where $\Gamma(i_1,\ldots,i_n)$ stands for function (3), under the condition that the set $\mathcal{J}$ is defined by (5). Into function (3) is introduced the complex normalizing coefficient C, which must provide us with the convergence of the sequence $\langle i\rangle^{(o)}$, $\langle i\rangle^{(1)}$, ..., $\langle i_n\rangle$ to the desired distribution $\langle \tilde{i}\rangle \in \mathcal{J}$. Physically it signifies the possibility of adjusting the radiation of the array to the level that is optimal in the sense of the uniform proximity of two curves: the normalized given radiation pattern $F(\theta)$:

$$\max_{\theta\in\Omega} F(\theta) = 1; \quad \Omega = \left[-\frac{\pi}{2}, \frac{\pi}{2}\right] \tag{9}$$

and the radiation diagram of the array $f(\theta)$. The magnitude of the coefficient C is selected by solving the following auxiliary problem for a known (calculated) current

$$\begin{aligned} \Delta &= \max_{\theta} \left| F(\theta) - \tilde{C}\varphi(\theta)\sum_{n=1}^{N} i_n e^{jnd n \sin\theta} \right| = \\ &= \min_{C} \max_{\theta} \left| F(\theta) - C\varphi(\theta)\sum_{n=1}^{N} i_n e^{jnd n \sin\theta} \right| \end{aligned} \tag{10}$$

The solution of problem (10) is obvious:

$$\begin{aligned} \tilde{C} = \frac{1}{2}\Big[&\Big(\max_{\theta} \operatorname{Re}\frac{F(\theta)}{f(\theta)} + \min_{\theta} \operatorname{Re}\frac{F(\theta)}{f(\theta)}\Big) + \\ &+ i\Big(\max_{\theta} \operatorname{Im}\frac{F(\theta)}{f(\theta)} + \min_{\theta} \operatorname{Im}\frac{F(\theta)}{f(\theta)}\Big)\Big] \end{aligned} \tag{11}$$

The soundness of the introduction of this coefficient follows from the fact that the left- and right-hand members of Eq. (1) can be multiplied by an arbitrary number. The essentials of the proposed algorithm will consist in constructing a sequence of current distributions, each term of which has a smaller quantity

$$\Delta^{(k)} = \max_{\theta} |F(\theta) - \tilde{C}^{(k)} \varphi(\theta) \sum_{n=1}^{N} i_n^{(k)} e^{jkdn\sin\theta}|$$

compared with $\Delta^{(k-1)}$.

To calculate the quantity Δ, we partition the interval of angles on which $F(\theta)$ and $f(\theta)$ is defined with a closely spaced net and we calculate Δ at the nodes of this net. Let us adopt the calculated initial values of load impedances $X_1^{(0)}, X_2^{(0)}, \ldots X_n^{(0)}$ and insert them into Eq. (1). From the system of equations (1) we calculate the current

$$\langle i\rangle^{(0)} = \{[Z] + [E]\langle X\rangle^{(0)}\}^{-1} \langle \varepsilon\rangle \tag{12}$$

From Eq. (11) we calculate the normalized coefficient $C^{(o)}$ corresponding to these currents, and then the quantity $\Delta^{(o)}$. In the following text we leave unchanged all the initial values of the load impedances of the dipoles, except for the load impedance of the first dipole. By varying the quantity jX_1, each time we calculate the values of <i>, $\tilde{C}$, and Δ, attempting to find a $j\tilde{X}_1$, such that

$$\min_{X_1} \Delta(jX_1) = \Delta(j\tilde{X}_1) \tag{13}$$

To calculate the currents corresponding to each new value of the quantity jX_1 generally speaking each time we must invert the matrix $\{[Z]+[E]\langle X\rangle\}$. If the number of attempts for the search will be large and the matrix is large in size, this procedure requires more machine time. This difficulty is cleared away with two procedures:

1) The matrix $\{[Z]+[E]\langle X\rangle\}$ corresponding to each new value of $jX_1^{(m)}$ can be obtained not by inversion, but by correcting the inverted matrix corresponding to the previous value of $jX_1^{(m-1)}$. The correction is carried out using the following formulas [23]. Let

$$\{[Z] + [E]\langle X\rangle^{(m)}\}^{-1} = [m] \tag{14}$$

and

$$\{[Z] + [E]\langle X_1^{(m)} X_2^{(m)} \ldots X_n^{(m)}\rangle_1\}^{-1} = [m]^{(m)}$$

then $m_{rs}^{(m)} = m_{rs} - t m_{ri} m_{js}$

where $t = \frac{d'}{1+m_{jj}}$, $d = j(X_1^{(i)} - X_1^{(m)})$

2) The strategy of searching for $j\bar{X}_1$ must be such that finding $j\bar{X}_1$ occurs in the smallest number of attempts. This optimal strategy can be developed only by relying on the form of the function $\Delta(jX_1)$. For an arbitrary number of dipoles, the form of this function cannot be analytically investigated, but for two dipoles it is shown in Fig. 1. For the form of function shown the optimal strategy was constructed using a Fibonacci series. The function $\Delta(jX_1)$ was computed at the following points:

$$\begin{matrix} jX_1^{(m)}, & j(X_1^{(m)} + \ell_1 a), \ldots & j(X_1^{(m-1)} + \ell_n a); \\ \Delta_1^{(m)}, & \Delta_1^{(1)}, & \Delta_1^{(n)}. \end{matrix} \tag{15}$$

In Eq. (15) ℓ_k is the k-th member of the Fibonacci series 1, 1, 2, 3, 5, 8, ...; a is the initial interval, equal to ± 0.05; ± 0.5; and ± 5, which is derived in order to occupy a section to the left of jX_1^{*}. The condition

$$\Delta_1^{(n-1)} - \Delta_1^{(n)} > 10^{-4} \tag{16}$$

is a criterion for converting from one term of the sequence (15) to another. The search for $j\tilde{X}_1$ ends when (16) is not satisfied for any values of the parameter $a = \pm 0.05$, ± 0.5, and ± 5.

To continue the process, we now record the value of $j\bar{X}_1$ found and carry out an analogous procedure for jX_2, where all $jX_3^{(0)} \ldots jX_n^{(m)}$ remain unchanged, as before. All the load impedances are selected in this way.

We have described one cycle of the algorithm. The entire algorithm consists of these repeating cycles. A quantity

analogous to (16) is the criterion for termination. The convergence of this process to $\langle\tilde{X}\rangle$ can be easily demonstrated if ΔjX_n has the form shown in Fig. 1.

As an example, let us examine the synthesis of an equidistant reflection array if the given radiation pattern has the following form:

$$F(\theta)=\begin{cases} \left|\dfrac{\sin 10(\theta-\frac{\pi}{3})}{10(\theta-\frac{\pi}{3})}\right|, & -\frac{\pi}{2}\leq\theta<-\frac{\pi}{3};\ \frac{\pi}{3}<\theta<\frac{\pi}{2} \\ 1, & -\frac{\pi}{3}<\theta<\frac{\pi}{3} \end{cases} \tag{17}$$

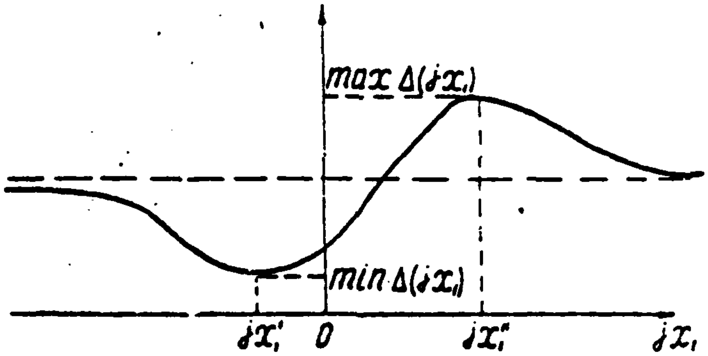

Fig. 1

Considering the plane θ as the plane of isotropicity of the lattice $\Phi(\theta)=1$, we get the following results by applying the above-described algorithm to problem (3)-(4). For N=28 and d=0.25λ, when the number of points of partitioning of the interval [0,π/2] is equal to m=19, the desired load impedances <X> in ohms as shown in Table 1 are obtained. The assigned and the obtained radiation patterns are presented in Fig. 2. From Fig. 2 we see that the approximation proves to be quite good if we omit consideration of the large side lobe.

In conclusion we must note that all the algorithms proposed in this article can be classed with local methods of analysis of

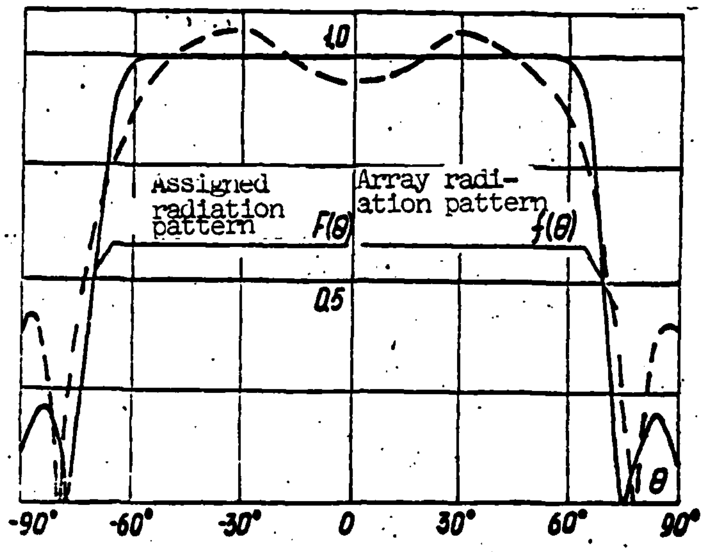

Fig. 2

multiextremal problems. To be fully convinced that the minima found are global, we must apply more complex nonlocal methods of analysis, for example, the I. M. Gel'fand method of troughs. Naturally, converting to nonlocal methods is necessary when the magnitude of the local minimum does not suit the investigator.

Table 1

$X_{\pm 1}$	$X_{\pm 2}$	$X_{\pm 3}$	$X_{\pm 4}$	$X_{\pm 5}$	$X_{\pm 6}$	$X_{\pm 7}$	$X_{\pm 8}$	$X_{\pm 9}$	$X_{\pm 10}$
$-j22$	$1-j8$	$1-j3$	$1-j30$	$1-j7.8$	$1-j10.5$	$1-j18$	$1-j5$	$1-j16$	$1-j18$

ENERGY METHOD OF SYNTHESIZING MICROWAVE ANTENNAS

A. F. Chaplin

At the present time, the problem of finding the current distribution or the distribution of the tangential field component in the antenna aperture for a given radiation pattern has been formulated and solved in the literature on antenna synthesis. It must be stated that with this formulation of the problem, the antenna must be represented as the distribution of extrinsic current (electric or magnetic) sustained by current or voltage generators. At the same time we know that microwave antennas are characterized generally by a free excitation mode [29], in which the antenna is fed a flow of incident power arriving from a constant power output generator. In addition, with the usual formulation of the antenna synthesis problem, estimates of antenna energy characteristics grow in complexity. This is evidenced by the fact that in most studies on synthesis the antenna power is calculated as the integral of the square of the radiation pattern module with respect to field intensity. We can easily show that this estimate is invalid above all in the calculation of the total and reactive antenna power. Examined below is a formulation of the antenna synthesis problem in which there is an association between the distribution of normalized voltage in the far zone and in the antenna aperture.

As a working model, we adopt a linear-array antenna with length 2ℓ, arranged along the y-axis and irradiating a field in the form of TM-waves with respect to the z-axis perpendicular to the antenna. Let us examine the two-dimensional problem when the field does not depend on the x coordinate. The free-space field is represented in the form of a superpositioning of plane waves; to do this, we use expressions from the monograph [13]:

$$
\begin{aligned}
E_z &= \int_{-\infty}^{\infty} \frac{F(\varkappa)}{\sqrt{\varkappa^2-k^2}}\, e^{-i\varkappa y-\sqrt{\varkappa^2-k^2}\,z}\, d\varkappa\,,\\
E_y &= -\int_{-\infty}^{\infty} \frac{F(\varkappa)}{\varkappa}\, e^{-i\varkappa y-\sqrt{\varkappa^2-k^2}\,z}\, d\varkappa\,,\\
H_x &= i\omega\varepsilon \int_{-\infty}^{\infty} \frac{F(\varkappa)}{\varkappa\sqrt{\varkappa^2-k^2}}\, e^{-i\varkappa y-\sqrt{\varkappa^2-k^2}\,z}\, d\varkappa
\end{aligned}
\tag{1}
$$

Here it is assumed that the observation point is located above the extrinsic sources, whose spectral density is represented by the function $F(\varkappa)$.

Each plane wave produces a power flow perpendicular to the antenna and equal to

$$\Pi_z = \frac{\omega\varepsilon}{2}\,\frac{|F(\varkappa)|^2}{\varkappa^2\sqrt{k^2-\varkappa^2}}$$

Let us represent the quantity Π_z in the form of the product of two symmetrical cofactors

$$\Pi_z = \frac{1}{2}\,\varphi(\varkappa)\,\overset{*}{\varphi}(\varkappa),$$

where

$$\varphi(\varkappa) = \sqrt{\omega\varepsilon}\,\frac{F(\varkappa)}{\varkappa\sqrt[4]{k^2-\varkappa^2}}\,;\quad \overset{*}{\varphi}(\varkappa) = \sqrt{\omega\varepsilon}\,\frac{F(\varkappa)}{\varkappa\sqrt[4]{k^2-\varkappa^2}} \tag{2}$$

This representation is similar to the representation widely used in microwave circuit theory for normalized voltage waves in waveguides. The quantity $\varphi(\varkappa)$ has the dimension of $(\text{watts})^{1/2}$.

As we know, the current distribution along the linear-array antenna is associated with the field intensity in the far zone by

means of a Fourier transform. In the same way, we can associate the function $\Phi(y)$ and $\varphi(\varkappa)$, which are the power distributions to the exponent 1/2 along the linear-array antenna and in the far zone, respectively.

$$\varphi(\varkappa) = \int_{-\ell}^{\ell} \Phi(y)\, e^{-i\varkappa y}\, dy, \tag{3a}$$

$$\Phi(y) = \frac{1}{2\pi} \int_{-\infty}^{\infty} \varphi(\varkappa)\, e^{i\varkappa y}\, d\varkappa \tag{3b}$$

If the antenna is located in loss-free space, the values of the function $\varphi(\varkappa)$ along the segment $[-k, k]$ define the active radiation power, and the values of this function at the semiinfinite segments $[-\infty, -k]$ and $[k, \infty]$ define the reactive energy stored in the near field of the antenna.

Thus, the problem of synthesizing microwave antennas can be posed and solved as follows: we assign the function $\varphi(\varkappa)$ and with the solution of the integral Fredholm equation of the first kind (3a) we find the function $\Phi(y)$ from which we can calculate the distribution of the flow of complex power along the antenna. If the function $\varphi(\varkappa)$ is defined along the entire $\varkappa$ axis, to solve the synthesis problem we can use the inversion formula (3b).

To solve the problem posed we can develop methods similar to methods of solving the conventional antenna synthesis problem: the Fourier integral method, the method of partial radiation patterns, and the A. N. Tikhonov regularization method. It must be noted that now all energy estimates will have an explicit physical meaning.

In addition to calculating the flow of complex power along the antenna, we can find the distribution of the surface impedance or the input impedance at each antenna point. The surface impedance

Z(y) can be found with the formula

$$Z(y)=\frac{E_y(y)}{H_x(y)}=\frac{i}{\omega\varepsilon}\,\frac{\int_{-\infty}^{\infty}\Phi(\varkappa)\sqrt[4]{\varkappa^2-\kappa^2}\,e^{-i\varkappa y}\,d\varkappa}{\int_{-\infty}^{\infty}\frac{\Phi(\varkappa)}{\sqrt[4]{\varkappa^2-\kappa^2}}\,e^{-i\varkappa y}\,d\varkappa} \tag{4}$$

Let us dwell on two properties of the functions $\Phi(\varkappa)$ and (y) we have introduced

1. Function $\Phi(\varkappa)$ and $\Phi(y)$ exhibit the property of local separation of power into active and reactive at each antenna point. Let us take two plane waves with the wave numbers $\varkappa_1$ and $\varkappa_2$: $\Phi_1(\varkappa)=A\delta(\varkappa-\varkappa_1)$, $\Phi_2=B\delta(\varkappa-\varkappa_2)$. Let $|\varkappa_1|>\kappa$ and $|\varkappa_2|>\kappa$. Let us find the conditional power flow at some point p(y,0) of the antenna.

$$\Pi_z(y)=\frac{i}{2}\left(\frac{Ae^{-i\varkappa_1 y}}{\sqrt[4]{\varkappa_1^2-\kappa^2}}+\frac{Be^{-i\varkappa_2 y}}{\sqrt[4]{\varkappa_2^2-\kappa^2}}\right)\left(\frac{\bar{A}e^{i\varkappa_1 y}}{\sqrt[4]{\varkappa_1^2-\kappa^2}}+\right.$$
$$\left.+\frac{\bar{B}e^{i\varkappa_2 y}}{\sqrt[4]{\varkappa_2^2-\kappa^2}}\right)=\frac{i}{2}\,\frac{|A|^2}{\sqrt{\varkappa_1^2-\kappa^2}}+\frac{i}{2}\,\frac{|B|^2}{\sqrt{\varkappa_2^2-\kappa^2}}+$$
$$+\,i\,\frac{|A||B|\cos[\arg A-\arg B+(\varkappa_2-\varkappa_1)y]}{\sqrt[4]{\varkappa_1^2-\kappa^2}\,\sqrt[4]{\varkappa_2^2-\kappa^2}}$$

The power flow of two slow plane waves represented with the functions $\Phi_1(y)$ and $\Phi_2(y)$ remains reactive at each point on the plane z=0.

Let $|\varkappa_1|<\kappa$ and $|\varkappa_2|<\kappa$. Then we have the expressions

$$\Pi_z(y)=\frac{1}{2}\,\frac{|A|^2}{\sqrt{\kappa^2-\varkappa_1^2}}+\frac{1}{2}\,\frac{|B|^2}{\sqrt{\kappa^2-\varkappa_2^2}}+$$
$$+\,\frac{|A||B|\cos[\arg A-\arg B+(\varkappa_2-\varkappa_1)y]}{\sqrt[4]{\kappa^2-\varkappa_1^2}\,\sqrt[4]{\kappa^2-\varkappa_2^2}}$$

The power flow of two fast plane waves represented by the functions $\Phi_1(y)$ and $\Phi_2(y)$ remains active at each point on the plane z=0. But if we examine the power flow of one fast and one slow wave $|\varkappa_1|<\kappa$ and $|\varkappa_2|<\kappa$, it proves to be complex at some point p(y,0):

$$\Pi_z(y) = \frac{1}{2}\frac{|A|^2}{\sqrt{\kappa^2-\varkappa_1^2}} + \frac{i}{2}\frac{|B|^2}{\sqrt{\varkappa_2^2-\kappa^2}} + \frac{|A||B|\cos[\arg A - \arg B + (\varkappa_2-\varkappa_1)y]}{e^{i\pi/4}\sqrt[4]{\kappa^2-\varkappa_1^2}\sqrt[4]{\varkappa_2^2-\kappa^2}}$$

2. The transition to the normalized voltage waves $\Phi(y)$ signifies the symmetrizing of the kernel of the integral equation, which associates $E_y(y)$ (or the surface magnetic flux $\mathcal{J}_z^m(y)$) with the distribution of the surface impedance $Z(y)$ and can be derived from Eq. (4):

$$E_y(y) = -\frac{\omega\varepsilon}{2} Z(y) \int_{-\infty}^{\infty} H_0^{(2)}(\kappa|y-y'|) E_y(y')\, dy' \qquad (5)$$

Actually, by designating $E_y(y)/\sqrt{Z(y)} = \Phi(y)$, we bring Eq. (7) to the form

$$\Phi(y) = -\frac{\omega\varepsilon}{2} \int_{-\infty}^{\infty} \sqrt{Z(y)}\sqrt{Z(y')} H_0^{(2)}(\kappa|y-y'|) \Phi(y')\, dy',$$

where the kernel is already symmetrical.

DIFFRACTION OF PLANE WAVES BY AN ARBITRARY SMOOTH CONVEX BODY AND THE KELLER METHOD OF DIFFRACTION WAVES

N. S. Orlova and Yu. I. Orlov

A shortwave asymptotic representation for an electromagnetic field was derived in [30], which is valid in the boundary layer near an ideally conducting surface S in the region of deep shadow and semishadow. Using the expressions for currents at the surface of a body derived in [30], in this paper the diffraction field in the wave zone in the shadow region is determined. The solution obtained generalizes the Keller formula [31] for the region of shadow and is utilized for refining the concept of diffraction rays (the geometrical theory of diffraction) [31]. Analogous problems in the two-dimensional case were investigated, in particular, in the studies [33-37].

1. Scalar Problem

Suppose that at a smooth convex surface a plane wave is incident at $U^{0}=e^{-ik(\vec{n}\vec{r})}$. Let us examine the first and second boundary value problems for the Helmholtz equation

$$\Delta U+k^{2}U=0,$$
$$U=U^{0}+U^{s},\quad \Omega U|_{S}=0,\quad \frac{\partial U^{s}}{\partial r}+ikU^{s}=o(r^{-1}), \tag{1}$$

where $\Omega=1$, for the Dirichlet problem, and $\Omega = \frac{\partial}{\partial n}$, for the Neumann problem (n is the normal to the surface S).

Near the surface S the field U(P') in the shadow region can be defined with the formulas given in [30]. In this case we use the coordinates of the boundary layer v,u,n (Fig. 1), where $u = QQ_0 + Q_0P_0$, the shortest distance between point Q on the incident wavefront and the point P_0, and $v = \overline{Q_1Q_0}$, the distance along the boundary of the geometrical shadow (Q_1 is the initial reference point), and $n=P'P_0$, the distance along the normal $\bar{n}_0(u, v)$ to the surface S, whose equation is $\bar{r} = \bar{r}_0(u, v)$. The system of coordinates u, v on S is semigeodetic; in this case, the first principal quadratic form of the surface is of the form

$ds^2 = du^2 + h_v^2(u,v)\,dv^2$, where $\left(\frac{\partial \bar{r}_0}{\partial v}\right)^2 = h_v^2$, $\left(\frac{\partial \bar{r}_0}{\partial u}\right)^2 = 1$.

To define the field in the shadow region far removed from the surface let us use Green's formula [38], with can be written approximately as follows, with reference to the results in [39]:

$$U(\bar{r}) = \frac{1}{4\pi}\int_{S_t} \left\{ \begin{matrix} -\frac{\partial U}{\partial n}\frac{e^{-ikR}}{R} \\ U\frac{\partial}{\partial n}\left(\frac{e^{-ikR}}{R}\right) \end{matrix} \right\} dS, \tag{2}$$

where $R = |\bar{r} - \bar{r}_0(u,v)|$, and the integration is performed over the shadow part S_t of surface S. Here and everywhere in the following text the first (second) row in the double formulas applies to the Dirichlet (Neumann) problem.

The expressions for the quantities $\left.\frac{\partial U}{\partial n}\right|_s$ and U_s, which appear in Eqs. (2) can can be called the "currents" I, follow from the boundary layer formulas given in [30] when m=0:

$$I = \left\{ \begin{matrix} \left.\frac{\partial U}{\partial n}\right|_s \\ U|_s \end{matrix} \right\} = \left(\frac{h_{v0}}{h_v}\right)^{1/2}\left(\frac{\rho_0}{\rho}\right)^{1/6} e^{-iku} \left\{ \begin{matrix} \left(\frac{2k^2}{\rho}\right)^{1/3} f^*(Z), \\ g^*(Z) \end{matrix} \right. \tag{3}$$

where f*(Z) and g*(Z) are functions complexly adjoint to the

Foch functions [40]

$$f(Z)=\frac{1}{\sqrt{\pi}}\int_{\Gamma}\frac{e^{iZt}}{w_1(t)}\,dt,\qquad g(Z)=\frac{1}{\sqrt{\pi}}\int_{\Gamma}\frac{e^{iZt}}{w_1'(t)}\,dt,$$
$$Z=\int_{u_{P}}^{u}\frac{M}{\rho}\,du,\quad M=\left(\frac{k\rho}{2}\right)^{1/3}\gg 1$$

ρ is the radius of curvature of a geodetic (ray), and v=const; in Eq. (3) and in the following treatment

$$h_v=h_v(P),\ \rho=\rho(P)\ \text{and}\ u_{P}=u(Q_0),\ h_{v_P}=h_v(Q),$$

$\rho_P=\rho(Q)$ (Fig. 1). The region of applicability for Eqs. (3) for currents is the region of shadow and semishadow, all the way to merger with geometrical optics formulas. By inserting (3) into (2), when kR>>1 we get

$$U(\bar r)=\frac{1}{4\pi}\iint_{\Delta}\left(\frac{h_{vP}}{h_v}\right)^{1/2}\left(\frac{\rho_P}{\rho}\right)^{1/6}h_v\frac{e^{-ik(\dots)}}{R}\begin{Bmatrix}\left(\frac{2k^2}{\rho}\right)^{1/3}f^*(Z)\\ ik(\bar n,\bar e_R)\,g^*(Z)\end{Bmatrix}dv\,du, \tag{4}$$

where $\bar e_R=R^{-1}\bar R$, and Δ is the region of variation of u and v corresponding to the shadow part of the surface S_T.

The double integral in (4) we calculate with the stationary phase method. Here the classical stationary phase method [39] turns out to be inapplicable. So first the interior integral in v is computed asymptotically, and then the refined stationary phase method is applied to the resulting integral in u [37]. As a result we get the following expressions for the field in the shadow region at large enough distances from the surface S (kR_0>>1).

$$U(\bar r)=-\sqrt{\frac{\pi}{k}}\left(\frac{1}{R_0(1+R_0\frac{1}{h_v}\frac{\partial h_v}{\partial v})}\right)^{1/2}\left(\frac{h_{v0}}{h_v}\right)^{1/2}\left(\frac{k\rho_0}{2}\right)^{1/6}\left(\frac{k\rho_P}{2}\right)^{1/6}e^{-ik(\dots)}\begin{Bmatrix}\hat f^*(Z_0)\\ \hat g^*(Z_0)\end{Bmatrix} \tag{5}$$

where $\hat f^*(Z_0)$ and $\hat g^*(Z_0)$ are functions complexly adjoint to the Foch functions [37,40,41]

$$\hat f(Z_0)=\frac{e^{i\frac{\pi}{4}}}{\sqrt{\pi}}\int_{\Gamma}e^{iZ_0t}\frac{v(t)}{w_1(t)}\,dt,\qquad \hat g(Z_0)=\frac{e^{i\frac{\pi}{4}}}{\sqrt{\pi}}\int_{\Gamma}e^{iZ_0t}\frac{v'(t)}{w_1'(t)}\,dt,$$

R_0 is the length of the tangent PP_0, $\rho_0=\rho(u_0,v_0)$, $h_0=h_v(u_0,v_0)$;

u_0, v_0 are the coordinates of the separation point of the diffraction ray $v = v_0 = \mathrm{const}$, $Z_0 = \int_{u_{Q_0}}^{u_0} M(u, v_0)\rho^{-1}(u, v_0)\,du$. .

Eqs. (5) are a generalization of Keller's [31] geometrical diffraction formulas, since they are valid also in the semishadow region.

Vector Problem

Let us examine the problem of the incidence of a plane electromagnetic wave $\bar{E} = \bar{E}^0 e^{-i\bar{k}\bar{r}}$, $\bar{H} = \frac{1}{\omega\mu}[\bar{k}\bar{E}] = \bar{H}^0 e^{-i\bar{k}\bar{r}}$ by an arbitrary, smooth convex, ideally conducting body. The field in a boundary layer with thickness $kn \lesssim M$ $(M = (\frac{k\rho}{2})^{1/3} \gg 1)$ near the surface of the body in the shadow region is determined by the equations in [30]. To determine the field in the shadow region far from the body surface let us use the equivalency theorem [13], which with reference to [39] can be approximately represented, analogously to (2), in the form:

$$\bar{E}(\bar{r}) \approx \frac{1}{4\pi i\omega\varepsilon}\,\mathrm{rot}_r \int_{S_T} [\bar{I}^0 \,\mathrm{grad}_s \frac{e^{-ikR}}{R}]\,dS, \qquad (6)$$

$$\bar{H}(\bar{r}) \approx \frac{1}{4\pi}\int_{S_T} [\bar{I}^0 \,\mathrm{grad}_s \frac{e^{-ikR}}{R}]\,dS, \qquad (7)$$

where $\bar{I}^0 = [\bar{n}_0 \bar{H}]|_s$ is the surface density of the electric current in the shadow part S_T of the metal surface S. In accordance with [30] we have:

$$\bar{I}^0 = H_v \bar{e}_u - H_u \bar{e}_v = H^0_{vQ_0} U_1|_s \bar{e}_u - \frac{i}{k}\sqrt{\frac{\varepsilon}{\mu}}\, E^0_{vQ_0} \frac{\partial U_1}{\partial n}\Big|_s \bar{e}_v \qquad (8)$$

Here $\bar{e}_u = \frac{\partial \bar{r}_0}{\partial u}$ and $\bar{e}_v = |\frac{\partial \bar{r}_0}{\partial v}|^{-1}\frac{\partial \bar{r}_0}{\partial v}$ are the unit vectors of the semigeodetic system of coordinates u,v, where $\bar{n}_0 = [\bar{e}_v \bar{e}_u]$; $H^0_{vQ_0}$, $E^0_{vQ_0}$ – v are the components of the incident field at the boundary points Q_0

(Fig. 1), $\frac{\partial U_1}{\partial n}\big|_S$ and $U_2\big|_S$ are the "currents" defined by Eqs. (5) in the Dirichlet and Neumann problems, respectively.

From Eqs. (6) and (7), with reference to Eq. (8), as $kR \gg 1$, we get

$$\begin{aligned} \bar{E}(\bar{r}) &= \frac{1}{4\pi}\int_{S_T}\left\{E^{\circ}_{v\varphi}\frac{\partial U_1}{\partial n}\Big|_S [\bar{a}_1,\bar{e}_R] + ik\sqrt{\frac{\mu}{\varepsilon}}H^{\circ}_{v\varphi}U_2\Big|_S[\bar{a}_2,\bar{e}_R]\right\}\frac{e^{-ikR}}{R}\,dS, \\ \bar{H}(\bar{r}) &= \frac{1}{4\pi}\int_{S_T}\left\{-\sqrt{\frac{\varepsilon}{\mu}}E^{\circ}_{v\varphi}\frac{\partial U_1}{\partial n}\Big|_S\bar{a}_1 + ikH^{\circ}_{v\varphi}U_2\Big|_S\bar{a}_2\right\}\frac{e^{-ikR}}{R}\,dS, \end{aligned} \qquad (9)$$

where $\bar{a}_1 = (\bar{e}_R\bar{n}_0)\bar{e}_u + \frac{\partial R}{\partial u}\bar{n}_0$, $\bar{a}_2 = (\bar{e}_R\bar{n}_0)\bar{e}_v + \frac{1}{h_v}\frac{\partial R}{\partial v}\bar{n}_0$. By removing the slowly varying cofactors from under the integral sign at the stationary point u_0, v_0, defined by the condition $\bar{e}_R = \frac{\partial \bar{r}_0}{\partial u}$, from Eq. (9) with reference to (2) it is not hard to find the following expressions for the field in the shadow region at large enough distances from the surface S ($kR_0 \gg 1$)

$$\begin{aligned} \bar{E}(\bar{r}) &= E^{\circ}_{n\varphi}U_2(\bar{r})\bar{n}_0(u_0,v_0) + E^{\circ}_{v\varphi}U_1(\bar{r})\bar{\tau}_v(u_0,v_0), \\ \bar{H}(\bar{r}) &= \sqrt{\frac{\varepsilon}{\mu}}[\bar{e}_R(u_0,v_0)\bar{E}(\bar{r})] = \\ &= H^{\circ}_{n\varphi}U_1(\bar{r})\bar{n}_0(u_0,v_0) + H^{\circ}_{v\varphi}U_2(\bar{r})\bar{\tau}_v(u_0,v_0), \end{aligned} \qquad (10)$$

where $H^{\circ}_{n\varphi} = -\sqrt{\frac{\varepsilon}{\mu}}E^{\circ}_{v\varphi}$, $E^{\circ}_{n\varphi} = \sqrt{\frac{\mu}{\varepsilon}}H^{\circ}_{v\varphi}$ are the normal components of the incident field at the boundary points Q_0 (Fig. 1), $U_1(\vec{r})$ and $U_2(\vec{r})$ of solution (5) of the Dirichlet and Neumann problems, $\bar{n}_0(u_0,v_0)$ and $\bar{\tau}_v(u_0,v_0)$ are the unit vectors of the principal normal and of the binormal of the geodetic $v=v_0=\text{const}$ at the separation point P_0 of the diffraction ray PP_0.

The region of applicability of Eqs. (10) is the same as in the scalar case.

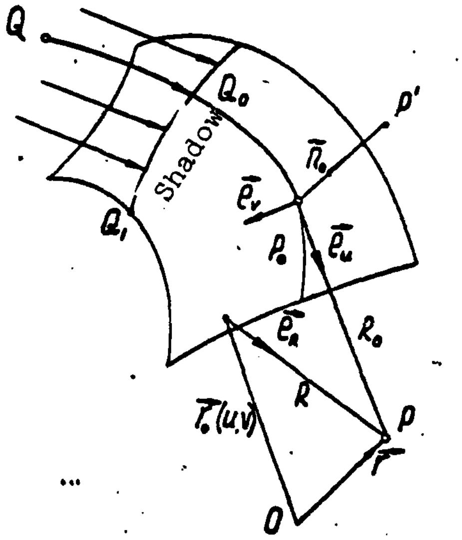

Q
Q₀
P'
Shadow
$\vec{n}_0$
$\vec{e}_v$
Q_1
P_0
$\vec{e}_u$
$\vec{e}_R$
R_0
$\vec{r}_0(u,v)$
R
P
$\vec{r}$
O

Fig. 1

DIFFRACTION OF A PLANE ELECTROMAGNETIC WAVE BY AN IDEALLY CONDUCTING BODY OF REVOLUTION

N. S. Orlova

1. Let the plane electromagnetic wave

$$\dot{\bar{E}}=\bar{E}^{0}e^{-i(\omega t)}=(E^{0}_{\theta}\bar{e}_{\theta}+E^{0}_{\varphi}\bar{e}_{\varphi})\,e^{ik(z\cos\theta^{0}-x\sin\theta^{0}\cos\varphi^{0}+y\sin\theta^{0}\sin\varphi^{0})} \tag{1}$$

be incident on a smooth, convex surface of revolution S, whose radii of curvature are much larger than the wavelength, and the equation of the generatrix in a cylindrical system of coordinates is of the form

$$z=f(r) \quad \text{or} \quad r=\psi(z) \tag{2}$$

According to [30], let us introduce near S the semigeodetic system of coordinates v,u,n normally associated with it and formed by the single-parametric family of geodetics v=const and the curves u=const orthogonal to it; n is the length of the segment of the normal to the surface. As we know [42], the trajectories of the geodetic lines at a convex body of revolution fluctuate between two parallels r=h and are governed by the following equations

$$r\sin\beta=h, \tag{3}$$

$$\frac{d\varphi}{du}=\frac{h}{r^{2}}, \quad \frac{dz}{du}=-\frac{\sqrt{r^{2}-h^{2}}}{r\sqrt{1+r'^{2}}}, \tag{4}$$

where du is an element of the length of the geodetic, β is the angle between the geodetic and the meridian, and h is the radius of the smallest parallel that is tangent to the given geodetic.

The geodetic lines v=const are envelope rays at the surface issuing from the boundary points of the geodetic shadow on S and serves as an extension of the incident rays

$$\vec{t}^0 = \kappa^{-1}\vec{\kappa} \qquad (5)$$

($\vec{t}^0$ is the unit vector of the envelope ray).

The equation of the boundary of the geometric shadow at the surface is found by determining the common points on the surface S and the family of planes tangent to it and parallel to the vector of the wave normal of the incident wave $\vec{k}$

$$\cos(\varphi_{\text{т}} - \varphi^0) = \operatorname{ctg}\theta^0 \dot{r}_{\text{т}}, \qquad (6)$$

where $\dot{r}_{\text{т}} = \frac{\partial r}{\partial z}\Big|_{z=z_{\text{т}}}$

By solving jointly Eqs. (3) and (5), let us determine the parameter of the geodetic $h = h(z_{\text{т}}, \varphi_{\text{т}}; \vec{\kappa})$

$$|h| = r_{\text{т}} \sin\theta^0 |\sin(\varphi_{\text{т}} - \varphi^0)| \qquad (7)$$

Thus, for the geodetics v=const, Eqs. (4) can be written in the form

$$\varphi = \varphi_{\text{т}} + \int_z^{z_{\text{т}}} \frac{h}{r} \frac{\sqrt{1+\dot{r}^2}}{\sqrt{r^2-h^2}} dz \quad (h \lessgtr 0) \qquad (8)$$

$$u = u_{\text{т}} + \int_z^{z_{\text{т}}} \frac{r\sqrt{1+\dot{r}^2}}{\sqrt{r^2-h^2}} dz, \qquad (9)$$

where $\varphi_{\text{т}}$ and $z_{\text{т}}$ are determined by Eq. (6), and $u_{\text{т}}$ is the phase of the incident field at the exit point of the geodetic at the boundary of the shadow

$$u_{\text{т}} = -(z_{\text{т}} + r_{\text{т}}\dot{r}_{\text{т}})\cos\theta^0 \qquad (10)$$

Eqs. (8) and (9) are valid when $\varphi < \varphi_{\text{пов}}$, where the angle of rotation $\varphi_{\text{пов}}$ corresponds to the tangency point of the geodetic with the parallel r=h. When $\varphi > \varphi_{\text{пов}}$, in Eqs. (8) and (9) we must use the partitioning of the integrals in terms of the rotation point, with reference to the symmetry of the geodetic with respect to $\varphi = \varphi_{\text{пов}}$.

As the coordinate v it is convenient to select

$$v = z_{\beta} \tag{11}$$

It is not difficult to show that the curvilinear coordinates v and u selected are orthogonal. The system of coordinates v,u,n, generally speaking, is orthogonal only near the surface. The Lame coefficients of the resulting semigeodetic coordinate system, for small n, can be expressed as follows:

$$\bar{h}_n = 1, \quad \bar{h}_u = 1, \quad \bar{h}_v = h_v, \tag{12}$$

where

$$h_v = \frac{\partial\varphi}{\partial v}\sqrt{r^2-h^2}$$

2. Following the study [80], let us write out expressions for the diffraction fields $\vec{E}$ and $\vec{H}$ near the surface

$$\begin{aligned}
\begin{Bmatrix} E_v \\ H_v \end{Bmatrix} &= \begin{Bmatrix} E_{v0n} \\ H_{v0n} \end{Bmatrix}\left(\frac{h_{v0n}}{h_v}\right)^{1/2}\left(\frac{\rho_0}{\rho}\right)^{1/6} e^{-i\kappa(u+\beta n^2)} V_1^*\left(Z, Y, \begin{Bmatrix} - \\ 0 \end{Bmatrix}\right), \\
\begin{Bmatrix} E_n \\ H_n \end{Bmatrix} &= \begin{Bmatrix} \sqrt{\frac{\mu}{\varepsilon}}\, H_{v0n} \\ -\sqrt{\frac{\varepsilon}{\mu}}\, E_{v0n} \end{Bmatrix}\left(\frac{h_{v0n}}{h_v}\right)^{1/2}\left(\frac{\rho_0}{\rho}\right)^{1/6} e^{-i\kappa(u+\beta n^2)} V_1^*\left(Z, Y, \begin{Bmatrix} 0 \\ - \end{Bmatrix}\right), \\
\begin{Bmatrix} E_u \\ H_u \end{Bmatrix} &= \left(\frac{h_{v0n}}{h_v}\right)^{1/2}\left(\frac{\rho_0}{\rho}\right)^{1/6} e^{-i\kappa(u+\beta n^2)}\left[\frac{i}{M}\begin{Bmatrix} -\sqrt{\frac{\mu}{\varepsilon}}\, H_{v0n} \\ \sqrt{\frac{\varepsilon}{\mu}}\, E_{v0n} \end{Bmatrix}\frac{\partial V_1^*}{\partial Y}\left(Z, Y, \begin{Bmatrix} 0 \\ - \end{Bmatrix}\right) - \right. \\
&\left. - \frac{i}{\kappa h_v} V_1^*\left(Z, Y, \begin{Bmatrix} - \\ 0 \end{Bmatrix}\right)\left[\begin{Bmatrix} E_{v0n} \\ H_{v0n} \end{Bmatrix}\left(\frac{1}{2}\frac{\partial \ln h_v}{\partial v} - \frac{1}{6}\frac{\partial \ln \rho}{\partial v}\right) + \begin{Bmatrix} \frac{\partial E_{v0n}}{\partial v} \\ \frac{\partial H_{v0n}}{\partial v} \end{Bmatrix}\right]\right]
\end{aligned} \tag{13}$$

Here $\quad Z = \int_{u_{0n}}^{u} \frac{M}{\rho}\, du, \quad Y = M^2\frac{2n}{\rho}, \quad M = \left(\frac{\kappa\rho}{2}\right)^{1/3}, \quad \beta = \frac{1}{6\rho}\frac{\partial\rho}{\partial u},$

$\rho = \frac{R_1 R_2}{R_1\sin^2\beta + R_2\cos^2\beta}$ is the radius of curvature of the geodetic, R_1 and R_2 are the principal radii of curvature S

$V_1^*(Z,Y,q)$ are functions complexly adjoint to the Foch functions [43]

The quantities $h_{\phi_{rp}}$ and ρ_{rp} can be calculated at the exit point of the diffraction ray from the shadow boundary. $E_{\phi_{rp}}$ and $H_{\phi_{rp}}$ are determined by the expansion of the components of the incident field (1) with respect to the coordinates v,u,n at the shadow boundary

$$E_{\phi_{rp}} = \Delta_1 E_\theta^\circ + \Delta_2 E_\phi^\circ, \quad H_{\phi_{rp}} = \sqrt{\frac{\varepsilon}{\mu}}\left(\Delta_2 E_\theta^\circ - \Delta_1 E_\phi^\circ\right), \tag{14}$$

where

$$\Delta_1 = \sin\Delta\varphi \frac{1+\sin^2\theta^\circ\cos^2\Delta\varphi}{\sqrt{1+tg^2\theta^\circ\cos^2\Delta\varphi}}, \quad \Delta_2 = \cos\theta^\circ\cos\Delta\varphi\sqrt{1+tg^2\theta^\circ\cos^2\Delta\varphi},$$
$$\Delta\varphi = \phi_{rp} - \varphi^\circ$$

The conversion from the semigeodetic system of the coordinates v,u,n to the spherical coordinates θ,ϕ at the surface is carried out based on the formulas

$$\bar{e}_\varphi = \bar{e}_u \sin\beta - \bar{e}_v \cos\beta, \quad \bar{e}_\theta = \bar{e}_u \cos\beta + \bar{e}_v \sin\beta \tag{15}$$

Eqs. (13) define the field corresponding to a single diffraction ray arriving at the observation point. In the simplest case, the field in the shadow region of the body of revolution is formed by means of two diffraction rays enveloping the surface on opposite sides. But the ray pattern of the field depends on the specific form of the surface and in the general case can be quite complex. In particular, investigation of the pattern of diffraction rays at the ellipsoid of revolution conducted as per Eq. (8) with a numerical method shows that the number of rays arriving at the arbitrary point P of the surface depends strongly on the elongation of the ellipsoid and on the angle of incidence of the plane wave (Fig. 1).

Thus, calculation of the fields at each specific surface must be preceded by the determination of the number of diffraction rays arriving at different zones of the shadow region. The fields of all rays are determined by Eqs. (13) and differ from each other only by the values of the variables u and v arriving there.

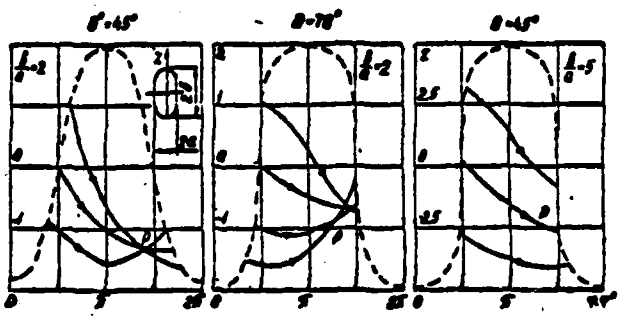

– – – – – – shadow boundary

Fig. 1

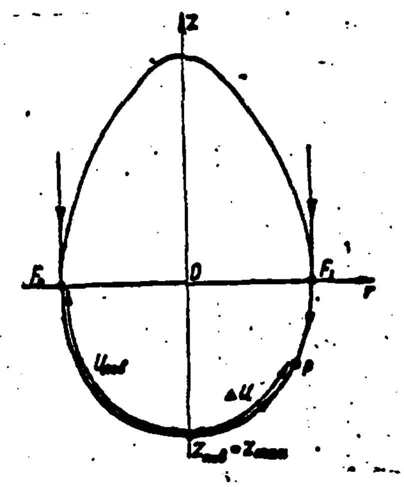

Fig. 2

3. The solution (13) that we derived cannot be used near the caustics (when $h_v \to 0$). In the cases when the ray pattern at the surface has a caustic, the solution (13) must be analytically extended into the caustic region, for example, using the method given in [44].

In the case of the axial incidence ($\theta^{\circ}=0$) of a plane wave, an axial caustic always originates on the body of revolution of arbitrary shape; to determine the field near the axial caustic Eqs. (13) can be similarly modified [45]. In this case, h=0 and the diffraction rays are propagated along the meridians, so it is sufficient to examine the ray pattern in the plane $\varphi = \varphi_{r_p} = const$ (Fig. 2). At each observation point two rays arrive, each propagating along the shortest path, and the other envelopes the "dark pole" ($z=-z_{max}$), thereby acquiring an additional lead in phase $\pi/2$.

As we can see from Fig. 2 and Eq. (12), for both rays we have the expressions

$$h_\varphi = \pm r, \quad z_{r_p} = 0, \quad r_{r_p} = r_{max} \tag{16}$$

The coordinates of the rays arriving at point P from points F_I and F_{II} can be written in the form

$$u^{I,II} = \left(\int_{-z_{max}}^{z_{r_p}} \mp \int_{-z_{max}}^{z}\right)\sqrt{1+\dot{r}^2}\,dz = u_{max} \mp \int_{-z_{max}}^{z}\sqrt{1+\dot{r}^2}\,dz = u_{max} \mp \Delta u, \tag{17}$$

where u_{max} is the ray coordinate of the rotation point $z=-z_{mzx}$.

Assuming that the following is true near the axial caustic

$$Z^{I} = Z^{II} = Z_{max} = \int_0^{u_{max}} \frac{M}{\rho}\,du$$

and referring to Eqs. (16) and (17) and the additional lead in phase at the caustic, let us represent the composite field near the axial caustic as follows:

$$\begin{Bmatrix} H_\varphi \\ E_\varphi \end{Bmatrix} = \begin{Bmatrix} H_{\vartheta_{r_p}} \\ E_{\vartheta_{r_p}} \end{Bmatrix} \left(\frac{r_{max}}{r}\right)^{1/2} \left(\frac{\rho_0}{\rho}\right)^{1/6} V_1^{e}\left(Z_{max}, Y, \begin{Bmatrix} 0 \\ \infty \end{Bmatrix}\right) = e^{i\frac{\pi}{4} - i\omega(u_{max} + \rho t)}\left(e^{i\omega\Delta u - i\frac{\pi}{4}} + e^{-i\omega\Delta u + i\frac{\pi}{4}}\right) \tag{18}$$

Using the familiar expansion of Bessel functions [46]

$$J_n(x) = \sqrt{\frac{2}{\pi x}}\left[\cos\left(x - \frac{n\pi}{2} - \frac{\pi}{4}\right) + O\left(\frac{1}{x}\right)\right], \tag{19}$$

from Eq. (18) we get

$$\begin{Bmatrix} H_\varphi \\ E_\varphi \end{Bmatrix} = \begin{Bmatrix} H_{\vartheta_{sh}} \\ E_{\vartheta_{sh}} \end{Bmatrix} \left(\frac{r_{max}}{r}\right)^{1/2} \left(\frac{\rho_0}{\rho}\right)^{1/6} V_1^*\left(Z_{max}, Y, \begin{Bmatrix} 0 \\ \infty \end{Bmatrix}\right) \sqrt{2\pi\kappa\Delta u}\, J_0(\kappa\Delta u) \times e^{i\frac{\pi}{4} - i\kappa(u_{max} + \beta r^2)} =$$
$$= \begin{Bmatrix} H_{\vartheta_{sh}} \\ E_{\vartheta_{sh}} \end{Bmatrix} \sqrt{2\pi\kappa r_{max}} \left(\frac{\Delta u}{r}\right)^{1/2} \left(\frac{\rho_0}{\rho}\right)^{1/6} V_1^*\left(Z_{max}, Y, \begin{Bmatrix} 0 \\ \infty \end{Bmatrix}\right) \times e^{i\frac{\pi}{4} - i\kappa(u_{max} + \beta r^2)} J_0(\kappa\Delta u) \tag{20}$$

Here $H_{\vartheta_{sh}}$ and $E_{\vartheta_{sh}}$ are calculated at any point on the shadow boundary. We note that $\lim_{r \to 0} \frac{\Delta u}{r} = 1$.

Similarly, by referring to the mutual orientation of the vectors $\vec{v},\vec{u},\vec{n}$ for the first and second rays, we get

$$\begin{Bmatrix} E_n \\ H_n \end{Bmatrix} = \begin{Bmatrix} \sqrt{\frac{\mu}{\varepsilon}} H_{\vartheta_{sh}} \\ -\sqrt{\frac{\varepsilon}{\mu}} E_{\vartheta_{sh}} \end{Bmatrix} \sqrt{2\pi\kappa r_{max}} \left(\frac{\rho_0}{\rho}\right)^{1/6} \left(\frac{\Delta u}{r}\right)^{1/2} V_1^*\left(Z_{max}, Y, \begin{Bmatrix} 0 \\ \infty \end{Bmatrix}\right) \times e^{i\frac{\pi}{4} - i\kappa(u_{max} + \beta r^2)} J_1(\kappa\Delta u),$$
$$\begin{Bmatrix} E_u \\ H_u \end{Bmatrix} = \sqrt{2\pi\kappa r_{max}} \left(\frac{\rho_0}{\rho}\right)^{1/6} \left(\frac{\Delta u}{r}\right)^{1/2} e^{i\frac{\pi}{4} - i\kappa(u_{max} + \beta r^2)} \times$$
$$\times \left[\frac{i}{M}\begin{Bmatrix} -\sqrt{\frac{\mu}{\varepsilon}} H_{\vartheta_{sh}} \\ \sqrt{\frac{\varepsilon}{\mu}} E_{\vartheta_{sh}} \end{Bmatrix} \frac{\partial V_1^*}{\partial Y}\left(Z_{max}, Y, \begin{Bmatrix} 0 \\ \infty \end{Bmatrix}\right) J_0(\kappa\Delta u) - \frac{i}{\kappa r_{max}} \begin{Bmatrix} \frac{\partial E_{\vartheta_{sh}}}{\partial \vartheta} \\ \frac{\partial H_{\vartheta_{sh}}}{\partial \vartheta} \end{Bmatrix} V_1^*\left(Z_{max}, Y, \begin{Bmatrix} \infty \\ 0 \end{Bmatrix}\right) J_1(\kappa\Delta u)\right] \tag{21}$$

We note that Eqs. (20) and (21), in contrast to Eqs. (13), describe the total field, considering all the rays focussing on the axial caustic.

The expressions we have derived for the diffraction field of the plane wave are valid near the surface of the body of revolution with an arbitrary shape; in the case of a sphere they wholly coincide with the asymptotic exact solution [47], including the caustic region. The resulting solution makes it

possible, by employing the reciprocity theorem, to derive formulas for calculating the radiation characteristics of arbitrarily oriented electric and magnetic dipoles located near the surface of the body.

PART 3

RECORDING ELECTROMAGNETIC RADIATION

POSSIBLE USE OF THE MAGNETIC MOMENT OF SEMICONDUCTOR PLASMA ELECTRONS FOR RECORDING CARBON DIOXIDE LASER RADIATION

G. D. Lobov, V. V. Shtykov, and Ye. I. Gratsianskaya

The presence of a nonlinear effect in a semiconductor caused by the magnetic moment of conduction zone electrons was indicated in [48]. Also made in this publication were estimates of the magnitude of this effect in the millimeter wave band. In principle, a frequency converter based on this effect in the infrared band can be constructed using semiconductors with small effective mass. From the results obtained in [48] it follows that to intensify this nonlinear effect, the product of the frequency of the effective radiation and the pulse relaxation time $\omega\tau_0$ of the semiconductor must be larger than unity. This condition can be met in the infrared band at room temperature; evidently this makes it possible to solve the problem of the uncooled low-inertia detector in this band.

In applications, directing the permanent magnetic field parallel to the propagation of electromagnetic waves may prove to be more convenient. So in this paper, in contrast to [48], magnetization will be found in the longitudinal propagation of plane electromagnetic waves in a semiconductor plasma. Since in actual frequency converters the semiconductor has finite dimensions, when we set out to find magnetization we take into account reflections from

the interface. Let the semiconductor occupy a half-space that has the boundary z=0, and let electromagnetic waves propagate along the z-axis. Then the solution of the differential equation of magnetization presented in [48], with reference to the transmission coefficient T of the electromagnetic waves in the semiconductor, will be of the form

$$\dot{M}_z(\omega_3) = \frac{\varepsilon_0 \varepsilon_p e \omega_0^2 \tau_0^2}{4 m^* \omega} |\dot{T}_0|^2 \dot{E}_0^{\sim}(\omega_1) \dot{E}_0^{\sim *}(\omega_2) [(\omega - \omega_0)^2 \tau_0^2 - 1]^{-1} \exp\{-j[\gamma(\omega_1) - \gamma^*(\omega_2)] z\}, \quad (1)$$

where $\omega_1 \cong \omega_2 = \omega$

$\gamma(\omega_i) = \frac{2\pi n_0(\omega_i)}{\lambda_i} + \frac{2\pi \varkappa_0(\omega_i)}{\lambda_i}$ are the constants of propagation at the corresponding frequencies

$\omega_0^2 = \frac{\varepsilon_0 \varepsilon_p e^2 N}{m^*}$ is the plasma frequency of the semiconductor

τ_0 is the relaxation time of a pulse in the semiconductor

m^* is the effective mass of the conduction zone electron of the semiconductor

ε_p is the dielectric constant of the semiconductor lattice

$n_0(\omega)$ is the index of refraction of the semiconductor at the given frequency

$\varkappa_0(\omega)$ is the attenuation coefficient at the given frequency

In Eq. (1) we take into account the contribution to the magnetization of the semiconductor of only the wave for which the direction of rotation of the electric field intensity vector coincides with the direction of rotation of electrons in the semiconductor.

Using the results obtained in [42], the square of the modulus of the transmission coefficient can be represented in the form

$$|\dot{T}_0|^2 = 4\left[1 + \sqrt{2\varepsilon_p}\sqrt{\frac{\sqrt{[a(a-Y^2)+b^2]^2+b^2Y^2}+a(a-Y^2)+b^2}{a^2+b^2}} + \varepsilon_p \frac{\sqrt{[a(a-Y^2)+b^2]^2+b^2Y^2}}{a^2+b^2}\right]^{-1}, \quad (2)$$

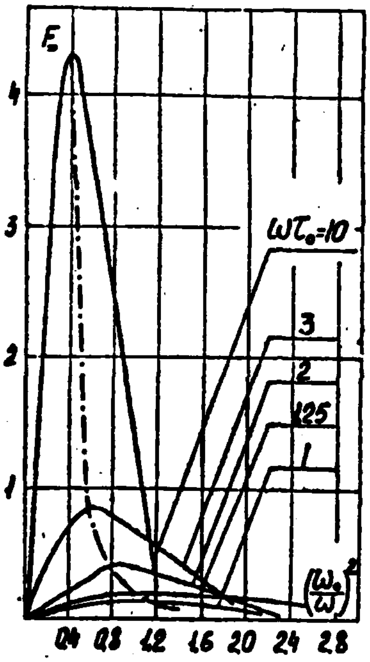

E
4
3
2
1
$\omega\tau_0=10$
3
2
1.25
1
$\left(\frac{\omega_0}{\omega}\right)^2$
0.4
0.8
1.2
1.6
2.0
2.4
2.8

Fig. 1

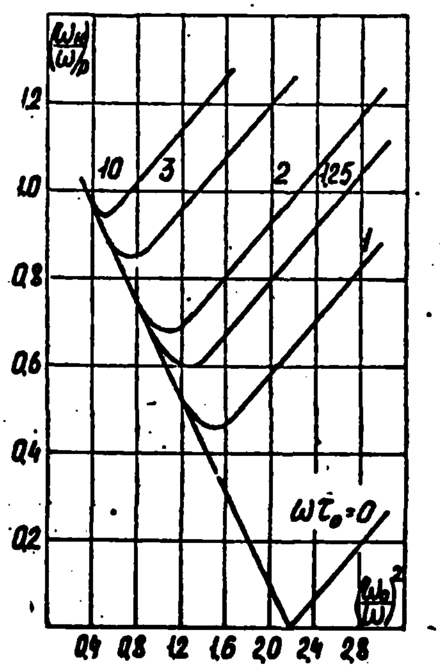

$\left(\frac{\omega_H}{\omega}\right)_p$
1.2
1.0
0.8
0.6
0.4
0.2
10
3
2
1.25
1
$\omega\tau_0=0$
$\left(\frac{\omega_0}{\omega}\right)^2$
0.4
0.8
1.2
1.6
2.0
2.4
2.8

Fig. 2

where $z = 1 - \frac{\omega_H}{\omega}$, $Y = \frac{\omega_0^2}{\omega^2}$, $\delta = \frac{1}{\omega\tau_0}$,

$\omega_H = \frac{eB}{m^*}$ is the cyclotron frequency of the semiconductor

With respect to Eq. (2), in Eq. (1) we isolate the part dependent on the concentration of the conduction zone electrons ω_0^2/ω^2, the pulse relaxation time $\omega\tau_0$, and the magnetic field intensity (ω_H/ω)

$$\dot{M}_z(\omega_2) = \frac{\varepsilon_0 \varepsilon_p e}{4m^* \omega} \dot{E}_+^{\text{nad}}(\omega_1) \dot{E}_+^{\text{nad}*}(\omega_1) F\left(\frac{\omega_0^2}{\omega^2}, \omega\tau_0, \frac{\omega_H}{\omega}\right), \qquad (3)$$

where

$$F = \frac{4Y}{(z^2+\delta^2)\left[1+\sqrt{\varepsilon_H}\sqrt{\frac{[\text{illegible}]+\delta^2 Y^2+z(z-Y)+\delta^2}{z^2+\delta^2}}+\varepsilon_p\frac{(z(z-Y)+\delta^2)^2+\delta^2 Y^2}{z^2+\delta^2}\right]}$$

Presented in Figs. 1 and 2 are the above-indicated functions. From Fig. 1 we see that the maximum value of $M_2(\omega_2)$ rapidly rises when $\omega\tau_0 > 3$. From Fig. 2 can be found the value of the permanent magnetic field for certain $\omega\tau_0$ and ω_0^2/ω^2. From a comparison of Figs. 1 and 2, it follows that to obtain the maximum value of $M_2(\omega_2)$ when $\omega\tau_0 > 3$, the required magnetic field is approximately equal to its value at the point of cyclotron resonance.

The variable part of the magnetization of the semiconductor can be recorded with an induction coil enclosing the semiconductor and located perpendicular to the external magnetic field. Let us estimate the parameters of the frequency converter at $\lambda = 10.6$ micrometers, in which a semiinfinite, longitudinally magnetized plasma cylinder with radius $R \gg \lambda$ is used.

The above-named condition allows us to use the results derived above in making estimates of the converter parameters. If the recording induction coil directly surrounds the semiconductor cylinder, the open-circuit voltage at coil ends is [50]

$$|\dot{U}_{xx}| = \omega_2 \mu_0 S_{\text{poper.}} N_{\text{vitk.}} |\dot{M}_z(\omega_2)|, \qquad (4)$$

where $S_{\text{вит}}$ is the cross sectional area of a coil turn and $N_{\text{вит}}$ is the number of coil turns. If the laser beam illuminates the entire plasma cylinder cross section, then Eq. (4), with reference to Eq. (3) takes on the form

$$|\dot{U}_{xx}| = \frac{\varepsilon_p e \omega_3 \mu_0 N_{\text{вит}}}{2cm^* \omega} \cdot \sqrt{P_1 P_2} \cdot F \qquad (5)$$

In [5] it is considered that the intensity of electromagnetic waves incident at the interface is $P = \frac{|E|^2}{2W} S$, where $W = \sqrt{\frac{\mu_0}{\varepsilon_0}}$ is the characteristic impedance in vacuo, and S is the beam cross sectional area.

Estimate calculations showed that at the output of the frequency converter at $\lambda=10.6$ micrometers (CO_2 laser), for InSb with $m^*=1.52 \cdot 10^{-32}$ kg, $\varepsilon_p=16$, $\omega\tau_0=10$, the latter corresponds to $\mu=0.6$ $m^2/V \cdot s$ [51], when $P_1=P_2=1$ W and to the coil turn number $N_{\text{вит}}=10$; the open-circuit voltage is approximately 5 microvolts and is attained for a magnetic field intensity of 160,000 gauss. To lower the magnetic field intensity, semiconductors with a lower effective mass can be used. If an HgTe semiconductor or a ternary compound $Cd_xHg_{1-x}Te$ is used as the working material in the above-described converter, with an effective conduction zone electron mass of $0.003m_e$, the open-circuit voltage for these parameters will be approximately 26 microvolts, for a mobility $\mu=2.5$ $m^2/V \cdot sec$, and a magnetic field intensity of 31.6 kilogauss.

Thus, utilizing $Cd_xHg_{1-x}Te$ in this converter is preferred over InSb. Synthesizing semiconductor compounds with an even lower effective mass makes it possible to substantially lower the required magnetic field and to build detectors for $\lambda=10.06$ micrometers with magnetic fields realistically attainable at the present time without cooling.

CONVERSION OF CO_2 LASER RADIATION TO MILLIMETER BAND RADIATION USING THE MAGNETIC MOMENT OF CONDUCTION ZONE ELECTRONS OF SEMICONDUCTORS

V. V. Shtykov

The problem of the conversion of infrared radiation frequency in a semiconductor placed in a constant magnetic field is examined in [113]. An induction coil is suggested in recording the variable magnetic moment, varying with time with the difference frequency ω_3. But there is some interest in investigating phenomena when infrared radiation is converted to millimeter band radiation, since the frequency ω_3 can be 10^{10} to 10^{11} hertz (see equation for the magnetization vector $\overline{M}$ in [48]). The high value of the difference frequency precludes the use of an induction coil in recording the variable part of $\overline{M}$. In this case a system suitable for microwave applications must be used; in the system an electromagnetic wave with the frequency ω_3 will be excited.

Let us examine, by way of example, a variant of an infrared radiation frequency converter in which a rectangular metal waveguide is used (see Fig. 1).

To solve the problem of wave excitation in a waveguide we will assume that the nonlinearity in the semiconductor is small [48].

This allows us to regard the magnitude of the variable part of the vector $\overline{M}$ as a given function and set it in correspondence to the outside magnetic flux with the complex amplitude

$$\dot{\bar{J}}^{m} = j\omega_3\mu_0 \dot{\bar{M}}(\omega_3) \tag{1}$$

The complex amplitude of the variable part $\dot{\bar{M}}(\omega_3)$, which appears in Eq. (1), was found for two limiting cases of the propagation of electromagnetic waves with frequencies ω_1 and ω_2 with respect to the vector of the constant magnetic field H_0 in [48] and [113].

From the results of these studies it follows that if the principal waves are traveling waves, then $\dot{\bar{M}}(\omega_3)$ is also a traveling wave. This circumstance imposes a number of features on the conversion of infrared radiation to a millimeter band wave. It turns out, for example, that when several phase relationships are satisfied, waves from individual regions of the semiconductor may be added together; this may lead to a larger conversion coefficient. This phenomenon is an analog of phenomena that are discussed in studies on nonlinear optics [54].

If we consider that the component $\dot{M}_z(\omega_3)$ parallel to the field H_0 has a maximum magnitude, and that for the most efficient wave excitation the vector $\bar{J}^{m}$ must be parallel to the vector $\overline{H}$ of the excited wave [10], H_0 must be oriented parallel to $\overline{H}$. When the principal type of oscillations in a rectangular waveguide is used, the last-named condition can be satisfied by orienting H_0 either perpendicular to the narrow wall of the waveguide or along its longitudinal axis. If also, as in [113], we consider the case of longitudinal propagation of the principal waves, the variant shown in Fig. 1 makes it possible to use longer waveguide specimens.

By employing the method outlined in [10] and Eq. (1), we can find the complex amplitude of the electric field at the waveguide center in the cross section z=L

$$\dot{E}_m(\omega_3) = j\frac{\pi\omega_3\mu_0}{a^2bh} e^{-jh^0L}\int \dot{M}_z(\omega_3) e^{jh^0z} dV \tag{2}$$

In deriving Eq. (2) we neglected the effect of the semiconductor wafer for waves in the waveguide, since a>>A. In the expression derived the attenuation of waves in the waveguide was allowed for by introducing the complex longitudinal wave number h=h'-jh".

If waves with circular polarization propagate in the semiconductor, the direction of rotation of vector E of the waves coinciding with the direction of electron spin, then $\dot{M}_z(\omega_3)$ can be represented in the form

$$\dot{M}_z(\omega_3) = \dot{M}_{z0} \exp[-j(\gamma_1-\gamma_2^*)z]$$

Assuming that $\dot{M}_{z0}$ does not depend on x and y, by performing integration in Eq. (2) with respect to z from 0 to L, we get

$$\dot{E}_{x0}(\omega_3, L) = -\frac{\omega_3 \mu_0 \pi}{a^2 b h} \dot{M}_{z0} AB \frac{1-\exp[-j(\gamma_1-\gamma_2^*-h)L]}{\gamma_1-\gamma_2^*-h} \exp(-h''L)$$

The dependence of the field $\dot{E}_{x0}$ on the length of the wave interaction region can be described with a function conveniently represented in the complex plane (see Fig. 1), if we transform it to the form

$$f(L) = \exp\left(-\frac{h''}{\Delta K}\varphi\right) - \exp\left[-j\varphi - \frac{\alpha_1+\alpha_2}{\Delta K}\varphi\right] \qquad (3)$$

by introducing the parameter $\varphi = (\beta_1-\beta_2-h')L = \Delta K L$.

From Fig. 1 it follows that when $\alpha_1+\alpha_2 < \Delta K$, f(L) is oscillatory, and when $\alpha_1+\alpha_2 > \Delta K$, the oscillations are weakly manifested. Emphasis is given to the case $\beta_1-\beta_2-h'=0$. In this case, f(L) is a real variable. This regime corresponds to the condition of phase matching, discussed in studies on nonlinear optics.

From Fig. 1 it follows that the deviation from this regime is not large when $\alpha_1+\alpha_2 \geq 10\Delta K$. When this condition is satisfied,

$$f(L) = \exp(-h''L) - \exp[-(\alpha_1+\alpha_2)L] \qquad (4)$$

Eq. (4) attains a maximum value when

$$h''L_m = \frac{Z \ln Z}{Z-1}, \quad \text{where} \quad Z = \frac{h''}{\alpha_1+\alpha_2}$$

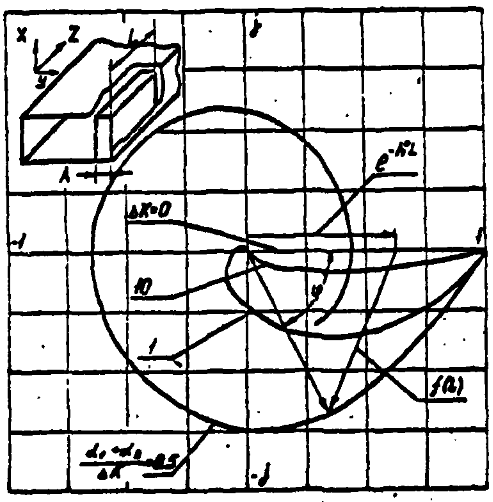

Fig. 1

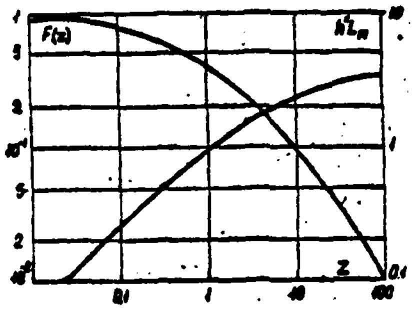

Fig. 2

The field amplitude E_{x0} in this case attains a maximum value, equal to

$$\dot{E}_{m0}(\omega_3;L_m) = j\frac{\pi\omega_3\mu_0}{a^2bh}\dot{M}_{z0}AB\frac{F(z)}{\alpha_1+\alpha_2},$$

where

$$F(z) = Z^{\frac{Z}{1-Z}}$$

Shown in Fig. 2 are $h''L_m$ and F(Z) as functions of the parameter Z. From the figure it follows that it is best to function when $\frac{h''}{\alpha_1+\alpha_2} \leq 0.1$, which corresponds to the length $L_m < \frac{0.3}{h''}$.

Corresponding to the value $\dot{E}_{x0}$ found when $\alpha_1 = \alpha_2 = \alpha$ is the intensity of waves with a difference frequency equal to

$$P(\omega_3;L_m) = \frac{\pi^2\omega_3\mu_0}{4a^2bh}|\dot{M}_{z0}|\frac{A^2B^2}{4\alpha^2}\cdot F^2(Z)$$

Using the expression from $\dot{M}_{z0}$ obtained in [113] and considering $\sigma_+\frac{|E|^2}{2} = \mathrm{div}\,\Pi_+ = 2\alpha\Pi_+$, where $\sigma_+ = \varepsilon_0\varepsilon_p\omega_0^2\tau_0[(\omega-\omega_H)^2\tau_0^2+1]^{-1}$ is an element of the conductivity tensor; when h'>>h", the expression for $P(\omega_3;L_m)$ can be represented in the form

$$P(\omega_3;L_m) = \frac{\pi^4 W_B B_e^2}{64a^2b\omega^2}P_1P_2F^2(Z) \tag{5}$$

Here P_1 and P_2 are the intensities of the principal waves in the crystal, B_e is electron mobility, and W_B is the characteristic impedance of the waveguide.

Let us estimate the intensity of difference-frequency waves when radiation from a CO_2 laser ($\omega \approx 1.78\cdot10^{14}$) is converted to millimeter band radiation with wavelength equal to approximately 5.6 mm (see [115]). When a standard 4 millimeter waveguide is used and with $Z \leq 0.01$, the intensity $P(\omega_3)$ is

$$P(\omega_3;L_m) \approx 10^{-17}B_e^2P_1P_2$$

If an InSb semiconductor crystal is used as the material, 77°K B_e can reach 70 m^2/s at the temperature of liquid nitrogen. When $P_1=P_2=100$ W, which is quite realistic for a CO_2 laser, the difference-frequency intensity will be $5\cdot10^{-10}$ W.

Thus, there is the opportunity of the experimental observation of the conversion of coherent infrared radiation to millimeter band radiation using the magnetic moment of the semiconductor conduction zone electrons.

CONVERTER OF FREQUENCY OF COHERENT INFRARED RADIATION TO THE MICROWAVE BAND USING A WAVEGUIDE WITH AN ELECTROOPTICAL CRYSTAL

V. I. Bogatkin

The conversion of the frequency of coherent infrared radiation to the microwave band can be attained by the excitation of a waveguide filled with an electrooptical crystal with nonlinearly polarized current at the difference (intermediate) frequency $\omega_n = \omega_r - \omega_c$ induced when heterodyne waves and infrared band signals are propagated in the crystal with the frequencies ω_Γ and ω_c, respectively [52,56].

Below is outlined a method of calculating the parameters of these converters with reference to the structure of the fields of all three interacting waves and losses in the crystal; additionally, the transmission coefficient is calculated with respect to the experiment presented in [52]. The main symbols correspond to those adopted in [56].

The complex amplitude of the electric field of the intermediate-frequency wave in the waveguide can be described in the form [53]

$$\dot{E}_n = \dot{U}_n(z)\,\dot{E}_{on}(x,y)\,e^{-jK_0 z}$$

Here the function $\dot{E}_{on}(x,y)$ describes the structure of the field of the excited wave type in the waveguide cross section, and the slowly varying amplitude $\dot{U}_n(z)$ obeys the equation

AD-A114 457 FOREIGN TECHNOLOGY DIV WRIGHT-PATTERSON AFB OH F/6 20/9
PRINCIPLES OF RADIO ENGINEERING (SELECTED PAGES),(U)
APR 82 Y A FILATOVA, I I CHUGUNOV
UNCLASSIFIED FTD-ID(RS)T-0647-81 NL

2 of 2

END
DATE
FILMED
6-82
DTIC

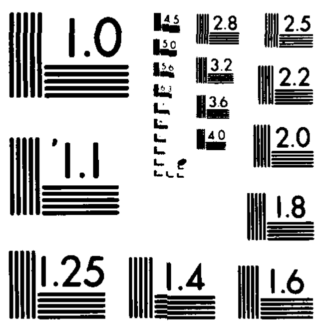

MICROCOPY RESOLUTION TEST CHART

$$\frac{d\dot{U}_n}{dz} + \alpha_n \dot{U}_n = -j\frac{\omega_n}{4\Pi_{on}} \dot{U}_r \dot{U}_c^* e^{-j\Delta\kappa z} \int_S \dot{\vec{E}}_{on}^* \hat{\chi}(\omega_n) \dot{\vec{E}}_{or} \dot{\vec{E}}_{oc}\, dx\, dy, \tag{1}$$

where

$$\Pi_{on} = \frac{1}{2} Re \int_S [\dot{\vec{E}}_{on} \dot{\vec{H}}_{on}^*]\, \vec{1}_z\, dx\, dy \tag{2}$$

is the normalized energy flow in the waveguide (neglecting the spatial dispersion of the crystal, see [53]). Integration is carried out over the waveguide cross section. The coefficient α_n is the attenuation coefficient with respect to the field of the excited wave with allowance for losses in the crystals and in the waveguide walls. The tensor $\hat{\chi}(\omega_n)$ describes the density of the nonlinearly polarized current induced in the crystal when acted on by the fields of the heterodyne wave and of the signal wave with the amplitudes

$$\dot{\vec{E}}_r = \dot{U}_r(z) \dot{\vec{E}}_{or}(x,y)\, e^{-j\kappa_r z} \quad \text{and} \quad \dot{\vec{E}}_c = \dot{U}_c(z) \dot{\vec{E}}_{oc}(x,y)\, e^{-j\kappa_c z}$$

respectively [53,54,55]. In Eq. (1), $\Delta\kappa = \kappa_r - \kappa_c - \kappa_n$. Equations analogous to (1) obtain also for the amplitudes of the heterodyne wave and of the signal wave; when combined with Eq. (1), they describe the interaction of waves with three frequencies.

For a small transmission coefficient of the converter with respect to power, Eq. (1) can be solved by assuming the quantities $\dot{U}_\Gamma$ and $\dot{U}_c$ to be assigned. Considering the losses in the crystal, we can write $\dot{U}_r(z) = U_{r_0} e^{-\alpha_r z}$, $\dot{U}_c(z) = U_{c_0} e^{-\alpha_c z}$, where the quantities $\dot{U}_{\Gamma_0}$ and $\dot{U}_{c_0}$ apply to some initial crystal cross section. In this case the solution of Eq. (1) coincides with the solution obtained from Eqs. (1) and (6) in [5], if the quantity $m\Gamma_n$ in [5] is replaced with

$$\frac{\omega_n}{4\Pi_{on}} \int_S \dot{\vec{E}}_{on}^* \hat{\chi}(\omega_n) \dot{\vec{E}}_{or} \dot{\vec{E}}_{oc}\, dx\, dy \tag{3}$$

and if $\kappa_n = \kappa_k$. In particular, all results applying to the optimal crystal length and the transmission coefficient as a function of the parameters (introduced in [56]) derived from analyzing the idealized case of the interaction of plane waves are valid for conversion in the waveguide. The results of the width of the

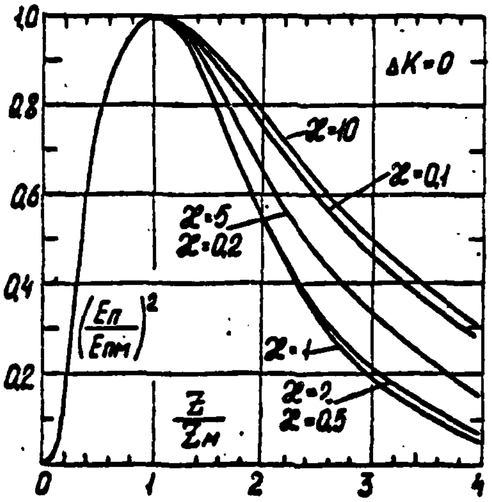
1,0
0,8
0,6
0,4
0,2
ΔK=0
æ=10
æ=0,1
æ=5
æ=0,2
æ=1
æ=2
æ=0,5
0
1
2
3
4

Fig. 1

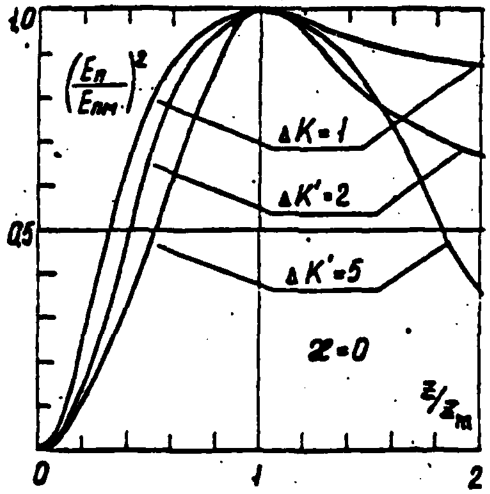
1,0
0,5
ΔK=1
ΔK'=2
ΔK'=5
æ=0
0
1
2

Fig. 2

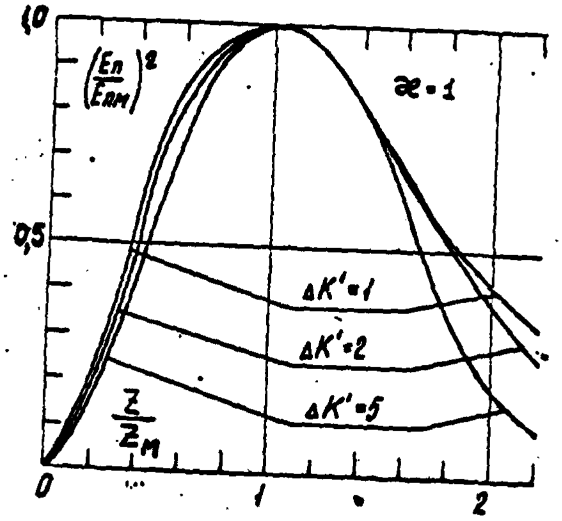

Fig. 3

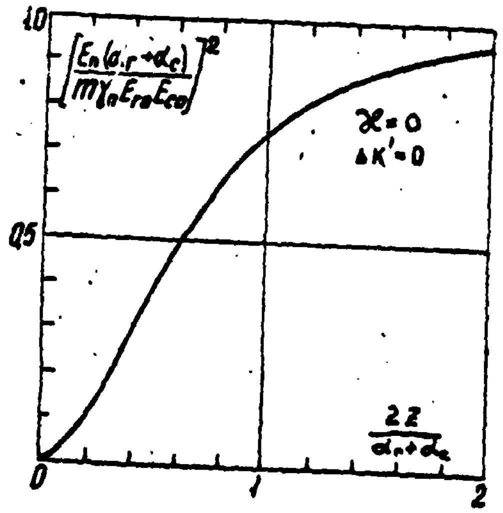

Fig. 4

radiation pattern in the passband, obtained in [56], can also be extended to the case of conversion in the waveguide.

Now let us calculate the transmission coefficient of the converter as applied to the experiment conducted in [52]. In it, the radiation from a CO_2 laser, containing oscillations at two frequencies, was focussed with a long-focal length lens at the center of a rectangular waveguide filled with GaAs crystal and excited H_{10} waves. By setting the waveguide cross-sectional dimensions equal to a and b, with respect to the x- and y-axes, respectively, we can describe the fields of laser radiation in the crystal in the form

$$\dot{\vec{E}}_r = \vec{1}_y \dot{E}_{r0} e^{-\alpha_r z} e^{-\frac{1}{R^2}\left[\left(x-\frac{a}{2}\right)^2+\left(y-\frac{b}{2}\right)^2\right]} e^{-j\kappa_r z}, \quad (4)$$
$$\dot{\vec{E}}_c = \vec{1}_y \dot{E}_{c0} e^{-\alpha_c z} e^{-\frac{1}{R^2}\left[\left(x-\frac{a}{2}\right)^2+\left(y-\frac{b}{2}\right)^2\right]} e^{-j\kappa_c z}$$

where R is the effective radius of the laser beam entering the crystal in the z=0 cross section. Strictly speaking, these functions cannot describe the field of waves propagating in the waveguide, but when R<<a,b and assuming that the geometrical optics is valid for the laser radiation in the waveguide, they are a good approximation. The eigenfunctions for the excited H_{10} wave we can write in the form $\dot{E}_{mny} = E_0 \sin\frac{\pi x}{a}$, $\dot{H}_{mnx} = \frac{E_0}{W_b} \sin\frac{\pi x}{a}$

where W_b is the characteristic impedance of the waveguide filled with an isotropic GaAs crystal. To construct Eq. (1), let us write Π_{mn} according to Eq. (2)

$$\Pi_{mn} = \frac{1}{2}\int_0^b dy \int_0^a \dot{E}_{mny} \dot{H}^*_{mnx} dx = \frac{ab}{4}\frac{E_0^2}{W_b} \quad (5)$$

Let us compute the integral in Eq. (3)

$$\int_S \dot{\vec{E}}^*_{mn} \hat{\chi} \dot{\vec{E}}_r \dot{\vec{E}}^*_c = m E_0 \int_0^b dy \int_0^a dx\, e^{-\frac{1}{R^2}\left[\left(x-\frac{a}{2}\right)^2+\left(y-\frac{b}{2}\right)^2\right]} \cdot \sin\frac{\pi x}{a}, \quad (6)$$

where

$$m = \vec{1}_y \hat{\chi} \vec{1}_y \vec{1}_y \quad (7)$$

When $R \ll a,b$, Eq. (6) can be easily computed:

$$\int_s \dot{\vec{E}}^{*}_{H} \hat{\chi} \dot{\vec{E}}_{\Gamma} \dot{\vec{E}}^{*}_{c} = \frac{\pi}{2} m R^2 E_0 \qquad (8)$$

By multiplying Eq. (1) by E_0 and inserting in it Eqs. (5) and (8), we get an equation for the complex amplitude of the field $\dot{E}$ of the H_{10} wave in the waveguide center

$$\frac{d\dot{E}}{dz} + \alpha_n \dot{E} = -j\frac{\pi}{2} m\omega_n \frac{R^2}{ab} W_b \dot{E}_{\Gamma_0} \dot{E}^{*}_{c_0} e^{-(\alpha_\Gamma+\alpha_c)z - j\Delta kz} \qquad (9)$$

If by selecting the waveguide dimension a the condition $\Delta k=0$ is satisfied and if the crystal length is small, such that we can neglect the attenuation of all waves, then by assuming in Eq. (9) that $\alpha_\Gamma = \alpha_c = \alpha_n = 0$ given the boundary condition $\dot{E}|_{z=0} = 0$ we get the solution

$$\dot{E}(z) = j\frac{\pi}{2} m\omega_n W_b \frac{R^2}{ab} \dot{E}_{\Gamma_0} \dot{E}^{*}_{c_0} z \qquad (10)$$

Considering that the power $P_n(z)$ transported by the excited wave in the z cross section is given by Eq. (5), when in place of E_0 we must substitute $E(z)$, and also that the amplitudes E_{Γ_0} and E_{c_0} are associated with the powers P_{Γ_0} and P_{c_0} of the heterodyne wave and the signal wave within the crystal at the converter input by the relationships

$$P_{\Gamma_0} = \frac{\pi}{4} \frac{R^2}{W_\Gamma} E^2_{\Gamma_0}, \quad P_{c_0} = \frac{\pi}{4} \frac{R^2}{W_c} E^2_{c_0}.$$

where W_Γ, W_c are the characteristic impedances of the crystal for the corresponding waves, we get the transmission coefficient with respect to power when the crystal length is z:

$$G = \frac{P_n(z)}{P_{c_0}} = m^2 \omega_n^2 W_\Gamma W_c W_b P_{\Gamma_0} \frac{z^2}{ab} \qquad (11)$$

Let us compute the nonlinearity parameter m in Eq. (11). The components of the nonlinear polarization vector for the GaAs crystal in the crystallographic coordinate system x',y',z' are equal to [54,55]

$$\dot P_{nx'}^{\omega\omega} = 2d_{14}(\dot E_{ry'}\dot E_{cz'}^{*} + \dot E_{cy'}^{*}\dot E_{rz'}),$$
$$\dot P_{ny'}^{\omega\omega} = 2d_{14}(\dot E_{rz'}\dot E_{cx'}^{*} + \dot E_{cz'}^{*}\dot E_{rx'}),$$
$$\dot P_{nz'}^{\omega\omega} = 2d_{14}(\dot E_{rx'}\dot E_{cy'}^{*} + \dot E_{cx'}^{*}\dot E_{ry'}).$$

In experimental conditions, in [52] the axis <111> of the crystal is directed along the y-axis of the waveguide, so the projection of the vectors of the heterodyne and signal fields onto the axes x',y',z' will be

$$\dot E_{rx'} = \dot E_{ry'} = \dot E_{rz'} = \frac{1}{\sqrt{3}}\dot E_r,$$
$$\dot E_{cx'} = \dot E_{cy'} = \dot E_{cz'} = \frac{1}{\sqrt{3}}\dot E_c$$

As a result, analogous projections of polarization prove to be equal to each other

$$\dot P_{nx'}^{\omega\omega} = \dot P_{ny'}^{\omega\omega} = \dot P_{nz'}^{\omega\omega} = \frac{4}{3} d_{14}\dot E_r \dot E_c^{*}$$

Thus, the vector $\vec P_n^{\omega\omega}$ is directed along the y-axis

$$\vec P_n^{\omega\omega} = \hat\chi \dot E_r \dot E_c^{*} = \dot E_r \dot E_c^{*} \hat\chi \vec 1_y \vec 1_y = \vec 1_y \frac{4}{\sqrt{3}} d_{14} \dot E_r \dot E_c^{*},$$

from which we get an expression for the parameter

$$m = \vec 1_y \hat\chi \vec 1_y \vec 1_y = 4/\sqrt{3}\, d_{14}$$

Eq. (11) can finally be written in the form

$$G = \frac{P_n(l)}{P_{c0}} = \frac{16}{3} d_{14}^2 \omega_n^2 W_r W_c W_b P_{r0} \frac{l^2}{ab} \qquad (12)$$

The numerical calculations based on Eq. (12), relying on data in [52] yield results that agree with those obtained in [52].

In conclusion we present plots (Figs. 1-4) characterizing the change in power of the intermediate-frequency wave at the converter output when the crystal length changes, with allowance for losses and the mismatch of phase velocities. The plots were constructed on the basis of the formulas derived in Eq. (5) when an analysis was made of the interaction of plane waves. They were normalized along the x-axis to the optimal crystal length, and along the y-axis, to the transmission coefficient, given an optimal crystal length. The symbols correspond to those adopted in [56].

CHARACTERISTICS OF THE CONVERSION OF COHERENT INFRARED RADIATION TO THE MICROWAVE BAND IN A RESONATOR CONTAINING AN ELECTROOPTICAL CRYSTAL

V. I. Bogatkin

Conversion of the frequency of coherent infrared radiation to the microwave band can be attained when an electrooptical crystal is placed not only in a waveguide [52,56,115], but only in a microwave resonator [56]. Certain properties of these converters are investigated in this article by analysis of idealized cases. The symbols and the subscripts correspond to the symbols and subscripts adopted in [115].

The power transmitted by nonlinearly polarized currents with the frequency ω_n to the excited type of resonator oscillations is

$$P_n = -\frac{1}{2} Re \int_V \dot{\vec{E}}_n^* \dot{\vec{J}}_n^{нл} dV, \tag{1}$$

here integration is carried out with respect to the resonator volume,

$$\dot{\vec{J}}_n^{нл} = j\omega_n \hat{\chi}(\omega_n) \dot{\vec{E}}_r \dot{\vec{E}}_c^* \tag{2}$$

is the density of the nonlinearly polarized current; $\dot{\vec{E}}_n = \dot{U}_n \vec{E}_{0n}(\vec{r})$ is the complex amplitude of the electric field vector of the excited oscillations; $\vec{E}_{0n}(\vec{r})$ is the function describing the

the spatial distribution of the field. The amplitude cofactor $\dot{U}_n$, assuming that ω_n equals the resonance frequency of the resonator, is given by the expression [53]

$$\dot{U}_n = -\frac{Q_n}{2W_{on}\omega_n}\int_V \dot{\vec{E}}^*_{on}\dot{\vec{J}}^{*\omega}_n \, dV, \tag{3}$$

where

$$W_{on} = \frac{1}{4}\int_V\left(\dot{\vec{E}}^*_{on}\frac{\partial\omega\hat{\varepsilon}_o}{\partial\omega}\Big|_{\omega=\omega_n}\dot{\vec{E}}_{on}+\dot{\vec{H}}^*_{on}\frac{\partial\omega\mu_o}{\partial\omega}\Big|_{\omega=\omega_n}\dot{\vec{H}}_{on}\right)dV \tag{4}$$

is the normalized energy of the resonator field; Q_n is the Q of the loaded resonator.

By substituting Eq. (2) in Eq. (3), and then Eqs. (2) and (3) in Eq. (1), we get

$$P_n = \frac{\omega_n Q_n}{4W_{on}}\left|\int_V \dot{\vec{E}}^*_{on}\hat{\chi}\dot{E}_r\dot{E}^*_c \, dV\right|^2 \tag{5}$$

Eq. (5) yields the total power transported by the nonlinearly polarized currents. Part of this power is dissipated in the resonator owing to the losses, and only part of it can be used in the form of a signal in the load associated with the resonator. We can show that the maximum power released in the load is

$$P_{load} = P_n\frac{Q_o}{4Q_n},$$

where Q_0 is the Q of the unloaded resonator. Therefore

$$P_{load} = \frac{\omega_n Q_o}{16W_{on}}\left|\int_V \dot{\vec{E}}^*_{on}\hat{\chi}\dot{E}_r\dot{E}^*_c \, dV\right|^2 \tag{6}$$

Let the resonator be formed of two infinite planes whose enclosed space is filled with an isotropic, nonlinear dielectric with thickness ℓ . Let us assume that the plane TEM wave with field components

$$\dot{\vec{E}}_{on} = \vec{i}_n\dot{E}_o\sin K_n z,$$

$$\dot{\vec{H}}_{on} = j[\vec{i}_n\vec{i}_z]\sqrt{\frac{\varepsilon_{on}}{\mu_{on}}}\dot{E}_o\cos K_n z, \tag{7}$$

is excited, where z is the coordinate measured along the z-axis perpendicular to the resonator walls; $\kappa_n l = \pi n$, $n = 1,2,3\ldots$; the unit vectors I_n and I_z are perpendicular. Let us calculate the quantity W_{on} in Eq. (4):

$$W_{on} = \frac{1}{4} S \int_0^l (\varepsilon_{an} E_o^2 \sin^2 \kappa_n z + \varepsilon_{an} E_o^2 \cos^2 \kappa_n z)\, dz = \frac{1}{4} S \varepsilon_{an} E_o^2 l \qquad (8)$$

Here S is the cross-sectional area of the resonator. Physically speaking, it is reasonable to calculate the power received per unit resonator cross-sectional area, so in the following we will assume S_1 to be equal to the unit area. When calculating Eq. (8), it is also assumed that ε_{an} and μ_{an} do not depend on frequency near ω_n.

Excitation of Currents by a Traveling Wave

We assume that plane heterodyne and signal waves of the TEM mode propagate through the resonator along the z-axis. In this case, we assume the resonator walls to be transparent to these waves. To some extent this case corresponds to the actual situation, when signal and heterodyne beams enter and exit through holes in the resonator walls. The wave amplitudes, with allowance for attenuation, we write in the form

$$\dot{E}_r = I_r \dot{E}_{ro} e^{-\alpha_r z} e^{-j\kappa_r z}; \quad \dot{E}_c = I_c \dot{E}_{co} e^{-\alpha_c z} e^{-j\kappa_c z} \qquad (9)$$

By inserting Eqs. (8) and (9) in Eq. (6) we get the power received per unit resonator area:

$$\Pi_{\text{кал}} = m^2 \frac{\omega_n Q_o}{\alpha \varepsilon_{an}} W_r W_c \Pi_{ro} \Pi_{co} f(\kappa_n, \kappa, \alpha, l) \qquad (10)$$

where $m = I_n \hat{\chi} I_r I_c$; $\alpha = \alpha_r + \alpha_c$; $\kappa = \kappa_r - \kappa_c$; W_r, W_c are characteristic impedances. Π_{ro}, Π_{co} are the Poynting vectors of the corresponding waves after their entrance into the resonator (when z=0). The function f is equal to the following expression:

$$f(\kappa_n, \kappa, \alpha, l) = \frac{(\alpha \kappa_n)^2 [1 + e^{-2\alpha l} - (-1)^n 2 e^{-\alpha l} \cos \kappa l]}{\alpha l \, [(\alpha^2 + \kappa_n^2 - \kappa^2)^2 + (2\alpha\kappa)^2]} \qquad (11)$$

Let us determine the conditions under which Eq. (11) is at a maximum; in view of the complexity of function f, let us limit ourselves to an approximate analysis. The expression in the square brackets in the denominator of Eq. (11) has a minimum with change in k, which is attained when

$$\kappa^2 = \kappa_n^2 - \alpha^2 \qquad (12)$$

The numerator has a maximum when the term in it is positive and $|\cos \kappa \ell| = 1$. This requires that $\kappa = \kappa_n - \frac{\pi}{\ell} q$, where q is a positive integer. By equating both values to k, we find that we must have

$$q = \frac{1}{2}\left(\frac{\alpha}{\kappa_n}\right)^2 n = \frac{1}{2\pi}\left(\frac{\alpha}{\kappa_n}\right)\alpha\ell$$

in order that the denominator minimum and the maximum of the numerator in Eq. (11) coincide.

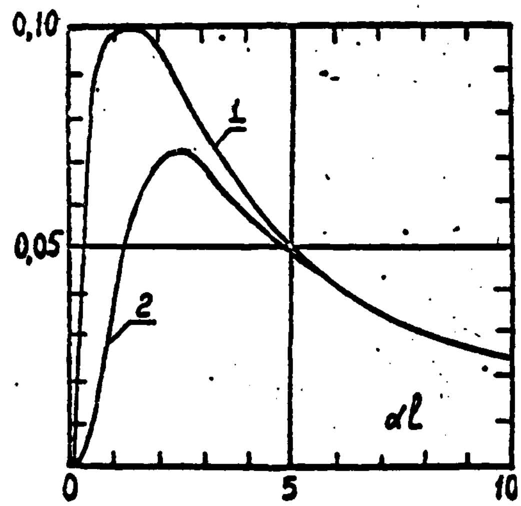

Fig. 1

In calculating q, it was assumed that $\alpha/\kappa_n \ll 1$. From the latter it will be clear that $\alpha\ell \sim 1$ is necessary in order to maximize f, therefore q<<1.

So, given the condition $\alpha/\kappa_n \ll 1$, we cannot carry out Eq. (12) and q=1 at the same time. So when k changes, the maximum of the numerator and the minimum of the denominator of Eq. (11) do not coincide. Further analysis shows that under condition (12) the

value of f exceeds by about one order of magnitude its value when $\varkappa = \varkappa_n - \frac{\pi}{\ell}$. So we assume that Eq. (11) is at a maximum when $\varkappa = \varkappa_n$, then we get

$$f(\alpha\ell) = \frac{1}{4\alpha\ell}(1-e^{-\alpha\ell})^2 \qquad (13)$$

A plot of function (13) is given in Fig. 1 (curve 1). The curve has a maximum when

$$\alpha\ell \approx 1{,}25, \qquad (14)$$

is approximately equal to 0.1.

Thus, the maximum possible transmission coefficient of the converter under study is

$$G_N = \frac{\Pi_{\text{вых}\,N}}{\Pi_{C0}} = 0{,}1 m^2 \frac{\omega_n Q_0}{\alpha\,\varepsilon_{0n}} W_r W_c \Pi_{r0} \qquad (15)$$

Excitation of Currents with a Standing Wave

Let us assume that in the resonator under study the heterodyne and signal waves are reflected from the internal wall when z=ℓ and, on propagating in the opposite direction, exit from the resonator when z=0. Then for the heterodyne and signal waves we will have the expression

$$\dot{\vec{E}}_r = \vec{I}_r[\dot{E}_{r0} e^{-\alpha_r z} e^{-j\varkappa_r z} - \dot{E}_{r0} e^{-2\alpha_r \ell} e^{-j2\varkappa_r \ell} e^{\alpha_r z} e^{j\varkappa_r z}] \qquad (16)$$

$$\dot{\vec{E}}_c = \vec{I}_c[\dot{E}_{c0} e^{-\alpha_c z} e^{-j\varkappa_c z} - \dot{E}_{c0} e^{-2\alpha_c \ell} e^{-j2\varkappa_c \ell} e^{\alpha_c z} e^{j\varkappa_c z}] \qquad (17)$$

The minus sign in front of the second terms takes into account the loss of a half wave at reflection.

When computing the components $\dot{\vec{E}}_r \dot{\vec{E}}_c^*$ in Eq. (6), we will consider only the products of the first and second terms in Eqs. (16) and (17). The rejected terms correspond to the weak interaction of the heterodyne and signal waves moving in opposite directions. By calculating Eq. (6), we arrive at an expression

analogous to Eq. (10):

$$\Pi'_{\text{вых}} = m \frac{\omega_n Q_0}{\alpha \varepsilon_{on}} W_r W_c \Pi_{r0} \Pi_{c0} f_1(\kappa_n, \kappa, \alpha, \ell) \tag{18}$$

where

$$f_1(\kappa_n, \kappa, \alpha, \ell) = \frac{(\alpha \kappa_n)^2}{[(\alpha^2 + \kappa_n^2 - \kappa^2)^2 + (2\alpha\kappa)^2]} \frac{1}{\alpha \ell} \times$$
$$\times [1 + e^{-4\alpha\ell} + 4e^{-2\alpha\ell} + 2e^{-2\alpha\ell} \cos 2\kappa\ell + (-1)^{\xi} 4e^{-\alpha\ell}(1 + e^{-2\alpha\ell}) \cos \kappa\ell] \tag{19}$$

Analyzing this function at the maximum, like the above analysis, again leads to the condition of phase matching $\kappa = \kappa_n$. Here the function f_1 is transformed to

$$f_1(\alpha\ell) = \frac{1}{4\alpha\ell}(1 - e^{-\alpha\ell})^4 \tag{20}$$

Its plot is given in Fig. 1 (curve 2). It attains a maximum equal to 0.072 when $\alpha\ell$=2.5. The maximum transmission coefficient in this case is

$$G'_n = \frac{\Pi_{\text{вых}}}{\Pi_{c0}} = 0{,}072 m^2 \frac{\omega_n Q_0}{\alpha \varepsilon_{on}} W_r W_c \Pi_{r0} \tag{21}$$

By comparing Eq. (21) with Eq. (15) we discover that using the reflected heterodyne and signal waves led to a reduction of the transmission coefficient by a factor of 1.4 and to an increase in the optimal resonator length by a factor of 2. This result is explained by the fact that, when reflected by the resonator wall, both waves (heterodyne and signal) change phase by π. Since Eq. (2) includes the products of wave amplitudes, the reflected waves will produce, near the wall, a nonlinear polarization vector in the same phase as the incident waves. The field of the excited oscillation (7) is formed by two waves moving in opposite directions and varying, at reflection by the wall, in phase by π. As a result, if, for example, the heterodyne and signal waves moving in the positive direction of the z-axis give up their energy to the intermediate-frequency wave moving in the same direction, after reflection of all three waves the energy will be pumped in the opposite direction because of the disturbed

matching of the phases of nonlinearly polarized currents and the electric field. So the conversion efficiency suffers. The presence of losses for the heterodyne and signal waves compensates the effect of the reverse transmission of energy, leading to an increase in the optimal resonator length.

Let us assume that the effect of phase discontinuity at reflection is eliminated. In actual conditions this can be achieved by making a hole in the resonator wall at $z=\ell$ and positioning the mirror reflecting the heterodyne and signal beams in a location outside the resonator at a distance of one-quarter intermediate-frequency wavelength in the dielectric. When making the calculations for this case, a plus sign must be placed at the second term, for example, in Eq. (17) (we neglect the attenuation in the dielectric section projecting from the resonator). Then in Eq. (18), in place of f_1, the function

$$f_2(\kappa_n,\kappa,\alpha,\ell)=\frac{(\alpha\kappa_n)^2}{\alpha\ell}\frac{[1-2e^{-2\alpha\ell}\cos\kappa\ell+e^{-4\alpha\ell}]}{[(\alpha^2+\kappa_n^2-\kappa^2)^2+(2\alpha\kappa)^2]} \tag{22}$$

will appear. As before, it will have a maximum at $\kappa=\kappa_n$ equal to

$$f_2(\alpha\ell)=2\frac{1}{4\alpha\ell}(1-e^{-2\alpha\ell})^2=2f(2\alpha\ell) \tag{23}$$

By comparing Eqs. (23) and (13) we see that when there is reflection with compensation of the half-wave loss, the optimal resonator length is reduced, and the transmission coefficient is increased by a factor of 2 compared with the case of excitation with a traveling wave.

We note that compensation of the half-wave loss is not required when there is excitation by TM waves (for example, in a cylindrical resonator [56]).

Comparison of Transmission Coefficients in Waveguide and Resonator Converters

If losses in the resonator are caused only by losses in the dielectric, we can find that

$$Q_0 = \frac{1}{2} \frac{\omega_n \varepsilon_{0n}}{\alpha_n} W_n, \tag{24}$$

where α_n is the attenuation coefficient of the amplitude of the plane wave with frequency ω_n in the dielectric.

The maximum transmission coefficient in the case of excitation with a standing wave with compensation for half-wave loss will then be written as

$$G_n'' = 0.1 \frac{m^2 \omega_n^2}{\alpha_n(\alpha_r + \alpha_c)} W_r W_c W_n \Pi_n \tag{25}$$

We can show that the idealized waveguide converter (examined in [56]) with a plane wave has a transmission coefficient equal to

$$G_{Mb} = 4 \frac{m^2 \omega_n^2}{(\alpha_r + \alpha_c)^2} W_r W_c W_n \Pi_n f^2(\varkappa, \Delta K'), \tag{26}$$

where $f(\varkappa, \Delta K')$ is a function in Eq. (12), in [56].

Let us inspect the ratio

$$\frac{G_n''}{G_{Mb}} = \frac{1}{40 \varkappa f^2(\varkappa, \Delta K')} \tag{27}$$

where $\varkappa = \alpha_n / \alpha_r + \alpha_c$. When $\varkappa = 1$ and $\Delta k' = 0$, the gain (26) in the transmission coefficient, for a resonator, is approximately 1.5. Calculations show that the optimal resonator length in this case is also shorter than the waveguide, by a factor of 1.5.

From Eq. (27) it follows that G_M'' can exceed G_{Mb} without bound, if $\varkappa \to 0$.

RECORDING SUBMILLIMETER AND INFRARED RADIATION WITH THE TUNNEL METAL-TO-DIELECTRIC-TO-METAL (MDM) JUNCTION

G. D. Lobov and A. N. Nenashev

Characteristics of Tuhnel Current for Weak Signals

Current flowing by tunnel penetration through the potential barrier in the MDM contact is defined as follows [57,58]:

$$I_{TV} = \frac{4\pi m e k T S}{h^3} \int_0^{E_m} D(E_x) \ln \left\{ \frac{1+\exp[(\eta - E_x)/kT]}{1+\exp[(\eta - E_x - eV)/kT]} \right\} dE_x, \tag{1}$$

here e and m are the electron charge and mass; k is the Boltzmann constant; η is the Fermi energy; T is temperature in degrees Kelvin; v is the applied voltage; h is the Planck constant; E_x is the fraction of the electron energy in the direction perpendicular to the potential barrier; E_m is the maximum electron energy; S is the contact area; ℓ is the dielectric thickness; $D(E_x) = \exp[-A \int_0^{1} [\Phi(x) + \eta - E_x]^{1/2} d(\frac{x}{\ell})]$ is the probability of tunnel penetration of an electron with energy E_x; $\Phi(x)$ is the shape of the potential barrier; and $A = 4\pi(2m)^{1/2}\ell/h$.

When T>0K, the representation of $D(E_x)$ in the form [59]

$$\ln D(E_x) = -[b + c(\eta - E_x) + f(\eta - E_x)^2 + \ldots] \tag{2}$$

If $1-c\kappa T>(2f)^{1/2}\kappa T$, we can neglect the third term in Eq. (2). In [58] it is shown that this condition is usually satisfied and the coefficients b and c are defined by the following expressions:

$$b=A\int_0^1[\varphi(x)]^{1/2}d\left(\frac{x}{l}\right);\quad c=qSA\int_0^1[\varphi(x)]^{-1/2}d\left(\frac{x}{l}\right) \tag{3}$$

If the voltage $v=V_0\sin\omega t$ is applied to an MDM system, the detected signal is determined by the following expression [57]:

$$\Delta V_{TY}=\Delta I_{TY}R_{TY}=\alpha V_0^2+\beta V_0^3, \tag{4}$$

where R_{TY} is the contact impedance for the tunnel current.

Using the representation of $D(E_x)$ in the form of Eq. (2) and expanding Eq. (1) in a series in terms of v, for the coefficients in Eq. (4) we get the expressions

$$\alpha=\frac{e}{4}\left[b_{21}-b_{11}+\frac{c_{21}+c_{11}}{c_{20}}(\pi\kappa Tc_{20})\,\mathrm{ctg}(\pi\kappa Tc_{20})\right], \tag{5}$$

$$\begin{aligned}\beta=\frac{2e^2}{3\pi}\Big\{&\frac{1}{c_{20}}\left(c_{20}b_{21}-c_{10}b_{11}-\frac{c_{22}-c_{12}}{2}\right)(\pi\kappa Tc_{20})\,\mathrm{ctg}(\pi\kappa Tc_{20})+\\&+\frac{c_{21}^2-c_{11}^2}{2c_{20}^2}(\pi\kappa Tc_{20})^2\,\mathrm{cosec}^2(\pi\kappa Tc_{20})[2-\sin^2(\pi\kappa Tc_{20})]+\\&+\frac{c_{22}-c_{12}}{2}(\pi\kappa Tc_{20})\,\mathrm{ctg}(\pi\kappa Tc_{20})\Big\}.\end{aligned} \tag{6}$$

$$R_{TY}=\frac{h^3c_{20}}{4\pi me^2S}e^{b_{20}}\frac{\sin(\pi\kappa Tc_{20})}{\pi\kappa Tc_{20}} \tag{7}$$

In Eqs. (5)-(7), the first digits in the subscripts at the coefficients b and c correspond to the following: "2" is the forward characteristic and "1" is the reverse characteristic. The second digits give the order of the derivative of the expressions in Eq. (3) in terms of the argument ev.

Allowing for the Effect of Mirror Image Forces

We will adopt the expression for the potential barrier with allowance for the mirror image forces, as in [60], in the form

$$\varphi(x) = \varphi_T(x) + V_i, \tag{8}$$

where $V_i = -\frac{1.15\lambda l^2}{x(l-x)}$; $\lambda = \frac{e^2 \ln 2}{8\pi\varepsilon_0 \varepsilon l}$; ε is the relative dielectric constant; and $\Phi_T(x)$ is the shape of the trapezoidal barrier.

Since it is difficult to derive expressions for b and c in final form from Eq. (3) with reference to Eq. (8), let us derive an approximate expression, considering that λ is a small quantity. Expanding Eq. (3) in series in terms of λ , after substituting Eq. (8) in it and neglecting the terms proportional to λ^2, we get

$$\begin{aligned}
b_{00} &= b_{00}^T - A(z\varphi_2^{3/2} + y\varphi_1^{3/2}) - 0.6\lambda A\left(\frac{\Gamma_1}{\varphi_1^{1/2}} + \frac{\Gamma_2}{\varphi_2^{1/2}}\right),\\
c_{00} &= c_{00}^T - A\left(\frac{z}{\varphi_2^{1/2}} + \frac{y}{\varphi_1^{1/2}}\right) + 0.6\lambda A\Big[\frac{2\Delta\varphi(\varphi_2^{1/2} - \varphi_1^{1/2})}{(\varphi_1\varphi_2)^{1/2}} + \\
&\qquad + \frac{\Gamma_1}{\varphi_1^{1/2}} + \frac{\Gamma_2}{\varphi_2^{1/2}}\Big],\\
b_{11} &= b_{11}^T + \frac{Az}{3\varphi_2} - \frac{0.6\lambda A}{\varphi_2^{1/2}}\left[\frac{\varphi_2^{1/2} - \varphi_1^{1/2}}{\varphi_1^{1/2}} + \frac{\Gamma_2}{2}\right],\\
b_{21} &= b_{21}^T + \frac{Ay}{3\varphi_1} - \frac{0.6\lambda A}{\varphi_1^{1/2}}\left[\frac{\varphi_1^{1/2} - \varphi_2^{1/2}}{\varphi_2^{1/2}} + \frac{\Gamma_1}{2}\right],\\
c_{11} &= c_{11}^T - \frac{Az}{4\varphi_2^{3/2}} + \frac{0.8\lambda A}{\varphi_2^{3/2}}\left[\frac{\varphi_2^{3/2} - \varphi_1^{3/2}}{3\varphi_1^{3/2}} + \frac{\varphi_2^{1/2} - \varphi_1^{1/2}}{\varphi_1^{1/2}} + \frac{\Gamma_2}{2}\right],\\
c_{21} &= c_{21}^T - \frac{Ay}{4\varphi_1^{3/2}} + \frac{0.8\lambda A}{\varphi_1^{3/2}}\left[\frac{\varphi_1^{3/2} - \varphi_2^{3/2}}{3\varphi_2^{3/2}} + \frac{\varphi_1^{1/2} - \varphi_2^{1/2}}{\varphi_2^{1/2}} + \frac{\Gamma_1}{2}\right],\\
c_{12} &= c_{12}^T - \frac{3Az}{8\varphi_2^{5/2}} + \frac{2\lambda A}{\varphi_2^{5/2}}\Big[\frac{(2\varphi_2 - \varphi_1)(\varphi_2^{5/2} - \varphi_1^{5/2})}{5\Delta\varphi\,\varphi_1^{5/2}} + \frac{\varphi_2^{3/2} - \varphi_1^{3/2}}{3\varphi_1^{3/2}} + \\
&\qquad + \frac{\varphi_2^{1/2} - \varphi_1^{1/2}}{\varphi_1^{1/2}} + \frac{\Gamma_2}{2}\Big],\\
c_{22} &= c_{22}^T - \frac{3Ay}{8\varphi_1^{5/2}} + \frac{2\lambda A}{\varphi_1^{5/2}}\left[\frac{(\varphi_2 - 2\varphi_1)(\varphi_1^{5/2} - \varphi_2^{5/2})}{5\Delta\varphi\,\varphi_2^{5/2}} + \frac{\varphi_1^{3/2} - \varphi_2^{3/2}}{3\varphi_2^{3/2}} + \frac{\varphi_1^{1/2} - \varphi_2^{1/2}}{\varphi_2^{1/2}} + \frac{\Gamma_1}{2}\right]
\end{aligned} \tag{9}$$

Here

$$y = \frac{9.2}{\varphi_2 + 2\varphi_1 + 4\lambda} - z; \quad z = \frac{1.2\lambda}{\varphi_2}; \quad \Delta\varphi = \varphi_2 - \varphi_1;$$

$$\Gamma_1 = \ln\frac{4\varphi_1}{y(\varphi_1^{1/2} + \varphi_2^{1/2})^2}; \quad \Gamma_2 = \ln\frac{4\varphi_2}{z(\varphi_1^{1/2} + \varphi_2^{1/2})^2}$$

The coefficients for the corresponding trapezoidal barrier are

$$
\begin{aligned}
&b_{10}^{T} = \frac{2A}{3\Delta\varphi}\left(\varphi_2^{3/2} - \varphi_1^{3/2}\right); \quad c_{10}^{T} = \frac{1}{\Delta\varphi}\left(\varphi_2^{1/2} - \varphi_1^{1/2}\right); \\
&b_{11}^{T} = \frac{1}{\Delta\varphi}\left(b_{10}^{T} - A\varphi_2^{1/2}\right); \quad b_{21} = -\frac{1}{\Delta\varphi}\left(b_{10}^{T} - A\varphi_1^{1/2}\right). \\
&c_{11}^{T} = \frac{1}{\Delta\varphi}\left(c_{10}^{T} - \frac{1}{2}A\varphi_2^{-1/2}\right); \quad c_{21}^{T} = -\frac{1}{\Delta\varphi}\left(c_{10}^{T} - \frac{1}{2}A\varphi_1^{-1/2}\right); \\
&c_{12}^{T} = \frac{1}{\Delta\varphi}\left(c_{11}^{T} - \frac{1}{8}A\varphi_2^{-3/2}\right); \quad c_{22}^{T} = -\frac{1}{\Delta\varphi}\left(c_{21}^{T} - \frac{1}{8}A\varphi_1^{-3/2}\right)
\end{aligned}
\tag{10}
$$

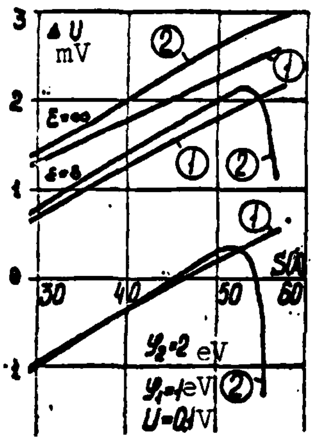

Fig. 1.
(1) Contact temperature 0°K
(2) Contact temperature 300°K

Shown in Fig. 1 (1) is the rectified voltage as a function of the dielectric thickness, derived from Eqs. (4)-(10). From the functions shown it is clear that the effect of the mirror image forces is quite large and even when ε<8, a signal with either positive or negative polarity can be obtained.

Allowing for the Thermionic Emission Current

If the contact temperature of an MDM is higher than 0°K, within the metal there will be electrons whose energy is larger than the work yield function ϕ. On leaving the metal, these electrons produce the thermionic emission current [61]

$$I_{\text{тэ}} = 4\pi h^{-3} m e \kappa^2 T^2 S\left[\exp\left(\frac{\varphi_{1m}}{\kappa T}\right) - \exp\left(-\frac{\varphi_{2m}}{\kappa T}\right)\right] =$$
$$= I_0\left[\exp\left(-\frac{\varphi_{1m}}{\kappa T}\right) - \exp\left(-\frac{\varphi_{2m}}{\kappa T}\right)\right],$$

where ϕ_{1m} and ϕ_{2m} are the potential barrier maxima in metals over the Fermi levels.

If the voltage v is applied between the electrons, then

$$\varphi_{2m} = \varphi_{1m} + v$$

and

$$I_{\text{тэ}} = I_0 \exp\left(-\frac{\varphi_{1m}}{\kappa T}\right)\left[1 - \exp\left(-\frac{e v}{\kappa T}\right)\right] \tag{11}$$

By defining ϕ_{1m} analogous to [61] for an electrode with a smaller work function, negatively charged, we find that [61]

$$\varphi_{1m} = \varphi_1 - ev - \left\{24[16 + \varepsilon l(\Delta\varphi - ev)]\varepsilon^{-2} l^{-2}\right\}^{1/2} \tag{12}$$

If the electrode with a larger work function is negatively charged, then

$$\varphi_{1m} = \varphi_2 - \left\{24[16 + \varepsilon l(\Delta\varphi + ev)]\varepsilon^{-2} l^{-2}\right\}^{1/2} \tag{13}$$

By expanding Eq. (11) in series in v, using Eqs. (12) and (13), we will have the following expression for the rectified voltage due to thermionic emission

$$\Delta V_{\text{тэ}} = \Delta I_{\text{тэ}} R_{\text{тэ}} = -\frac{e}{\kappa T}\left[1 - \left(\frac{24}{16 + \varepsilon l \Delta\varphi}\right)^{1/2}\right] V_0^2, \tag{14}$$

where

$$R_{\text{тэ}} = \frac{h^3}{4\pi m e^2 \kappa T S} \exp\left\{\frac{\varphi_1}{\kappa T} + \frac{[24(16 + \varepsilon l \Delta\varphi)]^{1/2}}{\varepsilon l \kappa T}\right\} \tag{15}$$

By representing $\Delta I_{\text{ту}}$ and $\Delta I_{\text{тэ}}$ as current generators with internal impedance $R_{\text{ту}}$ and $R_{\text{тэ}}$, for the total voltage at the contact ($R_{\text{тэ}} \| R_{\text{ту}} \ll R_{\text{н}}$) we get the expression

$$\Delta V_{\Sigma} = \frac{R_{\text{тэ}}}{R_{\text{ту}} + R_{\text{тэ}}} \Delta V_{\text{ту}} + \frac{R_{\text{ту}}}{R_{\text{ту}} + R_{\text{тэ}}} \Delta V_{\text{тэ}} \tag{16}$$

Shown in Fig. 1 (2) are the results of calculation based on Eq. (16) with the involvement of Eqs. (4), (7), (14), and (15) for the contact temperature T=300°K. From the figure it is clear that up to a certain dielectric thickness the effect of temperature is small. But when the dielectric thickness is increased, corresponding to an increase in contact impedance, a second change in the polarity of the rectified voltage is possible.

Experimental Results

The experiments were conducted with a point contact between a 15 micrometer tungsten wire and an aluminum base coated with a natural oxide layer. The tungsten wire was sharpened electrolytically and the tip was monitored with a microscope. The mechanical system made it possible to finely regulate the wire pressure on the base, by varying the thickness of the dielectric film. The relative changes in the dielectric thickness were monitored by the change in the contact at direct current. The following device was used as supplies of microwave oscillations: a klystron operating in the 5 mm range, and a CO_2 laser. In both cases amplitude modulation of the radiation was employed. In the experimental part of the study, the magnitude and shape of detected pulses were investigated as a function of dielectric film thickness.

Shown in Fig. 2 is the signal magnitude as a characteristic function of contact impedance on exposure to radiation with λ=5 mm. As we can see in the figure presented, the polarity of the detected signal varies by a factor of 2. In accordance with the theoretical assumptions elaborated above, this function can be accounted for by the effect of mirror image forces for small film thicknesses (small contact impedances) and by the presence of thermionic emission, which must be taken into account for high contact impedances (large film thicknesses). When this MDM contact is irradiated with radiation with λ=10.6 micrometers, the signal polarity was observed to vary only for small contact impedances. Evidently, the absence of

change in polarity for large contact impedances can be accounted for by a reduction in the effect of the thermionic emission current when the wavelength is shortened.

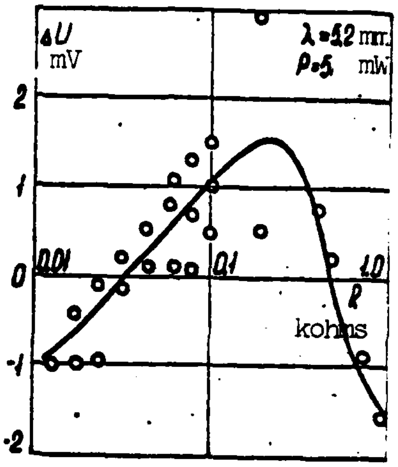

Fig. 2

Since the time constant of the RC junction depends strongly on the dielectric film thickness, as to be expected, for small contact impedances the rise time of the detected pulse front was small (less than 10^{-7} s). As the contact impedance was increased, this time rose to 10^{-4} to 10^{-3} s. These functions were analogous for both cases of irradiation.

PART 4

DIELECTRIC WAVEGUIDES

CALCULATION OF MULTILAYER DIELECTRIC WAVEGUIDE

G. D. Rozhkov, A. S. Belanov, and V. F. Vzyatyshev

Use of Dielectric Waveguides in Submillimeter Wave Band

Several factors at present impede the broad application of dielectric waveguides in the submillimeter wave band. Of these, the increase in attenuation and the need to reduce the transverse dimensions of dielectric waveguides in order to retain the single wave mode are leading barriers.

Attenuation in dielectric waveguides, although slower than in hollow metal waveguides, intensifies with shortening of the wavelength. Given existing materials, with consideration of losses of the order of $2 \cdot 10^{-4}$, for single wavelength waveguides[1] it reaches a value of 6-10 dB/m, somewhere on the boundary between the millimeter and the submillimeter bands.

Accordingly, in order to employ dielectric waveguides in the submillimeter band, first of all a considerable reduction in attenuation must be attained in these waveguides. One possible way of solving this problem consists of using dielectric waveguides made of special materials. In fact, because of features of the

[1] This refers to dielectric waveguides with considerable delay, which can be attained by bends and twists.

mechanism of propagation in dielectric waveguides [62], thermal losses in the waveguide material is the main cause of attenuation, so that attenuation is proportional to the material loss angle.

Is there a possibility of reducing the loss angle of materials in the millimeter and submillimeter bands? Specialists on electrical properties of dielectrics believe that these possibilities undoubtedly exist [63]. As early as 1964, polyethylene with $\tan \delta = 2.7 \cdot 10^{-5}$ at the frequency of 55.2 GHz [64] was prepared. But if this loss angle persists up to the frequency 300 GHz, dielectric waveguides made of this material would have an attenuation of about 1 dB/m at a wavelength of 1 mm.

Of late there have been reports about studies conducted by several British companies aimed at finding special materials for dielectric waveguides exhibiting much lower losses in the submillimeter band than known materials. The first achievements in this direction are reported in [65].

But even if materials with loss losses were prepared, the difficulties involved with the small cross-sectional dimensions will remain. These dielectric waveguides will be difficult to fabricate with the necessary tolerances complied with. In addition, for small dimensions of the dielectric waveguides the mating of waveguide leads of individual assemblies when devices are constructed of these will be difficult.

Specific difficulties also stem from the fact that when any external objects are brought close to dielectric waveguides, for reinforcement, for example, an external electromagnetic field of the dielectric waveguide will be excited and additional losses and radiation will appear. Satisfactory solutions to the problem of reinforcement have been found in the millimeter band by means of members made of foamed materials, and also with metal members.

In the submillimeter band, members made of foamed materials can become unsuitable because of the commensurability of their pore size and the wavelength, while ohmic losses increase drastically in the metal reinforcement members.

Since dielectric waveguides as such, especially when made of polymeric materials, exhibit low rigidity and become very difficult in imparting mechanical stiffness to devices on the dielectric waveguides, or the stability of the mutual arrangement of the dielectric waveguides in sections with space coupling.

It is known [66] that retaining the single wavelength mode requires that in the dielectric waveguide the so-called reduced dimension

$$\tilde{d} = d\sqrt{\varepsilon_1 - \varepsilon_2}/\lambda \tag{1}$$

not exceed some value that is critical for the higher wavelength types. From Eq. (1) it follows that the physical dimension of the dielectric waveguide d can be increased if the dielectric constant of the dielectric waveguide material ε_1 is made smaller. Unfortunately, the minimum value of ε of known homogeneous solid dielectrics is close to 2. But using porous materials of the foamed polystyrene type is hampered owing to the need to produce pores with a diameter much less than the wavelength, and also because the latter are not rigid enough.

However, there is another possibility of increasing the transverse dimensions of the dielectric waveguides. It consists of increasing the dielectric constant of the external medium ε_2 in Eq. (1). In practice, this corresponds to the transition to a multilayer dielectric waveguide.

Multilayer Dielectric Waveguides

A rod of a material with ε_1 in a massive homogeneous shell of material with ε_2 is the simplest example of this kind of

of dielectric waveguides. If this dielectric waveguide is constructed, for example, of polyethylene (ε_1=2.28) in a teflon jacket (ε_2=2.08), the transverse dimensions of the rod jacket can be increased by roughly threefold compared with the case of locating it in air (ε_2=1).

When a multilayer dielectric waveguide is used, it is also easy to solve the reinforcement problem, since the field in the jacket rapidly fades with increasing distance from the rod. The mating problem is also eased. However, if the jacket surrounds the dielectric waveguide core on all sides, access to the external field of the dielectric waveguide is impeded, as is the adjustment of the parameters of devices with space coupling.

We must not forget that, in addition to the useful effect, the increase in the transverse dimensions of the guide rod and the field region, the directional properties are degraded in the dielectric waveguide jacket. They can be characterized by the delay factor ξ_2 with respect to the external medium, which cannot be larger than the quantity $\xi_{вн} = \sqrt{\varepsilon_1/\varepsilon_2} - 1$, and in the single wavelength mode generally it cannot exceed the quantity $\xi_{до} = \xi_{вн}/2$. For example, in the above-discussed variant of a polyethylene-teflon dielectric waveguide $\xi \leq \xi_{до} = 2\%$.

The poor directional properties of the multilayer dielectric waveguide will be exhibited in that radiation at the bent sections will be induced even when the radii of curvature are very large. In this case, the most significant fact may be that the total (for radiation and thermal) angular attenuation for a section bent with the radius R

$$\alpha_{\Sigma\theta} = \alpha_{и} + \alpha_{т} R, \tag{2}$$

as shown in [66] cannot be smaller than some minimum quantity $\alpha_{\Sigma\theta\, мин}$, attained when there is an optimal bending radius $R_{опт}$. Let us evaluate these quantities.

For angular attenuation that arises due to radiation in dB/rad, from [66,67] we have

$$\alpha_{H} = 55R'\zeta_{2}\exp\left(-11{,}8R'\zeta_{2}^{1/2}\right), \tag{3}$$

where ζ is the delay of a wave with respect to the medium with ε_2

$R' = R/\lambda_2$ is the relative radius of bending in wavelengths in the ambient medium $\lambda_2 = \lambda/\sqrt{\varepsilon_2}$

For thermal attenuation (in dB/unit of length), from [66] we can write

$$\alpha_{T} = \frac{27{,}29}{\lambda_2}\left[\sqrt{\frac{\varepsilon_1}{\varepsilon_2}}\,tg\,\delta_1 K_1 + tg\,\delta_2 K_2\right], \tag{4}$$

where δ_1 and δ_2 are the loss angles in the media with ε_1 and ε_2; k_1 and k_2 are the structural attenuation coefficients. In our case, $\sqrt{\varepsilon_1/\varepsilon_2} = 1$; here, $K_1 + K_2 = 1$ independently of the shape of the waveguide cross section and independently of its dimensions. If we further set $\delta_1 = \delta_2 = \delta$, relation (4) becomes

$$\alpha_{T} = \frac{27{,}29}{\lambda_2}tg\,\delta \tag{5}$$

By substituting Eqs. (3) and (5) in Eq. (2) and differentiating with respect to R, for $R'_{\min}$ we get

$$R'_{\min} = 0{,}0848\,\zeta_2^{-\frac{3}{2}}\,y, \tag{6}$$

where y is a root of the equation

$$(y-1)e^{-y} = 0{,}497\,\zeta_2^{-1}\,tg\,\delta \tag{7}$$

By substituting Eqs. (6) and (7) in Eq. (2), we have

$$\alpha_{\Sigma\min} = 27{,}29\,tg\,\delta\,R'_{\min}\frac{y}{y-1} \tag{8}$$

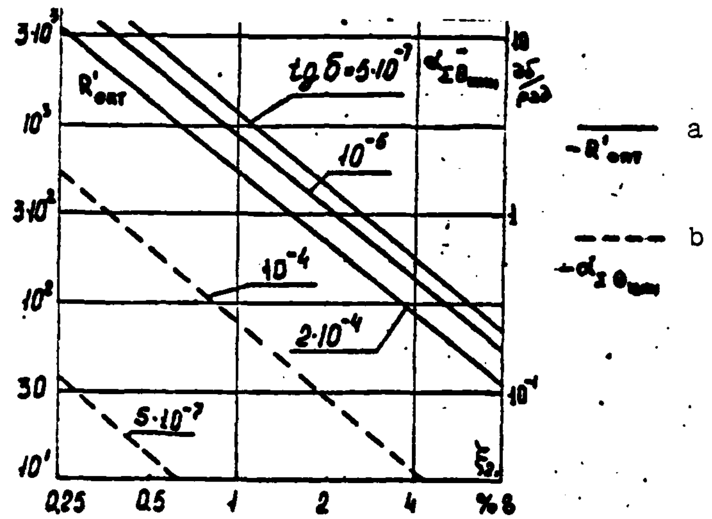

Fig. 1

The quantities $R'_{опт}$ (Fig. a) and $\alpha_{\Sigma\Theta min}$ (Fig. b) as functions of ξ_2 are presented in the plots in Fig. 1. From the plots we see that, given the existing materials (tan $\delta=2\cdot10^{-4}$), the minimum losses in bending become unacceptably large even when $\xi_2<0.02$ (larger than 2 dB/90°). Here the optimal radius of bending is about $220\lambda_2$ and is obviously applicable only in the short-wave part of the submillimeter band (when $\lambda=0.3$ mm and $\varepsilon_2=2.08$, $R_{опт}=45$ mm).

Bending losses can be reduced considerably when tan δ is made smaller. Thus, when tan $\delta=5\cdot10^{-7}$, even the quantity $\xi_2=2.5\cdot10^{-3}$ is applicable, which corresponds to $\varepsilon_1/\varepsilon_2\approx1.01$ and makes it possible to increase the transverse dimensions by about tenfold compared with the dielectric waveguide in air. But the bending radii required in this case ($R'_2\approx8\cdot10^3$) obviously are

unacceptable through the submillimeter band (even when λ=0.1 mm and ε=2.08, R_{min}=540 mm).

Thus, by applying the simplest variant of a multilayer dielectric waveguide in a situation when it must be subjected to bends, a substantial (by an order of magnitude) gain can be attained in the transverse dimensions only in the optical and in the near infrared regions, and even then under the condition that the loss angle of the materials will be not higher than 10^{-6} to 10^{-7}.

The transition to the multilayer dielectric waveguide with a heterogeneous jacket opens another possibility of controlling waveguide parameters. By varying the dimensions of the individual regions of the jacket and the parameters of their materials, we can vary the properties of the dielectric waveguide over wide limits and achieve the combination of materials that cannot be achieved with a dielectric waveguide with a homogeneous jacket. Let us refer to this kind of multilayer dielectric waveguide with a heterogeneous jacket as a "composite" type.

"Composite" Dielectric Waveguides

A composite dielectric waveguide is a rod made of a material with $\varepsilon_1>\varepsilon_2>\varepsilon_3$, abutting on several sides a material with ε_2, and in the remaining sides, with a medium that has ε_3, for example, with air. Some examples of these dielectric waveguides are satisfactorily described with models shown cross-sectionally in Fig. 2.

As will be shown below, the dimensions of the rod of this kind of dielectric waveguide, when the single wavelength mode is retained, can be nearly as large as the rod dimensions for a homogeneous jacket with ε_2. On the other hand, when ε_1=1, this kind of dielectric waveguide has a free access to the external field. But the feature of the behavior of the composite dielectric

waveguide in curved sections is the most attractive. Radiation from a bend of this dielectric waveguide must depend on the direction of the bend. In this case it can be expected that radiation from a bend such that the free side of the rod is the external side is determined by the delay factor ξ_3 with respect to a medium with ε_3. Then the dimensions of this bend can be considerably less than for a dielectric waveguide in a homogeneous jacket with ε_2.

Unfortunately, a rigorous calculation of the characteristics of the composite dielectric waveguides is exceptionally cumbersome. Because of additional interfaces, this calculation must be much more complicated than the calculation of a rectangular dielectric waveguide with a homogeneous jacket. The so-called asymmetric plane dielectric waveguide, a dielectric layer with ε_1, a thickness 2a, and whose medium on one side has the dielectric constant ε_3, and on the other, ε_2, is a relatively simple model satisfactorily describing this dielectric waveguide when $b \gg a$.

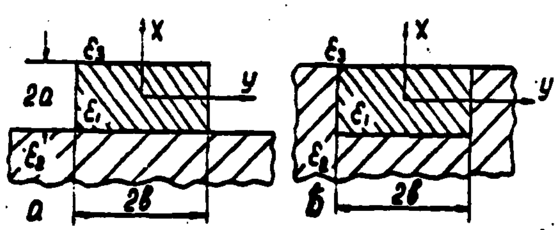

Fig. 2

Analysis of the asymmetric plane dielectric waveguide is reported by the studies [68,69]. We carried out a numerical solution of the characteristic equation and calculated the wave numbers, the constant of propagation, the effective field dimensions on both sides of the wafer, and the structural attenuation coefficients due to losses in the wafer material and in the adjacent media for the waves H_1, H_2, H_3, and E_1, E_2, E_3, and the following parametric ratios:

$\varepsilon_1 = 1.5$; $\varepsilon_3 = 1$; $\varepsilon_2 = 1$; 1.01;
; $\varepsilon_1 = 2.28$; $\varepsilon_3 = 1$; $\varepsilon_2 = 1$; 1.05; 1.3; and 2.08;
$\varepsilon_1 = 3.9$; $\varepsilon_3 = 1$; $\varepsilon_2 = 1$; 1.05 and 2.08 over a wide range of values of the reduced wafer thickness.

Lacking the possibility of presenting all the results in this present study, we give just the dispersion characteristics for the case ε_1=2.28 (polyethylene); ε_3=1; ε_2=2.08 (teflon). They are noted with the symbol ●● in the plots in Figs. 3 and 4. The upper curves correspond to the E_1 wave in Fig. a and to the H_1 wave in Fig. b, and the lower curves, to the E_2 and H_2 waves. The quantity U in the plots, the delay factor of the wave with respect to the medium with ε_3, is associated with the earlier discussed quantity ζ_2 by the relationship

$$U = \frac{c}{v_\varphi \sqrt{\varepsilon_3}} = (1+\zeta_2)\sqrt{\varepsilon_2} \tag{9}$$

As can be seen from the plots, the quantity U satisfies the inequalities

$$\sqrt{\varepsilon_2} \leqslant U \leqslant \sqrt{\varepsilon_1}, \tag{10}$$

here executing the leftmost equality in Eq. (10) corresponds to the critical frequency, and of the rightmost equality, to infinitely large frequencies. The physical meaning of the leftmost inequality in Eq. (10) corresponds to the case when the wave field in a medium with ε_2 decays exponentially with increasing distance from the guide rod with ε_1; when it is not satisfied, the field in a medium with ε_2 will taken on the form of plane waves propagating at some angle to the z-axis and entraining energy from the guide rod.

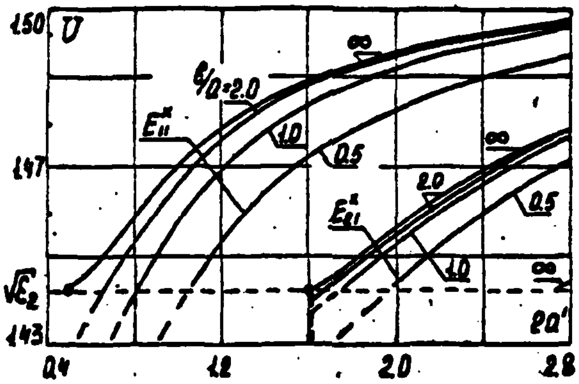
1.50
U
∞
b/a=2.0
E^x_{11}
1.0
0.5
1.47
∞
2.0
E^x_{21}
0.5
1.0
∞
$\sqrt{\varepsilon_2}$
2a'
1.43
0.4
1.2
2.0
2.8

a)

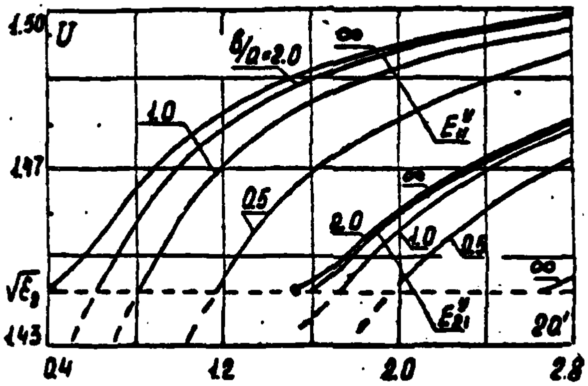
1.50
U
b/a=2.0
∞
1.0
E^y_{11}
1.47
0.5
∞
2.0
1.0
0.5
∞
$\sqrt{\varepsilon_2}$
E^y_{21}
2a'
1.43
0.4
1.2
2.0
2.8

b)

Fig. 3

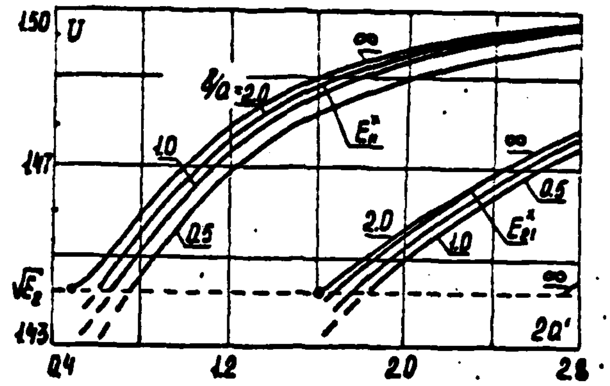

1.50
U
$\ell/a = 2.0$
1.0
0.5
∞
E_{11}^{x}
2.0
1.0
0.5
E_{21}^{x}
1.47
$\sqrt{E_2}$
1.43
$2a'$
0.4
1.2
2.0
2.8

a)

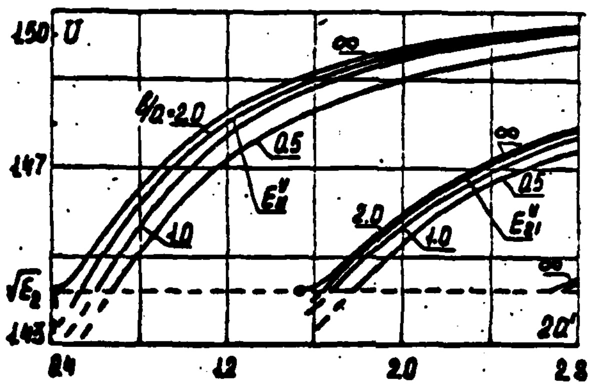

1.50
U
$\ell/a = 2.0$
0.5
1.0
∞
E_{11}^{y}
2.0
1.0
0.5
E_{21}^{y}
1.47
$\sqrt{E_2}$
1.43
$2a'$
0.4
1.2
2.0
2.8

b)

Fig. 4

Relative Dimensions and Band Dimensions of an Asymmetric Plane Dielectric Waveguide

Analysis of the critical conditions for the nearest highest wave type shows that the wafer thickness, at parameters characteristics of the curves in Figs. 3 and 4, can be chosen at values that are larger by a factor of 3.5 to 3.6 than the thickness of the wafer in air (ε_1=2.28; ε_2=1). Interestingly, in the case of a homogeneous setting (ε_1=2.28; ε_2=ε_3=2.08) an increase in wafer thickness of only a factor of 2.5 (by 30 percent less) is possible.

It is interesting also to compare the band properties of these dielectric waveguides. Considering that the minimum wavelength of the band λ_{min} corresponds to the critical conditions of the nearest highest wave type and assuming that at the maximum wavelength, the delay ξ_2 must be equal to some minimum value ξ_{2min} , for the band overlap factor $D=\lambda_{max}/\lambda_{min}$ we have

$$D=\frac{d'_{\kappa p}}{d'[\xi_2-\xi_{2min}]} \tag{11}$$

Assuming in this case ξ_{2min}=0.02, for the asymmetric dielectric waveguide we have D_{H_1}=1.67 and D_{E_1}=1.58, while for the symmetric variant D_{H_1}=1.56 and D_{E_1}=1.49 (9 to 11 percent less).

Thus the plane asymmetric dielectric waveguide will exceed the symmetric variant both with respect to the allowable transverse dimensions and with respect to the width of the working band.

Possibilities of Approximate Calculation

To calculate the models in Fig. 2 that are closer to the actual situation, we can employ an approximate approach first described by V. Shlosser in [70] and widely used by Ye. Markatili in [73]. It is described in detail also in the review [72]. This approach is based on the assumption that the fields in the regions $|x|\leq a$ and $|y|\leq b$ can be described with a single trigonometric function within

the rod and by a single exponential function outside the rod, and with fields in the region $|x|>a;\ |y|>b$ need not generally interest us. In [71] it is shown that this approach for small ε_1 yields satisfactory results, especially in the region that is far-removed from the critical frequency.

The characteristic equation derived by the method described can be represented in the form

$$U^2=U_H^2-\left(\frac{\beta}{4\pi b}\right)^2, \tag{12}$$

where β is a dimensionless internal wave number [66] of a plane dielectric waveguide with thickness 2b made of a material with ε_1 in a medium with ε_2, in the case of model 1, and in a medium with ε_2, in the case of model 2; and U_H is the delay coefficient (with respect to a medium with ε_3) of the above-examined plane asymmetric dielectric waveguide.

The results of calculating the delay with respect to Eq. (12) for dielectric waveguides with different b/a ratios are presented in Figs. 2 and 4.

The symbols for both wave types, as in [72], are as follows: the letter symbol [E] gives the field (in this case, electric), with respect to which the polarization direction is estimated; the letter superscript (x or y) gives the coordinate axis in whose direction the indicated field is generally polarized; the numerical subscripts give the number of field variations in the directions of the corresponding coordinate axes.

It is to be expected that the accuracy of these results improves as U grows larger. The values $U<\sqrt{\varepsilon_2}$ (dashed sections of the curves) will contradict the physical considerations, since the waves traveling with a delay $U<\sqrt{\varepsilon_2}$ must radiate.

Estimates of the width of the working band based on criterion (11) show that it decreases with decrease in b/a. When b/a=2, the

decrease is not large and amounts to 2-7%. When b/a=0.5, model 2 is a much more advantageous model from the standpoint of band properties.

EXPERIMENTAL STUDY OF A COMPOSITE DIELECTRIC WAVEGUIDE

V. F. Vzyatyshev, G. D. Rozhkov, and B. A. Ryabov

Formulation of Problem

When any microwave transmission line is investigated, it is necessary first to establish the conditions for single-wavelength or a virtually single-wavelength operating conditions and to study the main characteristics (delay, attenuation, and distribution of field) of the waves under these conditions. A method for the experimental resolution of these problems as applied to dielectric waveguides has been worked out (see [73,74]).

One feature of setting up experiments with a composite dielectric waveguide consists of the fact that at the present time there are still numerous assemblies (exciters, bends, and so on) that are needed for known methods of measuring. So we were compelled to work out a special method of measuring, using the minimum number of assemblies that are simplest in a design sense.

At the first stage we set up two main goals.

1. Investigation of the dispersion characteristics of the lower wave types.

2. Investigation of the behavior of these waves at the bend sections.

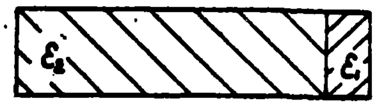

Fig. 1

The cross section of the waveguide investigated is shown in Fig. 1. Rod 1 is made of polyethylene (ε_1=2.28) and has the dimensions 10x4.5 mm^2. It is a rectangular PDV-12 dielectric waveguide that is truncated to make one of its faces planar [73]. Region 2 is made of teflon (ε_2=2.08) and has the dimensions 10x40 mm^2. This waveguide configuration is advantageous in that it provides for access to the external field of the dielectric waveguide from three sides.

Dispersion Characteristics

This investigation was conducted with a dielectric resonator and following the method described in [73,74], in the wavelength band from 4 to 10 mm. Serving as the resonator was a section of the above-described composite dielectric waveguide, 120 mm long, placed between a solid and a gridded reflector. The resonator is excited through the gridded reflector with the open end of a rectangular dielectric PDV-8 waveguide, with a cross section of 6.7x3.35 mm^2. The back wave is branched with a balanced waveguide joint on this same waveguide.

It was found that when the exciting dielectric waveguide is placed opposite the midsection of the teflon plate, a large number of resonances, partially superimposing on each other, is observed.

Identification of the type of these oscillations was made difficult owing to the high concentration of their field in the dielectric. When the exciting dielectric waveguide is placed opposite the polyethylene rod, the intensity of most resonances is reduced, and the intensity of resonances corresponding to the wave types we are interested in is even increased.

The longitudinal order of the resonance oscillation, N, the number of half-waves accommodated along the resonator length L, is determined with an electrical probe, and the resonance frequency f_p, with a wavemeter. Delay with respect to air is then calculated based on the relationship

$$U = \frac{NC}{2Lf_p} \qquad (1)$$

where C is the speed of light.

Polarization of the electric field of the observed oscillations and the number of its variations are determined with a thin plate made of metallized mica.

The experimental results are shown with curves marked by circles in Fig. 2. Also shown there are the calculated results obtained with the approximate method described in [118] (solid curves in the upper part of the plot). The symbols for the wave types correspond to those in [118]. Clearly, the discrepancy of the experimental results and the calculation is very substantial. Admittedly, the experimental waveguide (Fig. 1) differs from the calculation models (Fig. 1 in [118]), but this difference is generally not taken into account in the approximate calculation method.

The most characteristic experimental fact is the detection of waves with the delay $U < \sqrt{\varepsilon_2}$. This fact, which at first glance contradicts the physical principles advanced in [118], is easily explained if we consider that the region with ε_2 has a finite height

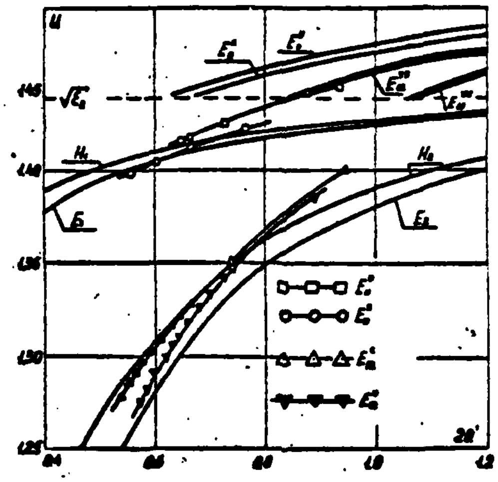

Fig. 2

(10 mm). So the waves entraining energy from the polyethylene rod at frequencies lower than the critical frequency must be not plane waves in an unbounded medium, but waves in the dielectric plate (ε_2=2.08; 2b=10 mm). The dispersion characteristics of these waves are indicated with solid curves in the lower part of the plot in Fig. 2. The symbols for these waves correspond to those in [66]. From the plots we see that some experimental points are below these curves, although from physical considerations it follows that they always must be higher and can be approached only in the critical-frequency region. But this fact cannot be accepted as proven, since the discrepance falls within the limits of experimental error (about $2 \cdot 10^{-3}$), the calculation (about $5 \cdot 10^{-9}$), and the dielectric constant of teflon (about $5 \cdot 10^{-3}$).

Behavior of Waves at Bend Sections

The measurements were made in the wavelength band of 3.9 to 5.7 mm using the following method.

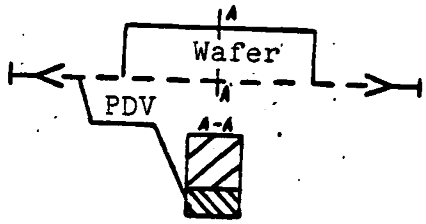

Fig. 3a

The transmission coefficient of the waveguide line consisting of a 1 m long section of a polyethylene PDV, with transverse dimensions of 10x4.5 mm, the midsection of which can be converted, by bringing up a rectangular teflon plate (Fig. 3a) or shaped teflon plates (Fig. 3b), into a section of a linear or a bent composite dielectric waveguide and two exciters in the form of smooth waveguide metal tapers with a 3.6x1.8 mm^2 cross section for a section with the dimensions of 5.5x11 mm^2 and a 100 mm length. The entrance and exit sections of the taper are turned by 90° in order for the electric field in the output section to be oriented parallel to its large side.

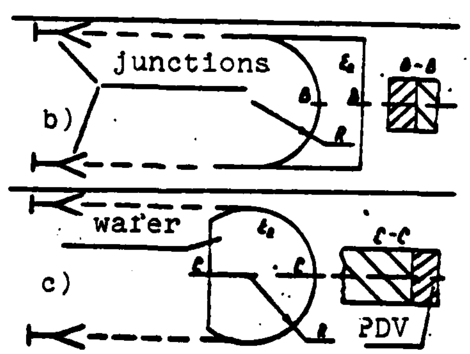

Fig. 3b and 3c

Losses in a line made up of a PDV with tapers for a wavelength of 3.9 mm came to about 6 dB. With the thermal losses in the dielectric waveguide material and in the tapers subtracted, the losses in excitation are about 1.2 dB per exciter. As the wavelength is made larger, the losses are reduced. In order to reduce the relative amplitude of the higher-type waves, special filters are inserted near the exciters. By applying an attenuation of about 5dB on the principal wave type, the filters serve simultaneously for decoupling the members being measured, the generator and the detector.

It was established that the PDV bends in the plane of its smaller facet with radii to 6 cm for an angle to 180° do not introduce additional losses of more than 0.8 dB. The losses observed do not depend monotonically on the angle of bending. Probably they are associated with the conversion to higher-type waveguide waves.

The main result of the measurements is the losses when shaped teflon plates (Figs. 3b and c) are brought up to the bent section of the PDV. This section is thus converted to a bent section of a composite dielectric waveguide (a bend of the kind shown in Fig. 3b, when the material with ε_2 is in the external side of the bend, we call an external bend, and a bend of the Fig. 3c type, an internal bend). It was found that the losses, especially in the external bend, depend strongly on the gap between the PDV and the plate. So measures were adopted to reduce the gap.

Since during transit through the section with the plate at the mating of the dielectric waveguide with the composite dielectric waveguide there must be some conversion into both the higher-type waves and into radiation waves, the characteristics of this converter were measured separately. To do this, the transmission coefficient was plotted as a function of the distance between the PDV and the Fig. 3a plate brought up to the PDV, so that on touching, the composite dielectric waveguide of Fig. 1 was constructed. This function in all cases proved to be monotonic, with the additional losses not exceeding 0.5 dB, λ=5.7 mm, and 0.2 dB, λ=3.9 mm.

Additional losses in the internal bend cannot be measured exactly because during the bringing up and pressing up of shaped plates, the position of the PDV ends in the exciters and the losses in excitation are changed. However, it can be ensured that additional losses do not exceed 1 dB at the wavelength of 5.7 mm and even less so at shorter wavelengths.

In the external bend, as to be expected [118], the losses prove to be much larger. They increase with increase in wavelength and amount to 20 dB at λ=3.9 mm and to 35 dB at λ=5.7 mm.

Thus, the composite dielectric waveguide with heterogeneous surrounding media actually has certain advantages when compared with the multilayer dielectric waveguide in a homogeneous setting.

DIELECTRIC WAVEGUIDE-BASED WAVE TYPE CONVERTER

A. N. Merkur'yev

Approach to Converter Analysis

As we know, when another single wavelength dielectric waveguide brought up to the wave field propagating along a first single wavelength dielectric waveguide, energy branches from the first to the second. Phenomena in this system can be described, with an accuracy suitable for a number of practical cases, with the theory of bound waves [75]. It is shown in [76] that the level of energy interchange between the dielectric waveguides is determined by the ratio $2c/\Delta\gamma$, where c is the linear coupling coefficient (LC) between the waves, and $\Delta\gamma$ is the difference of their constants of propagation. If $\Delta\gamma=0$, there may be total branching of energy from the initially excited dielectric waveguide into the second waveguide; this will occur when

$$cL = \frac{\pi}{2} + n\pi, \quad (n = 0,1,2 \ldots), \tag{1}$$

where L is the coupling section length.

But if $\Delta\gamma \neq 0$ and $2c/\Delta\gamma \ll 1$, as follows from [76,79], the fraction of energy branching into the second dielectric waveguide will not exceed $(2c/\Delta\gamma)^2$. This fact, first pointed out in [75] as applied

to hollow metal waveguides, then can be used in converting the principal wave of the single wavelength dielectric waveguide, for example, a multiwavelength dielectric waveguide, in particular, to an H_{01} wave of the circular dielectric waveguide.

Analysis of phenomena in the system of coupled single wavelength and multiwavelength dielectric waveguides is hampered by the fact that, since a single wavelength transmission line must be brought into correspondence with each propagating wave type, the number of differential equations in their system describing the coupling of the dielectric waveguides is relatively large, so that numerical methods must be used in the solution. The analysis can be simplied with allowance for the fact that the wave type converter must operate with minimum losses, that is, in it there must be a substantial coupling of the wave from the single wavelength dielectric waveguide only with a single wave type from the multiwavelength dielectric waveguide; coupling with other wave types, as an unwanted phenomenon degrading the device characteristics, must be brought to a minimum.

Obviously, this can be achieved by selecting the cross-sectional dimensions and the dielectric constant of the dielectric waveguide so that there is an equality of the constants of propagation of the converted wave types, and by reducing the linear coupling coefficient; this requires making the distance between the dielectric waveguides quite large [77].

Further, to describe the phenomena in the dielectric waveguide system we can use the approach presented, for example, in [78], that is, we can simultaneously examine the coupling of only two specified wave types without allowing for the transformation into parasitic wave types, and the latter can be estimated by the weak coupling method. To do this, the results obtained in [79] can be used directly in calculating the converter characteristics;

this however presupposes a knowledge of the linear coupling coefficient. Since it is not possible to calculate the linear coupling coefficients, we calculate them, more precisely, the linear coupling coefficients of the principal HE_{11} wave of the PDV and the H_{01} wave of the KDV, experimentally.

Measuring the Linear Coupling Coefficients of Waves HE_{11}^{PDV} and H_{01}^{KDV}

The experimental estimate of the linear coupling coefficients is conveniently done by investigating the characteristics of an adjustable converter mockup. The measurements were made according to the diagram in Fig. 1. The converter I as such consists of a KDV section 4.35 mm in diameter and a PDV section, with a cross section of 2.90x1.45 mm^2, parallel for a coupling section 280 mm long. These measurements of the dielectric waveguide sections provide, as is clear from the dispersion curves in Fig. 4, an equality of delays $\xi=\lambda/\lambda_b-1$ (λ_b is the wavelength in the dielectric waveguide) for the waves HE_{11}^{PDV} and H_{01}^{KDV} in the wavelength band $\lambda \approx 5.1$ mm. In this case (see Fig. 2), in addition to the principal wave HE_{II} and the wave H_{0I}, two more wave types can be propagated in the KDV: E_{01} and HE_{21}. Coupling with the first of these, E_{01}, is eliminated by selecting the mutual positioning of the dielectric waveguides such as in shown in the field in Fig. 3. In the Fig. 1 diagram the reflection coefficient of the converter is measured (reflector 2 is connected to the KDV of this converter). The following adjustments are possibled in the converter: varying the distance t between the dielectric waveguides (see Fig. 3) and shifting one dielectric waveguide along the other with constant t. Both adjustments were made without changing the length of the coupling section.

As shown by the experiment, when one dielectric waveguide is shifted along the other, the reflection coefficient rapidly oscillates; a slow aperiodic change is superimposed on the oscillation. The latter is evidently caused by some disturbance in the parallelity of the dielectric waveguides when they are shifted. Rapid

oscillations are explained by the interference in the detector of two (or possibly several) reflected waves. It turned out that near λ=5.1 mm, when $t \geq 2.5$ mm, the period of oscillations corresponds to the delay of the H_{01} wave in the KDV. Therefore, in the converter there must actually be the predominant coupling with the H_{01} wave in the KDV, and the oscillations are caused by the interference of the wave with the variable phase reflected from the converter, and the wave with a constant phase, caused by a nonideal matching of the arrangement elements.

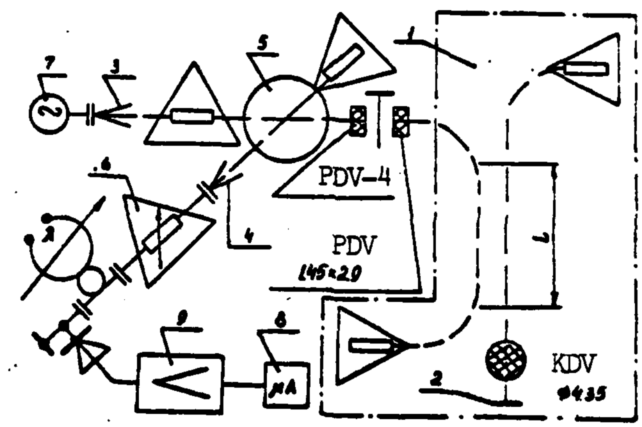

Fig. 1

1. adjustable converter
2. reflector
3,4. tapers to the PDV from metal waveguides
5. bridge (3 dB) for the PDV
6. attenuator
7. generator
8. recording microammeter
9. amplifier

The reflection coefficient as functions of the distance t between the dielectric waveguides in accordance with [77] is oscillatory. Applying the method given in [77], from these functions we found the linear coupling coefficients of the waves HE_{11}^{PDV} and H_{01}^{KDV}, whose plots are shown in Fig. 3.

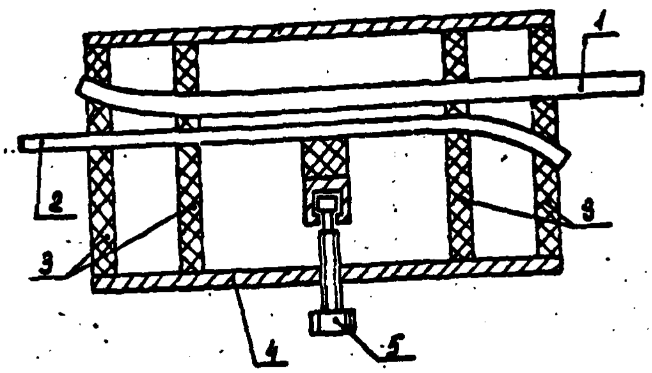

Fig. 2

1. KDV
2. PDV
3. supports
4. housing
5. tuning screw

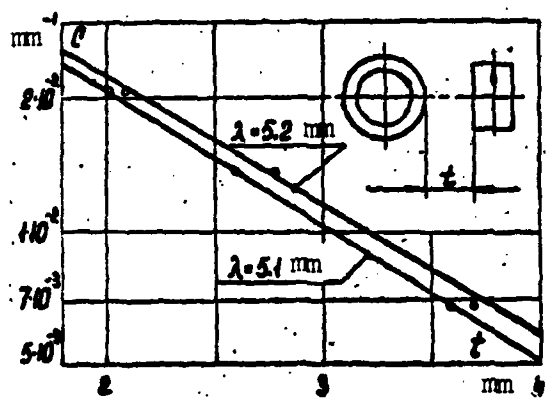

Fig. 3

Construction and Characteristics of Converter

Further study of a converter of HE_{11}^{PDV} and H_{01}^{KDV} wave types was made with a nonadjustable mockup (see Fig. 2). In it use was made of the dielectric waveguides of the same transverse dimensions and the same waveguide positioning as in the adjustable converter mockup. The dielectric waveguides were mounted in foam plastic supports. The ends of the dielectric waveguides were smoothly diverted from each other.

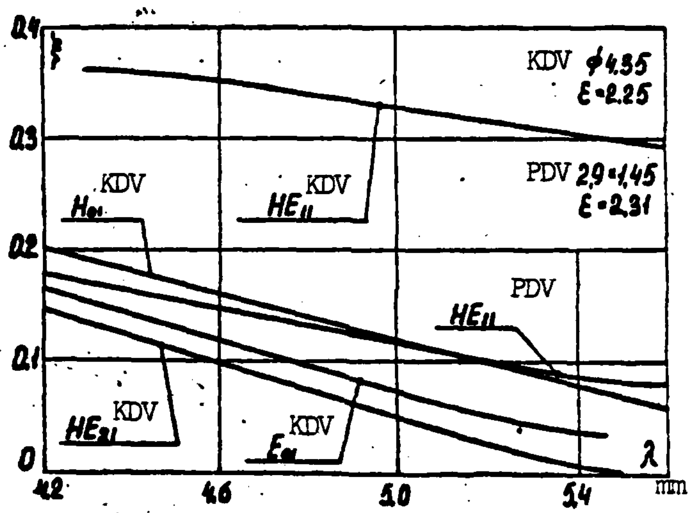

Fig. 4

In trying to attain small device dimensions, we selected the distance between dielectric waveguides t=2 mm. Further, on the basis of Fig. 3 and condition (1) for M=0, we found the length of the coupling section, L=90 mm.

The shape of the PDV axis in the coupling section can be modified somewhat with a tuning screw, attaining the maximum transmission coefficient.

In tuning, the two converters were connected in a cascade manner. By rotating the tuning screws, the minimum losses Δ

was attained, defined as the ratio of the input signal strength to the output signal strength. The plot of the minimum losses Δ_{min} for a single converter as a function of wavelength is presented in Fig. 5. The quantity Δ_{min} has its smallest value at λ=4.7 mm, and not at λ=5.1 mm, as would be expected on the basis of Fig. 4. The concern evidently is that, for total interchange of energy, it is required to have an equality of velocities of propagation of the coupled waves; this occurs at the point of the frequency scale not coinciding with the equality point of the phase velocities of the waves in the connected dielectric waveguides; and it does so the more strongly, the closer the coupled dielectric waveguides are to each other.

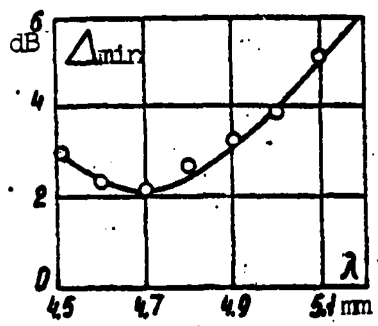

Fig. 5

When the frequency characteristic was being recorded, as before the two converters were connected cascadewise. The losses for a single converter as a function of wavelength $\Delta(\lambda)$ during the tuning of the converters at λ_0=4.7 mm is shown in Fig. 6. In the region λ=4.25 mm we observed a second hump of the frequency characteristic; this apparently is caused by the amplification of the coupling of the PDV wave HE_{11} and of the KDV wave HE_{21}. The concern is that, as shown experimentally, even at the wavelength 4.7 mm, the principal

PDV wave is partially converted to an HE_{21} wave existing in the KDV together with the H_{01} wave, and with a reduction in λ , the weakening of the coupling of the HE_{11}^{PDV} wave with the H_{01}^{KDV} wave is partially compensated by an amplification of the coupling of the HE_{11}^{PDV} and the HE_{21}^{KDV} waves.

Thus, the minimum losses occur at the wavelength of 4.7 mm and amount to 2 dB. In the wavelength band from 4.6 mm to 4.85 mm the losses do not exceed 3 dB. In this mockup, conversion of the KDV HE_{21} wave to the parasitic type was noted.

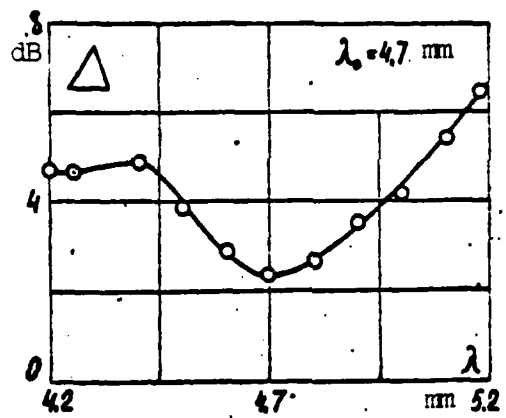

Fig. 6